Sensing the shape of spacetime: detector response and entanglement harvesting in curved space

by

Keith K. Ng

A thesis
presented to the University of Waterloo
in fulfillment of the
thesis requirement for the degree of
Doctor of Philosophy
in
Physics

Waterloo, Ontario, Canada, 2018

Examining Committee Membership

The following served on the Examining Committee for this thesis. The decision of the Examining Committee is by majority vote.

External Examiner:	Silke Weinfurtner Associate Professor, Dept. of Mathematics, University of Nottingham
Supervisor(s):	Robert B. Mann Professor, Dept. of Physics & Astronomy, University of Waterloo
Internal Member:	Niayesh Afshordi Associate Professor, Dept. of Physics & Astronomy, University of Waterloo
Internal Member:	Robert Spekkens Adjunct Professor, Dept. of Physics & Astronomy, University of Waterloo
Internal-External Examiner:	Eduardo Martin-Martinez Assistant Professor, Dept. of Applied Mathematics, University of Waterloo

I hereby declare that I am the sole author of this thesis. This is a true copy of the thesis, including any required final revisions, as accepted by my examiners.

I understand that my thesis may be made electronically available to the public.

Statement of contributions

This thesis is based on the following published and forthcoming articles.

- Chapter 3 is based on
  - Keith K. Ng, Robert B. Mann, and Eduardo Martín-Martínez. The equivalence principle and QFT: Can a particle detector tell if we live inside a hollow shell? *Phys. Rev. D*, 94(10):104041, 2016
- Chapter 4 is based on
  - Keith K. Ng, Robert B. Mann, and Eduardo Martín-Martínez. Over the horizon: distinguishing the Schwarzschild spacetime and the $\mathbb{RP}^3$ spacetime using an Unruh-DeWitt detector. *Phys. Rev. D*, 96(8):085004, 2017
- Chapter 5 is based on
  - Keith K. Ng, Robert B. Mann, and Eduardo Martíín-Martínez. New techniques for entanglement harvesting in flat and curved spacetimes. *Phys. Rev. D*, 97(12):125011, 2018
- Chapter 6 is based on
  - Keith K. Ng, Robert B. Mann, and Eduardo Martín-Martínez. Unruh-DeWitt detectors and entanglement: The anti–de Sitter space. *Phys. Rev. D*, 98(12):125005, 2018

Abstract

This thesis seeks to understand what information Unruh-DeWitt detectors can gain about the structure of spacetime. By coupling to the quantum state of a field on a curved space, the detectors can gain information about their surroundings, beyond their proper acceleration. They can then receive more information than a naïve application of the equivalence principle might suggest. Therefore, we seek to characterize the response of detector(s) in curved space, and find the limits of their abilities.

We first consider the transition probability of a single detector. We show that the transition probability is sensitive to the quantum state of the field. Suppose a detector is enclosed by a shell of transparent matter: then, the gravitational field is completely flat inside. However, the detector can still determine it is not in flat space, and can do so faster than the signalling time to the shell. Thus, some information about the global structure of spacetime is stored locally in the vacuum state, and the detector can extract this information.

Next, we consider the question of the (3+1)-dimensional geon, a Schwarzschild black hole which has a topological identification behind its horizon. Even though it is identical to the usual black hole outside the event horizon, the detector can still distinguish the geon from an ordinary black hole. We compare our results in (3+1) dimensions to those already found for the BTZ geon in (2+1) dimensions. Thus, the vacuum state contains information about the global structure of spacetime, and this information can be extracted by a single detector.

We then consider two detectors, and the entanglement they gain by being coupled to the field. The quantity of entanglement harvested is, once again, sensitive to the structure of the spacetime in which the detectors live; we thus seek to characterize the dependence of entanglement on spacetime structure. We find a new formula for calculating the harvested entanglement, and apply it to find a new analytic expression in flat space. This new method is optimized for calculating the entanglement harvested from a state where only the mode expansion is known, as in most spacetimes; and in the special case where the detectors are spacelike separated, the formula simplifies dramatically.

Lastly, we apply our new formula to (3+1)-dimensional Anti-de Sitter spacetime, a highly symmetric space of constant negative curvature. We use our new expression to find the entanglement harvested by two detectors, both in geodesic and static configurations. We find that the entanglement is indeed affected by global structures and choices in AdS_4. However, we also find many new and novel phenomena in the static case, where two detectors remain static at different redshifts; these phenomena merit further investigation.

Acknowledgements

In my time at Waterloo, I have been so very fortunate to meet and learn from a great many wonderful people. First, I would like to thank my supervisor Robert Mann, who has supported me every step of the way. When I first signed on at Waterloo, he suggested I attempt to calculate the effect of *superradiant* Kerr black holes on detector *entanglement.* It was quite the surprise to us how open the field was back then; I would like to think that we have helped fill it in a little. He has been with me every step of the way, and I would like to thank him for that.

Next, I would like to thank Eduardo Martín-Martínez, who has been like a co-supervisor to me these many years. His enthusiasm for relativistic quantum information, for detectors, proved infectious. I would like to think that his influence is a large part of why I decided to stay in the field, and pursue a PhD., after I completed my Master's thesis. I wish him the best of luck with his endeavours, and his many, many students.

I would also like to thank the many friends I made along the way. While working in Robb's group, I encountered many wonderful people, and found many good friends, who continue to inspire me with their brilliance. Wilson Brenna, Dan Grimmer, Robie Hennigar, Alex Smith, and Erickson Tjoa, just to name a few. Thank you for supporting me and inspiring me, and I wish you the best of luck, wherever you are.

Finally, I would like to thank my family, without which none of this could have been possible. Thank you for your kind love and support. I will remember you always.

Table of Contents

List of Figures

Notation and conventions

- Throughout this thesis, we will use a mostly positive metric signature. That is, $g_{\mu\nu} = \text{Diag}[-+++]$.
- We normalize our units such that $c = \hbar = k_B = 1$. The length scale will be chosen for convenience in each spacetime.
- The following notation is used throughout this thesis:

i	Imaginary unit, i.e. $\text{i}^2 = -1$
D	Spacetime dimension
L	AdS length
$\alpha, \beta, \mu, \nu, ...$	Spacetime indices
$a, b, c, d...$	Spatial indices
$\hat{A}$	Quantum operator A
$\langle \hat{A} \rangle$	Expectation value of operator $\hat{A}$

"How wonderful that we have met with a paradox.
Now we have some hope of making progress."
—Niels Bohr.

Chapter 1

Introduction

If the business of physics is to make predictions, then one can only conclude that the field has been a massive success. In recent years, physicists have found the Higgs boson, and thus completed their description of the fundamental particles of nature; and have detected gravitational waves, a most extraordinary prediction of general relativity. From the very large to the very small, it might not be an exaggeration to say that the physics of the day-to-day has been figured out, and the physics of the extraordinary is well on its way.

Yet, tensions exist. On the most fundamental level, quantum mechanics and general relativity are quite incompatible. Most famously, general relativity predicts the existence of black holes, objects so massive and dense that nothing can escape from them; the object at the center of our galaxy, for instance, is almost certainly a black hole millions of stellar masses large, and efforts to directly observe its horizon continue. Now, suppose we were to drop an object into the black hole. By the No Hair Theorem [12], while the black hole is increased in mass and spin (and, possibly, charge), no other information remains accessible to those outside it. The precise state of that falling object is lost to the singularity inside the black hole. However, one of the most fundamental principles of quantum mechanics is unitarity: information cannot be destroyed. The laws of nature are, for the most part, reversible: a sufficiently powerful being could "rewind" the time evolution of a system to deduce its past.

Black holes, however, are different. Hawking showed [6] that black holes *evaporate:* eventually, after billions of years, their mass-energy is released as radiation, and they disappear. For an observer falling into a black hole, crossing the event horizon should not be a special event: for a sufficiently massive black hole, the change in the gravitational field is so gentle as to be unnoticeable, suggesting that simple quantum mechanics should still

hold. Therefore, the No Hair Theorem [12] suggests that the radiation emanating from the event horizon does not carry the information out of the black hole; the information is simply, permanently lost, violating the base principles of quantum mechanics. This situation is known as the Information Paradox: as a true contradiction between general relativity and quantum mechanics, it is believed that its resolution will point the way towards a unified theory of physics.

Naturally, as a promising topic decades old, many papers and careers have been made on its merits, promoting various solutions to this paradox. While we will seek to summarize a few possible solutions, for more detailed discussion see e.g. [29]. Perhaps the simplest (if not necessarily the most popular) is that the unitarity principle of quantum mechanics is simply, straightforwardly violated: that black holes really do destroy information, violating unitarity. However, unitarity is fundamental to the predictive power of quantum mechanics: without unitarity, there can be no predictions. Therefore, this solution is not favoured by the majority of quantum physicists. Moreover, the AdS/CFT conjecture [19] provides evidence against this theory: briefly, in the Anti-de Sitter (AdS) spacetime, a quantum gravity theory is equivalent to a gravity-free quantum field theory (the conformal field theory, or CFT) on the outer boundary of the spacetime. In such a spacetime, it is hard to see how a black hole could delete information, if the information cannot be deleted on the boundary.

Another solution involves the fate of the black hole itself. While Hawking suggested that the black hole should eventually evaporate into nothing, transformed into information-free radiation, some have suggested that the black hole might instead emit all its information at the end, or perhaps simply leave behind an information-rich 'remnant.' However, there are reasons to believe such information-dense objects cannot exist. Consider by analogy the production of pairs of quarks in particle collisions: in calculating how many quarks are produced, one must multiply by 3, the number of colors. Since even the largest black holes would presumably decay into these remnants, the remnants must have a correspondingly large number of internal microstates: in other words, these remnants would have an almost infinite number of 'colors' and a very small mass. Therefore, if these remnants exist, they should also be pair-produced in detector collisions with incredible abundance [29]. Needless to say, this has not been observed.

Another approach is to deny the nature of the black hole as a singularity. In this picture, what most physicists consider a black hole is actually a more complicated object composed of strings: a 'fuzzball'. Since this object has no singularity, the information is never really deleted; instead, Hawking radiation is comprised of information surfacing from the inside of the black hole, reaching the event horizon, and escaping. However, while this solution does not create any immediate paradoxes, it depends on the existence of string

theory, which has not been independently verified. As well, current fuzzball models do not yet fully replicate the behaviour of evaporating black holes.

Another hypothesis, and for a while the most popular, is known as Black Hole Complementarity. First posited by Susskind [37], it suggests that rather than delete information, black holes *duplicate* it: infalling information is both absorbed into the black hole, and reflected off the event horizon. (More precisely, this information would be encoded in correlations in the Hawking radiation emitted at early and late times.) While duplication of information is still not permitted by unitarity, Susskind argued that this kind of duplication is not observable: there is no observer who could compare both copies of the information, since one copy will be lost inside the black hole, while the other escapes.

However, a subtle problem with this picture was observed much later by a group known collectively as AMPS [1], after their initials (Almheiri, Marolf, Polchinski, and Sully). They observed that monogamy of entanglement (a form of quantum information conservation) suggests that the apparent 'duplication' involved in the Complementarity picture is not possible. Specifically, the late-time Hawking radiation cannot be entangled both with early-time Hawking radiation, and with infalling information. In order for monogamy to be observed, they argued that the information must not 'fall into' the black hole at all: an observer falling into a black hole encounters a high-energy boundary, and is incinerated, at its *event horizon* instead. This proposal, which has become known as the 'firewall', is also controversial: physicists have long argued (e.g. [37]) that by the equivalence principle, since a freefalling observer (that is, one freely accelerated by gravity alone) should be equivalent to a stationary observer in flat space, an observer in such a situation should see nothing at all, the so-called 'no-drama' postulate.

In order to understand what a local observer in such a spacetime observes, we will use the concept of the Unruh-DeWitt detector [38, 5]. A simple, compact two-level system, the UDW detector is a simple model of a local observer, which can interact with the quantum field. Initially, we wished to understand the detector's behaviour on simple trajectories around the black hole, before moving towards studying its behaviour as it falls towards the event horizon. Consider, for instance, the detector orbiting around the black hole. How does it respond to the Hawking radiation emanating from the black hole?

This simple question led to strange answers. One might naïvely invoke the equivalence principle to conclude that since an orbiting detector is in freefall, it must behave much like a detector in the absence of gravity. In particular, if the quantum field is in a state such that the black hole is not emitting particles, known as the Boulware state, the detector should not see anything at all. However, as was discovered first by Hodgkinson and Louko [10], then by us [24], this is not the case: the detector becomes excited, detecting that it

is not in flat space, even in the Boulware case, in which the black hole does not radiate.

Now, strictly speaking, the use of the equivalence principle here is unjustified: it properly applies only to small systems which do not interact with external fields (with the exception of gravity), such as a reflecting cavity. It cannot be applied to any system coupling to a spatially extended quantum state, e.g. a UDW detector. However, this discovery reveals a hidden truth: a quantum vacuum state can carry information about the shape of spacetime. This information may then be retrieved by a single local observer. We therefore argue that application of the equivalence principle to the 'no-drama' postulate may not be fully justified. The question of what drama may occur at the horizon requires further study.

This raises a natural question, then: how much information about the structure of spacetime can a detector discover, given a particular quantum state? For instance, Hodgkinson and Louko [10] demonstrated that a single detector can distinguish a geodesic orbit around a black hole from a static one in flat space. We explore this question in two other spacetimes: a transparent shell, and a topological identification of the black hole. In these two cases, we see that merely by locally coupling to a global field state, a detector can determine much about its spacetime.

After this, the next logical step is to consider how the behaviour of a pair of detectors depends on the structure of spacetime. A pair of detectors interacting with a quantum field state can become entangled, despite being spatially separated [39, 33], in a process known as entanglement harvesting. As was determined by [22, 36], the quantity of entanglement that is harvested is dependent on the structure of spacetime. Therefore, we develop tools to more rapidly calculate the entanglement harvested by two detectors in curved space, apply them to the Anti-de Sitter space in (3+1)-dimensions, and compare to results [7] in (2+1)-dimensions.

In brief, this thesis aims to collect our work on characterizing the response of a detector, or pair of detectors, to various structures in spacetime. We will see how much information about spacetime structure such local observers can obtain, and further understand how detectors interact with quantum fields in more exotic spacetimes. We will begin with a brief introduction to quantum field theory, introducing only the parts that we will require. Next, we determine how quickly a detector can detect a distant feature of spacetime: in this case, a shell of matter. We then demonstrate that a detector can, by measuring the Hawking radiation emitted by a geon, detect a topological feature behind the event horizon. We also develop a scheme for studying the quantum vacuum of any spacetime, using the mode solutions of the field equations, and apply it to four-dimensional Anti-de Sitter space. Lastly, we conclude with a few words about the meaning of our research, and possible future

issues that might be explored. We believe our work represents an important next step in developing UDW detectors as a tool for understanding the structure of spacetime.

Chapter 2

Preliminary Theory

In order to calculate what a local observer measures on a given spacetime, we need a few things:

1. A way of expressing the quantum state of a field on the spacetime,
2. A model system representing the observer, and
3. A way of formalizing the concept of 'measurement'.

Each of these is complicated by the fact that we will be studying curved spacetimes; as we will see, certain intuitions from Minkowski space break down in the presence of curvature. However, with the proper theoretical background, we can still make calculations and predictions, in surprisingly complicated situations.

First, we will need to use a few basic concepts [3] from quantum field theory in order to express the state of the field. Then, we will introduce the concept of an Unruh-DeWitt particle detector [38, 5], our model observer. Finally, we will show from perturbation theory how to derive the probability that this observer detects a particle.

2.1 Quantum Field Theory Done Quickly

Let us start off in ordinary quantum mechanics, by considering a quantum harmonic oscillator, a particle in a harmonic potential. That is, the particle behaves according to the

following Hamiltonian:

$$\hat{H} = \frac{\hat{p}^2}{2m} + \frac{1}{2}m\omega^2\hat{x}^2 \tag{2.1}$$

where the momentum of the particle is $\hat{p} = -\mathrm{i}\hbar\hat{\partial}_x$. Rather than attack the Schrödinger equation directly, we instead will use Dirac's ladder operator approach. It is a standard exercise to show that the spectrum can first be found by considering the following two linear combinations of the position and momentum operators:

$$\hat{a} = \sqrt{\frac{m\omega}{2\hbar}}\left(\hat{x} + \frac{\mathrm{i}}{m\omega}\hat{p}\right) \tag{2.2}$$

$$\hat{a}^\dagger = \sqrt{\frac{m\omega}{2\hbar}}\left(\hat{x} - \frac{\mathrm{i}}{m\omega}\hat{p}\right). \tag{2.3}$$

It is a fairly straightforward calculation to show that these operators have the commutator

$$[\hat{a}, \hat{a}^\dagger] = 1. \tag{2.4}$$

Next, one shows that the Hamiltonian can be re-expressed in terms of these operators:

$$\hat{H} = \hbar\omega\left(\hat{a}^\dagger\hat{a} + \frac{1}{2}\right). \tag{2.5}$$

For reasons that will quickly become apparent, we will write $\hat{N} = \hat{a}^\dagger\hat{a}$, and call it the "number operator". Since this new operator only differs from the Hamiltonian by a constant, the eigenstates of the Hamiltonian are also eigenstates of $\hat{N}$. We will thus label the eigenstates as

$$\hat{H}|n\rangle = n|n\rangle. \tag{2.6}$$

The commutation relation (2.4) can then be used to show that

$$\hat{N}\hat{a}|n\rangle = (n-1)\hat{a}|n\rangle, \tag{2.7}$$

$$\hat{N}\hat{a}^\dagger|n\rangle = (n+1)\hat{a}^\dagger|n\rangle. \tag{2.8}$$

Thus the operators $\hat{a}, \hat{a}^\dagger$ must map eigenstates to eigenstates, up to a multiplicative constant.

Now, since $\langle n|\hat{N}|n\rangle = (\hat{a}|n\rangle)^\dagger(\hat{a}|n\rangle)$, we find that all eigenvalues of $\hat{N}$ must be non-negative. Therefore, there must be a state such that $\hat{a}|\psi\rangle = 0$; otherwise, we could produce states with negative eigenvalue. This state also has the lowest energy; in other words, we have proved the existence of a ground state. Our ladder operators $\hat{a}, \hat{a}^\dagger$, now called the

annihilation and creation operators respectively, are interpreted as subtracting and adding quanta of energy to the ground state. By repeatedly applying $\hat{a}^\dagger$ to the ground state, we can produce any excited eigenstate; the number operator $\hat{N}$ counts the quanta of energy contained in the oscillator. However, there is apparently an additional $\hbar\omega/2$ energy in the oscillator; since this energy is also contained in the ground state, it is not accessible. Still, this term has important consequences later.

Finally, to complete our analysis, we must solve for the wavefunction of the ground state, by using the position-basis form of $\hat{a}$ in $\hat{a}|0\rangle = 0$. We can then derive the excited state wavefunctions by repeatedly applying the explicit form of $\hat{a}^\dagger$ to $|0\rangle$. It can be shown that all possible states of the quantum harmonic oscillator can be formed by linear combination of these eigenstates; we have thus fully described all possible wavefunctions of the quantum harmonic oscillator. We are done.

In order to derive quantum field theory, we use something similar to quantize the wave equation of a field. This time, let us start with the classical massless Klein-Gordon equation, which in natural units is:

$$-\partial_t^2\phi + \nabla^2\phi = 0. \tag{2.9}$$

Instead of quantizing the position of a particle, we would like to quantize the value of the field at every point instead. So, $\hat{\phi}(\mathbf{x}, t)$ plays the role of $\hat{x}$ in the previous analysis. Then, by using the classical Lagrangian density,

$$\mathcal{L}[\phi, \partial_\mu\phi] = -\frac{1}{2}\partial^\mu\partial_\mu\phi, \tag{2.10}$$

we can find the conjugate momentum to be $\pi = \frac{\partial\mathcal{L}}{\partial(\partial_0)\phi} = \partial_0\phi$. This conjugate pair $\hat{\phi}, \hat{\pi}$ is the analogue of $\hat{x}, \hat{p}$ in the previous quantization procedure. In these terms, the quantum Hamiltonian density is

$$\hat{H} = \frac{1}{2}\hat{\pi}^2 + \frac{1}{2}(\nabla_\mu\hat{\phi}^2). \tag{2.11}$$

The canonical equal-time commutation relations are then (leaving in $\hbar$ for emphasis)

$$[\hat{\phi}(\mathbf{x}, t), \hat{\phi}(\mathbf{x}', t)] = 0 \tag{2.12}$$

$$[\hat{\pi}(\mathbf{x}, t), \hat{\pi}(\mathbf{x}', t)] = 0 \tag{2.13}$$

$$[\hat{\phi}(\mathbf{x}, t), \hat{\pi}(\mathbf{x}', t)] = \mathrm{i}\hbar\delta(x - x'). \tag{2.14}$$

In principle, we would then use the canonical equal-time commutation relation and the equation of motion to derive the evolution of $\hat{\phi}(\mathbf{x}, t)$ in time. In spacetimes that are not

static, this is often the only way to proceed. However, in the spacetimes we will consider, it is far simpler to instead express $\hat{\phi}(\mathbf{x}, t)$ in the particle basis. That is, we write:

$$\hat{\phi}(\mathbf{x}, t) = \int \frac{d^3\mathbf{k}}{(2\pi)^3} \left(\hat{a}_{\mathbf{k}} f_{\mathbf{k}}(\mathbf{x}, t) + \hat{a}^\dagger_{\mathbf{k}} f^*_{\mathbf{k}}(\mathbf{x}, t) \right) \tag{2.15}$$

where $\omega_{\mathbf{k}} = |\mathbf{k}|$ is the energy of the mode with momentum $\mathbf{k}$, and

$$f_{\mathbf{k}}(\mathbf{x}, t) = \frac{1}{\sqrt{2\omega_{\mathbf{k}}}} e^{\mathrm{i}(\mathbf{k}\cdot\mathbf{x} - \omega_{\mathbf{k}} t)} \tag{2.16}$$

is the mode itself, a positive-energy solution of the wave equation with momentum $\mathbf{k}$. As before, we can demonstrate that the Hamiltonian can be expressed with respect to these creation and annihilation operators, that all states can be built from a ground state (i.e. the vacuum state) using these operators, and so on. Of course, we are using the Heisenberg picture here, since our operators depend on time; this will facilitate the interaction picture we introduce later.

Of course, there is a small complication here. Our expression for the Hamiltonian now translates as (with time dependence suppressed)

$$\begin{aligned} \hat{H} =& \frac{1}{2} \int \frac{d^3\mathbf{k}}{(2\pi)^3} \omega_{\mathbf{k}} (\hat{a}_{\mathbf{k}} \hat{a}^\dagger_{\mathbf{k}} + \hat{a}^\dagger_{\mathbf{k}} \hat{a}_{\mathbf{k}}) \\ =& \int \frac{d^3\mathbf{k}}{(2\pi)^3} \omega_{\mathbf{k}} (\hat{a}^\dagger_{\mathbf{k}} \hat{a}_{\mathbf{k}} + \frac{1}{2} (2\pi)^3 \delta^3(0)) \end{aligned} \tag{2.17}$$

Clearly we have a problem here: there is a constant, infinite term in our Hamiltonian. It is similar to the $\hbar\omega/2$ found in the quantum harmonic oscillator Hamiltonian, repeated for every 'oscillator' in our system, and is sometimes referred to as the 'vacuum energy', as even the vacuum state posesses this infinite 'energy'. As it is constant, however, it is not accessible; we will simply remove it, without changing the dynamics of the system. Thus,

$$\hat{H} = \int \frac{d^3\mathbf{k}}{(2\pi)^3} \omega_{\mathbf{k}} \hat{a}^\dagger_{\mathbf{k}} \hat{a}_{\mathbf{k}}. \tag{2.18}$$

Notably, the translation of these concepts to curved space is quite straightforward. Substituting covariant derivatives for ordinary derivatives, we can simply write the classical Klein-Gordon equation of (2.9) as

$$0 = (-g^{\mu\nu} \nabla_\mu \nabla_\nu + \zeta R)\phi, \tag{2.19}$$

where ζ describes the field's coupling to the Ricci scalar R. In fact, this equation is often written even more briefly via the d'Alembertian, $\Box = -g^{\mu\nu}\nabla_\mu\nabla_\nu$. In (3+1)-dimensions, the choice of $\zeta = 1/6$ defines the conformally coupled scalar field; of the spacetimes we will study, this becomes relevant in the Anti-de Sitter and Schwarzschild-Anti-de Sitter spacetimes.

The modification in the Klein-Gordon equation leads to a change in the mode solutions (2.16), but (2.15) may still be used to express the field in terms of the particle basis. However, there is a particular problem with our approach: in non-static spacetimes, it is difficult to define a vacuum state [3]. For instance, in a spacetime which undergoes a temporary period of expansion, a state which has no particles before expansion will contain particles afterwards. We are left with the task of *choosing* which state to build upon, with the interpretational headaches that follow. However, in all of the cases we will consider, canonical choices of vacuum exist. We thus defer the discussion of which vacuum to pick to later chapters.

2.2 The Unruh-DeWitt detector

With the field theory out of the way, we can now discuss the matter of the observer and the measurement. The Unruh-DeWitt detector [38, 5] is perhaps the simplest possible model of a local detector, a two-level pointlike system of gap Ω coupled to a scalar field. Its interaction Hamiltonian is described by

$$\hat{H}_I(t) = \lambda \frac{d\tau}{dt} \chi(\tau(t)) \hat{\phi}(x(t)) \hat{\mu}(\tau(t)), \tag{2.20}$$

where $x(t)$ is the position of the detector at time t, λ is the (perturbatively small) coupling to the scalar field, $\chi(\tau(t))$ is a switching function, characterizing the time-dependence of the interaction, and

$$\hat{\mu}(\tau(t)) = e^{\mathrm{i}\Omega\tau}\sigma^+ + e^{-\mathrm{i}\Omega\tau}\sigma^- \tag{2.21}$$

is the monopole operator; more precisely,

$$\sigma^+ = |\Omega\rangle\langle 0|, \tag{2.22}$$
$$\sigma^- = |0\rangle\langle\Omega|. \tag{2.23}$$

While this is a fairly simplified model, it captures the essential features of the light-matter interaction when angular momentum is not involved [32, 21].

The measurement protocol is simple: we first initialize the detector in the state $|0\rangle$. In the cases where Ω is positive, this is the ground state. We then switch on the interaction for some time, before switching it off: $\chi(\tau)$ begins at zero, then takes nonzero value for some time, and then vanishes afterwards. Finally, the state of the detector is measured. In other words, the only projective measurement occurs after interaction has been completed. Mathematically, it is often convenient to use Gaussian switching functions, or other functions of non-compact support; in those cases, the measurement is only properly conducted 'at infinite time', where the switching function approaches zero.

Our analysis will not be solely restricted to $\Omega > 0$. For $\Omega < 0$, the setting corresponds to a detector initialized in an excited state; the transition probability is then the probability it is measured in its ground state after interaction. We will also consider $\Omega = 0$, where the detector is initialized in one of two degenerate states, and then calculate the probability it is found in the other state. For instance, one might initialize an atom in one of two spin states, then determine whether its spin flips after interaction.

Since we are working in curved space, we need to be clear about which quantities are in which frame. Our convention will be to take the switching function $\chi(\tau)$ and the gap Ω in the frame of the detector, which has proper time $\tau(t)$. On the other hand, the field operator evolves according to the coordinate time t, as do the mode functions of the field. Thus, the interaction Hamiltonian includes both time coordinates, as well as a redshift factor $d\tau/dt$.

For small λ, we may use perturbation theory to estimate the transition probability of a detector switched according to ϕ. To leading order [3]:

$$P = \lambda^2 |\langle \Omega | \mu(0) | 0 \rangle|^2 \mathcal{F}(\Omega) \tag{2.24}$$

where the 'transition function' $\mathcal{F}(\Omega)$ is independent of the properties of the detector, and may be expressed as

$$\mathcal{F}(\Omega) = \int_{-\infty}^{\infty} \mathrm{d}t \int_{-\infty}^{\infty} \mathrm{d}t' \chi(t)\chi(t') e^{\mathrm{i}\Omega(\tau(t)-\tau(t'))} W(t,t') \tag{2.25}$$

where

$$W(t,t') = W(\mathbf{x}(t), \mathbf{x}(t')) = \langle \Psi | \hat{\phi}(\mathbf{x}(t)) \hat{\phi}(\mathbf{x}(t')) | \Psi \rangle \tag{2.26}$$

is the pullback of the Wightman function, the two-point correlator of the field state $|\Psi\rangle$, to the worldline of the detector. Notably, since the transition function is related to the transition probability by a constant, some authors use the term interchangeably. Note that the dimensionality of the transition probability will be $[\lambda]^{-2}$; while this implies that

$\mathcal{F}(\Omega)$ is dimensionless for (3+1)-D space, it becomes dimensionful for other numbers of dimensions. In particular, since we only calculate the leading order terms, it is not *a priori* clear what coupling constant λ will be sufficiently small that the next perturbative order does not apply; a value of $\mathcal{F}(\Omega) = 1$ should therefore *not* be understood as reflecting a certainty of transition.

The probability of transition will serve as our main probe of spacetime for the next two chapters. It is therefore prudent to explain how one might experimentally measure a 'probability'. Instead of a single detector, one would have to implement an array of multiple detectors, then determine the proportion of detectors that underwent transitions; this proportion, then, is the measured result. Depending on the sensitivity required to distinguish between spacetimes, such an array could number in the thousands or more. In general, the faster the (array of) detector(s) is switched, the more the signal is dominated by switching noise, unrelated to the broader structure of spacetime. However, it is unclear whether the required sensitivity poses any *theoretical* bound on the time required to distinguish spacetimes.

2.3 Describing the vacuum

In order to complete our calculation, we need to determine the form of the Wightman function of the quantum state of the field. In this thesis, we will deal primarily with vacuum states of various kinds, which contain no particles. More precisely, $0 = \langle\Psi|\hat{a}^\dagger_{\mathbf{k}}\hat{a}_{\mathbf{k}}|\Psi\rangle$ for all possible modes. Using this fact, together with (2.15) and the commutation relations of $\hat{a}, \hat{a}^\dagger$ we immediately discover that

$$\begin{aligned} W(\mathbf{x}, t; \mathbf{x}', t') =& \langle\Psi|\hat{\phi}(\mathbf{x}, t)\hat{\phi}(\mathbf{x}'; t')|\Psi\rangle \\ =& \int \frac{\mathrm{d}^3\mathbf{k}}{(2\pi)^3} f_{\mathbf{k}}(\mathbf{x}, t) f^*_{\mathbf{k}}(\mathbf{x}', t'). \end{aligned} \tag{2.27}$$

Thus, describing the correlations of the vacuum state is mainly a matter of calculating the mode functions.

We note here that in other spacetimes, the nature of the mode indices varies; for instance, in Anti-de Sitter space, there are only a countable infinity of modes. This implies that the integral $\int \frac{\mathrm{d}^3\mathbf{k}}{(2\pi)^3}$ may be replaced by a sum, or some combination of sum and integral. However, the larger structure of the Wightman function of the vacuum state remains the same.

In principle, we now have a procedure for calculating the transition function: find the mode solutions, use them to find the Wightman function, then integrate over the worldline of the detector, in order to find the transition probability as a function of the gap. However, this is easier said than done: because (2.25) contains two time integrals and one sum over modes, it is important to either calculate the modes efficiently, or find some way to simplify the expression. Finding ways to reduce the computational complexity of the problem presented the main challenge in this research, and perhaps the main scientific merit as well.

Chapter 3

The massive transparent shell

The detector model we described in the previous chapter has an interesting history. When Unruh [38] originally proposed the idea of a local detector, he applied it to a simple question: what does Hawking radiation look like to an observer near a black hole? His answer was that it depends on the detector's state of motion: an accelerated detector observes a thermal bath of particles, even in flat space. A detector held fixed over a black hole feels an acceleration; the corresponding temperature matches the temperature of the radiation predicted by Hawking. He then suggested that a detector falling into a black hole should see nothing near the horizon, since it is not accelerated.

This description of effects so far matches what one would expect from applying the Equivalence Principle: a detector experiences thermal radiation whether its acceleration is due to motion in flat space, or gravity above a black hole. It was therefore something of a surprise to us when Hodgkinson [10] and we [24] found an apparent violation: the same is *not* true for a detector in circular geodesic motion around a black hole. Even though the detector is not accelerated, in the general relativistic sense, it still detects particles, even if the black hole is not emitting radiation. Further, as was shown by [10], the particles detector do not correspond to any thermal state. Therefore, in some sense, not only can this freefalling detector determine that it is not stationary in flat space, but it can even determine that it is not being accelerated in flat space either.

Now, as mentioned previously, this is not a violation of the equivalence principle *per se*. The equivalence principle does not apply when one can couple to a non-gravitational external field. It does, however, argue against naïve application of the principle. Once a detector is allowed to couple to an external field, we cannot assume its proper acceleration characterizes its response. Additionally, it also suggests the potential for further investiga-

tion. What features of spacetime can a detector detect by coupling to the field? This next example may be one of the simplest possible 'features': a change in the local gravitational potential, effected by a massive transparent shell around the detector.

More concretely, suppose we have a static detector located at the center of a massive transparent shell of matter. The gravitational field inside the shell is zero: no acceleration is felt by the detector. The detector is initialized in a reference state $|0\rangle$, its interaction is switched on and off, and then it is measured. Experimentally, if one prepared an ensemble of detectors, allowed them to interact, then measured them, one could make a precise measurement of the transition probability; therefore, we wish to show that the transition probability differs significantly from that of a detector in flat space. In fact, we will demonstrate that the interaction with the field may be done faster than one may naïvely believe possible.

3.1 The metric and the detector

Intuitively, our spacetime is fairly simple: it must be Minkowski inside the shell, and Schwarzschild outside. Suppose the shell's radius is R, and its ADM mass (that is, the mass characterizing the gravitational field at infinity) is M. The metric of such a shell is

$$\mathrm{d}s^2 = \begin{cases} -f(r)\mathrm{d}t^2 + \frac{1}{f(r)}\mathrm{d}r^2 + r^2\mathrm{d}\Omega^2, & r > R \\ -f(R)\mathrm{d}t^2 + \mathrm{d}r^2 + r^2\mathrm{d}\Omega^2, & r < R, \end{cases} \tag{3.1}$$

where $f(r) = 1 - 2M/r$.

There are a few things to note about this solution. First, strictly speaking, the metric is *not* Minkowski inside the shell, though it is flat. The change in gravitational potential causes the time component of the metric to change: the induced metric on the shell must be continuous, so g_{tt} is the same inside as outside. Of course, if we were to change coordinates, switching to the proper frame of a static detector inside the shell, we would produce the Minkowski metric again. However, the g_{rr} component is no longer continuous; it experiences a jump discontinuity, which we will have to handle carefully later.

Now, what does it mean to distinguish the shell from flat space? Suppose we switched the detector located at the centre according to some switching function

$$\chi(\tau) = e^{-\tau^2/2\sigma^2}. \tag{3.2}$$

Notably, we must define this switching with respect to the detector local time: the coordinate time t is merely a coordinate-dependent concept. We then wish to determine whether

the detector transition probability under this switching differs significantly between the two cases, and if so, how quickly it can be determined. 'Classically'—that is, without access to the quantum field—this is not possible if $\sigma \ll 2r^*(R)$, since the latter describes the time it would take for light to leave the detector, hit the shell (if any), and return. It would therefore be of interest to determine whether access to the quantum state of the field allows distinguishing the spacetimes much faster than that. (Strictly speaking, if we use a Gaussian switching function, the interaction does not vanish. However, we have found that the use of switching functions of compact support does not significantly affect results.)

3.2 The modes

Recall that the d'Alembertian, $\Box$, may be rewritten as

$$\Box\Psi = \frac{1}{\sqrt{-g}}\partial_\mu(\sqrt{-g}g^{\mu\nu}\partial_\nu\Psi), \tag{3.3}$$

where g is the determinant of the metric. Since our metric is spherically symmetric, it is simplest to express the modes in terms of angular and radial functions. In fact, it is fairly easy to see that since the angular part of the metric is precisely as in Minkowski space, the angular part of our modes will be precisely the spherical harmonics.

Let us then write the mode solutions as

$$\Psi_{\omega lm} = \frac{1}{\sqrt{4\pi\omega}}e^{-i\omega t}\psi_{\omega l}(r)Y_{lm}(\theta,\phi). \tag{3.4}$$

The radial modes now behave according to

$$0 = \omega^2\psi_{\omega l} + \frac{\alpha}{ar^2}\partial_r\left(\frac{\alpha}{a}r^2\partial_r\psi_{\omega l}\right) - \alpha^2\frac{l(l+1)}{r^2}\psi_{\omega l} \tag{3.5}$$

where

$$\alpha^2 \equiv -g_{tt} \tag{3.6}$$

$$a^2 \equiv g_{rr}. \tag{3.7}$$

We can rewrite this equation in a more familiar form. Let us define a tortoise coordinate, r^*, such that $\partial_{r^*} = \frac{\alpha}{a}\partial_r$, and define

$$\rho_{\omega l} \equiv r\psi_{\omega l}. \tag{3.8}$$

We then find

$$0 = \partial_{r^*}^2 \rho_{\omega l} + (\omega^2 - V_l(r))\rho_{\omega l} \tag{3.9}$$

where

$$V_l(r) = \alpha^2 \frac{l(l+1)}{r^2} + \frac{1}{r}\frac{\alpha}{a}\partial_r \frac{\alpha}{a}. \tag{3.10}$$

We emphasize that the effective potential is written here in terms of r, not r^*; in order to integrate this differential equation, we will need a way to transform between r and r^*.

3.3 Putting it together

First, evaluating (3.6) and (3.7) in terms of the metric defined in (3.1), and substituting the result into the expression for the effective potential (3.10), we find

$$V_l(r) = \begin{cases} f(r)\left(\frac{l(l+1)}{r^2} + \frac{2M}{r^3}\right), & r > R \\ f(R)\left(\frac{l(l+1)}{r^2}\right), & r < R. \end{cases} \tag{3.11}$$

This puts us in familiar territory: the outer potential is that of the Schwarzschild exterior solution, while the inner potential is a rescaling of the Minkowski spacetime's effective potential.

While what is left is mostly a matter of integration, we need to deal with the discontinuity at the shell. As a is discontinuous on the shell, the effective potential (3.10) is infinite there, so we instead look for a weak solution of (3.5), i.e. one that satisfies (3.5) in a distributional sense. More precisely, using the common notation

$$[X] = \lim_{r \to R^+} X - \lim_{r \to R^-} X; \tag{3.12}$$

we quickly find $0 = [r^2 \partial_{r^*}(\psi)]$, or more succinctly,

$$0 = [\partial_{r^*}\psi]\,. \tag{3.13}$$

In other words, in tortoise coordinates, a weak solution ψ to (3.5) must have a smooth derivative across the shell. It immediately follows that $\rho = r\psi$ does *not* have a smooth derivative with respect to r^*, so caution is required.

Since the tortoise coordinate is only defined up to a constant, we will set $r^*(r = 0) = 0$ at the centre. Note that this implies that our tortoise coordinate will not precisely match

the usual tortoise coordinate of the Schwarzschild exterior solution. Therefore, inside the shell, $r = \sqrt{f(R)}r^*$, and we can simplify (3.5) to find

$$0 = \tilde{r}^2\psi + 2\tilde{r}\partial_{\tilde{r}}\psi + \tilde{r}^2\partial_{\tilde{r}}^2\psi - l(l+1)\psi. \tag{3.14}$$

With $\tilde{r} = \omega r^*$, this is the Bessel equation, so the inner mode solutions are (up to normalization) $\psi \sim j_l(\omega r^*) = j_l(\tilde{\omega} r)$ where

$$\tilde{\omega} \equiv \omega/\sqrt{f(R)}\,. \tag{3.15}$$

While this appears to fully define the outer modes, there is a subtlety here: we need to normalize these modes in order to correctly define the Wightman function. Thus, we need to use (3.13) to connect these solutions to the outside of the shell, integrate to infinity, and then normalize according to the asymptotic coefficients.

$$\int_0^\infty dr^* \rho_{\omega_1 l}(r)\rho_{\omega_2 l}(r) = 2\pi\delta(\omega_1 - \omega_2). \tag{3.16}$$

Since $r^* \to r + r_S$ for some 'shift' r_S as $r \to \infty$, the modes must approach $\rho_{\omega l}(r) \to 2\sin(\omega r + \theta)$ as $r \to \infty$ for some phase θ. Thus, by affecting how the inner and outer solutions connect, the properties of the shell affect the amplitude of the modes. In contrast, in flat space, $j_l(\omega r) \to \sin(\omega r + \theta)/(\omega r)$ as $r \to \infty$, so the spherical Bessel function is multiplied by 2ω; thus $\psi = 2\omega j_l(\tilde{\omega} r)$ under this normalization scheme. (The detector 'sees' $\tilde{\omega}$ as the local energy, but in that case $\tilde{\omega} = \omega$.)

3.4 A Fourier transform

Our particular choice of detector configuration allows for some further simplification. Since our detector is static at the centre, we only need consider the $l = 0$ mode for each value of ω in the mode sum. Then, since $j_l(0) = 1$, and the time dependence of our modes is simple, we find

$$\mathcal{F}(\Omega) = \int_{\tau_i}^{\tau_f} d\tau_1 \int_{\tau_i}^{\tau_f} d\tau_2\, e^{-i\Omega(\tau_2-\tau_1)}\chi(\tau_1)\chi(\tau_2) \int_0^\infty d\omega\, e^{-i\omega(t_2-t_1)} \left|\frac{\psi_{\omega 0}(0)}{\sqrt{16\pi^2\omega}}\right|^2 \tag{3.17}$$

Next, using (3.6),

$$\mathcal{F}(\Omega) = \int_{\tau_i}^{\tau_f} d\tau_1 \int_{\tau_i}^{\tau_f} d\tau_2\, e^{-i\Omega(\tau_2-\tau_1)}\chi(\tau_1)\chi(\tau_2) \int_0^\infty d\omega\, e^{-i\tilde{\omega}(\tau_2-\tau_1)} \left|\frac{\psi_{\omega 0}(0)}{\sqrt{16\pi^2\omega}}\right|^2 . \tag{3.18}$$

Finally, since our switching function is smooth, we can swap the integrals, leaving us with

$$\mathcal{F}(\Omega) = \sum_l \int_0^\infty d\omega \int_{\tau_i}^{\tau_f} d\tau_1 \int_{\tau_i}^{\tau_f} d\tau_2 \, e^{-i(\Omega+\tilde{\omega})(\tau_2-\tau_1)} \chi(\tau_1)\chi(\tau_2) \frac{|\psi_{\omega 0}(0)|^2}{16\pi^2 \omega r^2} \,. \tag{3.19}$$

Since ω only appears via $d\omega/\omega$, we will rewrite the integrals with respect to the local energy $\tilde{\omega}$ instead.

Now, this integral is in quite a familiar form. Since the switching functions vanish outside of $[\tau_i, \tau_f]$, we can extend the integrals to infinity, leaving us with a Fourier-like integral. This leaves us with

$$\mathcal{F}(\Omega) = \int_0^\infty \frac{d\tilde{\omega}}{8\pi\tilde{\omega}} |\hat{\chi}(\Omega+\tilde{\omega})|^2 \, |\psi_{\omega 0}(0)|^2 \,, \tag{3.20}$$

where

$$\hat{\chi}(\tilde{\omega}) = \frac{1}{\sqrt{2\pi}} \int_{-\infty}^{\infty} e^{-i\tilde{\omega}\tau} \chi(\tau) \tag{3.21}$$

is the Fourier transform of the switching function. Equation (3.20) represents this chapter's main result. It implies that given the right switching function, *any* difference in the behaviour of the $l = 0$ modes at $r = 0$ can be detected.

In some sense, this expression also implies that distinguishing two spacetimes in this way is comparable to analyzing its spectrum. One could compare it to the familiar undergraduate task of determining the length of a tube by measuring its resonances. It is, nonetheless, quite interesting that this works even without a discrete spectrum. It may be interesting to try to characterize how this spectrum is related to the structure of the shell: that is, whether one could have a finite thickness shell of varying density, and determine the exact mass distribution thereof.

Still, even in this simple case, there are limits: if we wish to have a small characteristic switching time σ, the result is a broad distribution of $\hat{\chi}(k)$ in energy; a quick switching smears over modes of similar energies, so the finer details of the spectrum are lost. For instance, using the Fourier transform of the Gaussian,

$$\mathcal{F}(\Omega) = \int_0^\infty \frac{d\tilde{\omega}}{8\pi\tilde{\omega}} \sigma^2 e^{-\sigma^2(\Omega+\tilde{\omega})^2} \, |\psi_{\omega 0}(0)|^2 \,, \tag{3.22}$$

any feature much finer than $1/\sigma$ in energy cannot be seen. We will need to numerically determine precisely what σ suffices.

3.5 Results

For purposes of demonstration, we will work with distance units in terms of the Schwarzschild radius of the shell, so that $R = 1$ corresponds to the Schwarzschild radius. Of course, since we do not want the shell to be a black hole, we must set $R > 1$. On the other hand, since we want our switching time σ to be much smaller than $2R/c$, the light-crossing time of the shell, we pick $\sigma = 1/2$. We then use the methods previously described to solve for the modes, and calculate the transition function, for the shell and flat cases. Under our unit conventions, this implies that the energy scale is $k_B T_{Hloc} = 1/8\pi M\sqrt{f(R)}$: the Hawking temperature of a black hole of mass M, as measured by a static observer at distance R from the center. Of course, we are not considering a state with particles in it, so there is no 'temperature' to speak of, but as we will see, this is still a useful energy scale.

First, we pick $R = 3$, and plot the transition probabilities with and without the shell. The results are shown in Fig. 3.1. While the differences between the two are essentially invisible, note that at large negative Ω (i.e. when the detector is initialized in an excited state), the transition probability is almost linear, as is characteristic of (3+1)-dimensional space. On the other hand, at very small Ω, our finite switching time causes some excitation to be detected; we would expect this excitation to vanish as $\sigma \to \infty$.

Since the difference is smaller than can easily be seen, the absolute difference in responses $\mathcal{F}_{shell}(\Omega) - \mathcal{F}_{flat}(\Omega)$ is then plotted in Fig. 3.2. Remarkably, this difference is almost *symmetric* in Ω; it is of equal magnitude whether the detectors start in an excited or ground state.

From an experimental perspective, the relative difference $(\mathcal{F}_{shell}(\Omega) - \mathcal{F}_{flat}(\Omega))/\mathcal{F}_{flat}(\Omega)$ is also important: it reflects the sensitivity of the detector array required to distinguish the two cases, or rather the number of detector elements required. Therefore, we plot it in Fig. 3.3. Since the absolute difference was almost symmetric, we find that the relative difference is significantly larger for positive gaps than negative gaps. We also find that the maximum relative difference is approximately 2%, at a gap approximately 90 times the local Hawking temperature; much larger than the energy scale of black hole radiation, but much smaller than its mass-energy.

We also plot the detector response function for $\Omega = 0, \sigma = 0.2$ for varying radii of shell, in Fig. 3.4, against the flat space value. As one would expect, the observable difference is largest when the shell is most compact, and decays rapidly as the shell increases in size. Evidently, this effect is only noticeable when the shell itself is almost a black hole.

As one might have anticipated, although we have provided strong evidence that this effect exists, it is quite unlikely to be experimentally observable. The miniscule energy scales

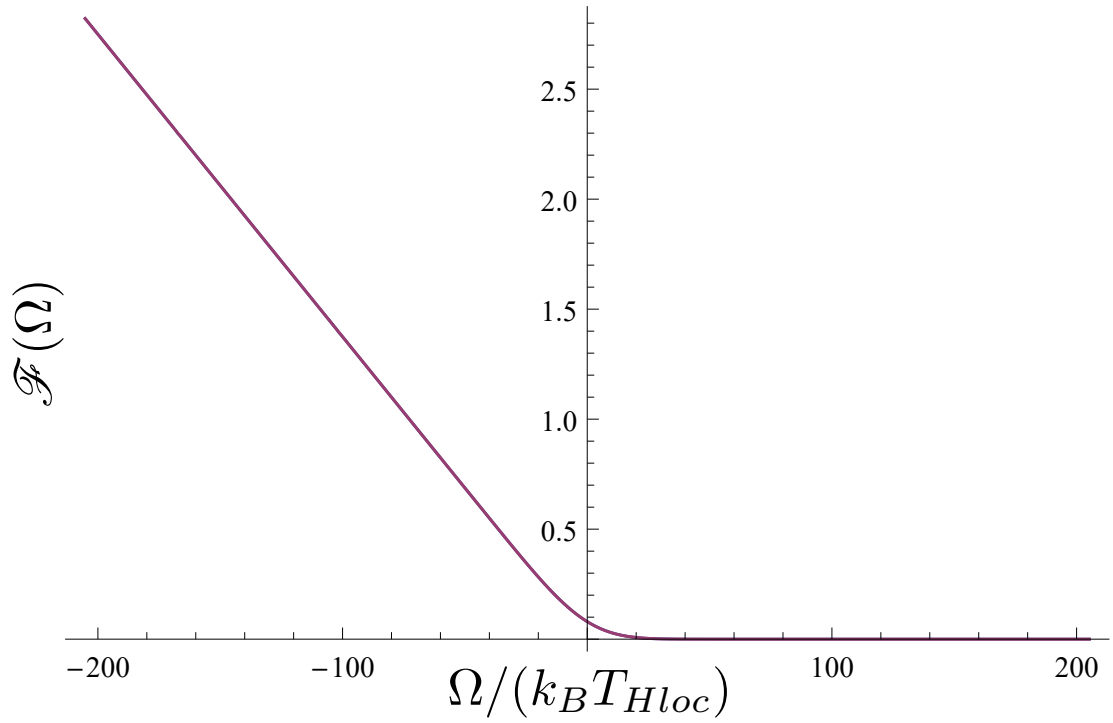

Figure 3.1: Response function for a detector with (blue) vs. without (red) the shell, for varying detector gaps

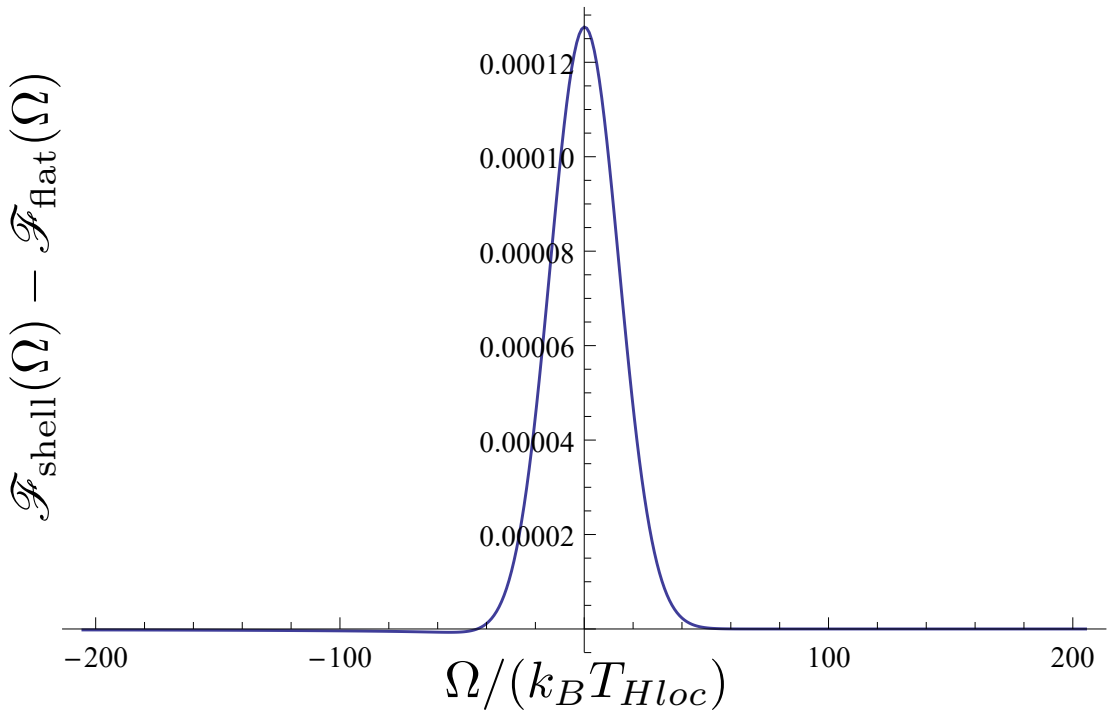

Figure 3.2: Absolute difference in response function between a detector in a shell vs. in flat space, for varying detector gaps.

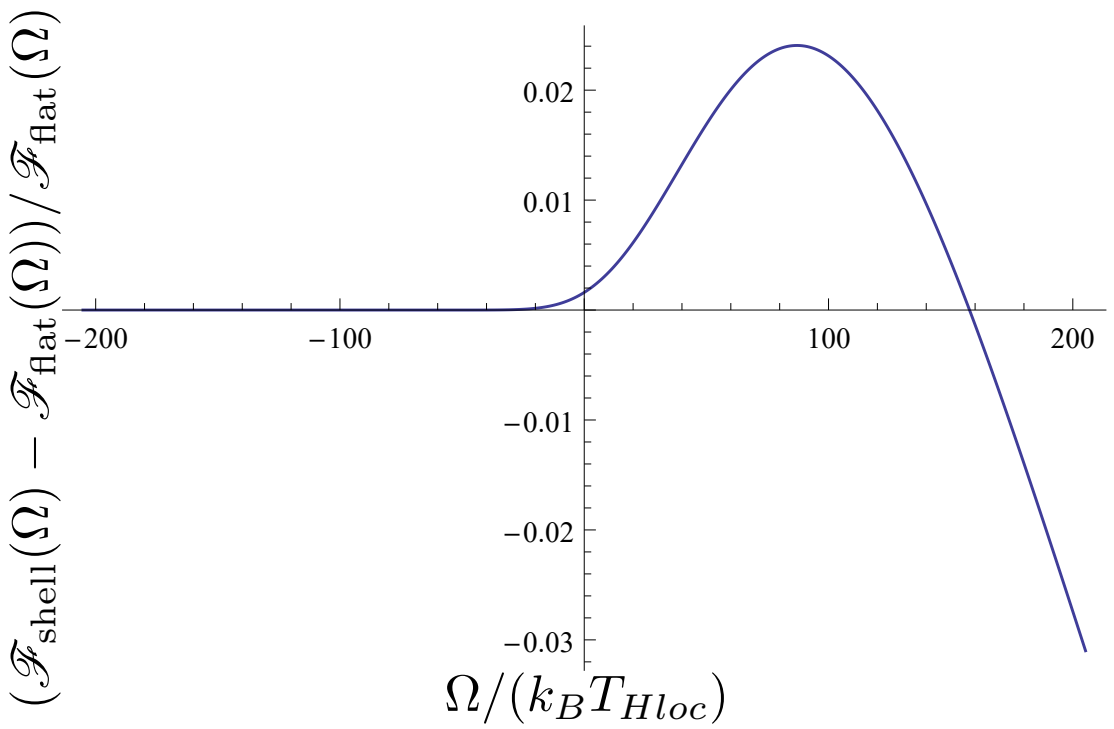

Figure 3.3: Relative difference in response function between a detector in a shell vs. in flat space, for varying detector gaps.

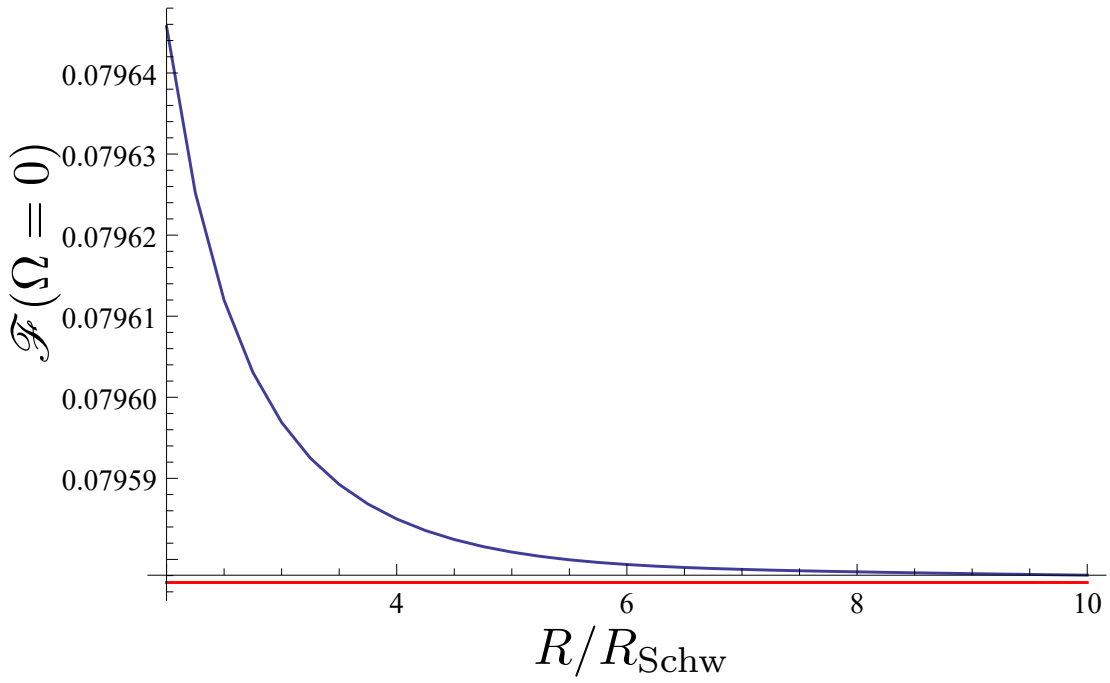

Figure 3.4: Response function vs. shell radius. Value for flat case in red.

involved, and the compactness of shell required, imply that any attempt to measure this effect would be subject to many of the same problems facing direct detection of Hawking temperature: the low energy scales required will cause issues with background radiation, cosmic microwave and otherwise, and require an extraordinarily sensitive detector array. It is, however, of some interest that this task is possible at all: we have provided evidence that the vacuum state contains information about the presence or absence of a shell.

Chapter 4

Looking inside a black hole

While the event horizon of a black hole marks the point of no return for information, many physicists believe that that information may escape in some form, carried away by correlations in the Hawking radiation. It has therefore been a matter of scientific interest to calculate how a detector responds to the Hawking radiation, to determine whether a local observer might be able to reconstruct that information. Indeed, determining the response of a detector near the event horizon was the first application of the Unruh-DeWitt detector concept [38]. More recently, the response of a UDW detector to a radiating black hole was calculated for a broader variety of trajectories and configurations, both in asymptotically flat [10] and Anti-de Sitter [24] spacetimes.

Therefore, we next choose to study how the Hawking radiation of a black hole is determined by its internal structure. More precisely, we work with the maximal analytic extension of the Schwarzschild black hole: it is possible to define a second spacetime, $\mathbb{RP}^3$, by topologically identifying the interior of the black hole. This 'geon' structure is isometric to the Schwarzschild spacetime everywhere outside the black hole. However, this difference in internal structure affects the Hawking radiation emitted in a subtle way, and we now demonstrate that this difference can allow an external observer to distinguish an ordinary (3+1)-dimensional black hole from a geon, and compare our results with those of [35] for the (2+1)-dimensional BTZ black hole.

4.1 Identifying a black hole

The metric of Schwarzschild spacetime one most usually uses is as follows:

$$\mathrm{d}s^2 = -f(r)\mathrm{d}t^2 + \frac{1}{f(r)}\mathrm{d}r^2 + r^2\mathrm{d}\Omega^2, \tag{4.1}$$

where $f(r) = 1 - 2M/r$. Immediately, one problem becomes clear: the metric is singular at both $r = 0$ and $r = 2M$. However, this is not a problem with the spacetime itself, but with the metric, or rather the choice of coordinates. This *coordinate* singularity may be removed by picking a different set of coordinates, allowing us to speak about the interior of the event horizon. For further discussion, see e.g. [23].

Let us use the Kruskal-Szekeres coordinates [23]. Outside the event horizon, i.e. for $r > 2M$, we have

$$T = \left(\sqrt{1 - \frac{2M}{r}}\right) e^{r/4M} \sinh\left(\frac{t}{4M}\right) \tag{4.2}$$

$$X = \left(\sqrt{1 - \frac{2M}{r}}\right) e^{r/4M} \cosh\left(\frac{t}{4M}\right) \tag{4.3}$$

while for $r < 2M$, inside the event horizon,

$$T = \left(\sqrt{\frac{2M}{r} - 1}\right) e^{r/4M} \cosh\left(\frac{t}{4M}\right) \tag{4.4}$$

$$X = \left(\sqrt{\frac{2M}{r} - 1}\right) e^{r/4M} \sinh\left(\frac{t}{4M}\right), \tag{4.5}$$

where T is always timelike and X is always spacelike. While these coordinates do *not* yield a manifestly static spacetime, they do cover the interior of the black hole. In particular, they also have a particular useful property: the speed of light in these coordinates, dX/dT, is always unity. This makes the Kruskal-Szekeres coordinates ideal for understanding the causal structure of this spacetime, the extended Schwarzschild solution.

A conformal transformation of a metric retains the same casual and geometric structure: events that are lightlike connected remain so, and the same applies to timelike separated events and to spacelike separated events. Therefore, in order to visualize the causal structure of the extended Schwarzschild solution, one often uses Penrose diagrams. In Fig. 4.1,

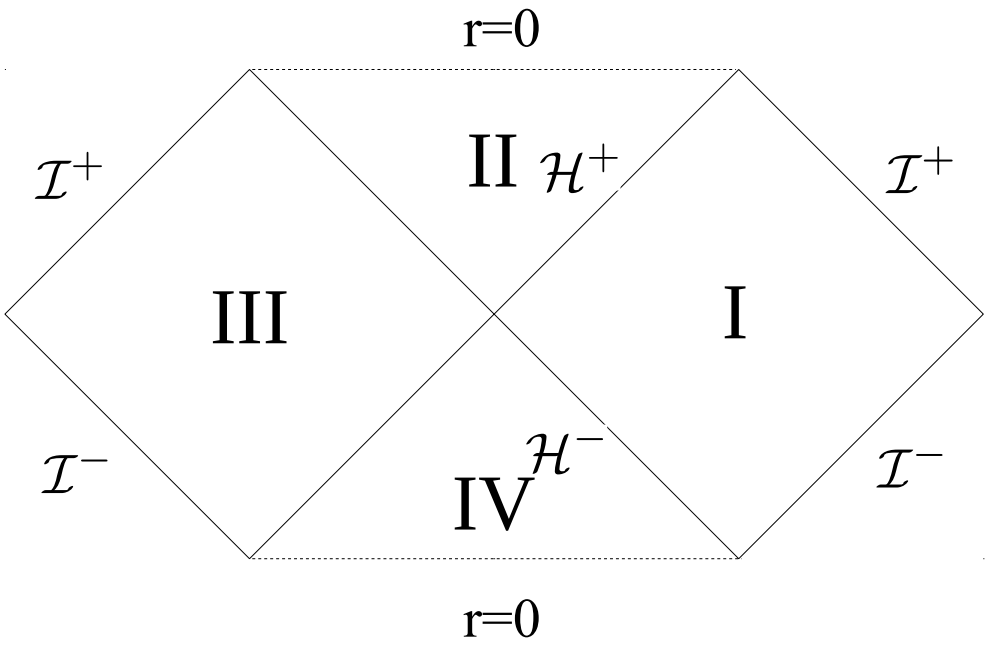

Figure 4.1: Penrose diagram of extended Schwarzschild solution

any two points connected by a 45 degree line are lightlike connected, while the flow of time is upwards. In particular, one can clearly see how objects entering the event horizon $\mathcal{H}^+$ from region I are doomed to hit the singularity $r = 0$ inside the black hole.

However, the Penrose diagram reveals other, more unusual features. It describes a spacetime with *two* singularities: one in the future, the usual black hole singularity, in region II; and one in the past, a *white hole* singularity, in region IV. Additionally, there are now two asymptotically flat regions, rather than one. Region I is the exterior of the black hole, and is bounded by the black hole horizon $\mathcal{H}^+$, the white hole horizon $\mathcal{H}^-$, the future lightlike infinity $\mathcal{I}^+$, and the past lightlike infinity $\mathcal{I}^-$. However, one other asymptotically flat region, region III, appears to be behind the horizon, and is only reachable by travelling faster than light.

In order to demonstrate how one topologically identifies the interior of a black hole, it is perhaps most expedient to use the corresponding Kruskal diagrams. While there is some mathematical nuance, a geon intuitively is a black hole 'with only one exterior'; that is, as shown in Fig. 4.2, while the extended Schwarzschild spacetime has an inaccessible 'parallel exterior', region III in Fig. 4.1, the geon does not. Instead, it is as though a mirror has been placed 'inside' it.

More formally, in order to define the topological identification, we define an involution, which in Kruskal coordinates is

$$J(T, X, \theta, \phi) = (T, -X, \pi - \theta, \phi + \pi). \tag{4.6}$$

That is, while the angular part of a point in space is mapped to the antipode, the other part is 'reflected' across the middle of the Kruskal diagram. This identification maps the usual exterior to the 'parallel exterior' of the extended Schwarzschild spacetime; if we allow ourselves to use (t, r, θ, ϕ) to refer to both exterior regions,

$$J(t, r, \theta, \phi) = (-t, r, \pi - \theta, \phi + \pi). \tag{4.7}$$

As should be apparent, this involution is *not* time-invariant, at least with respect to t. This might not seem to be an issue at first, since the exterior of the Schwarzschild black hole is never identified with a causally connected point. However, because the Hartle-Hawking state of the black hole is defined globally, this identification introduces a time-dependence in the quantum state of the field.

More concretely, it is fairly simple to use the method of images to determine the Wightman function of the $\mathbb{RP}^3$ geon, in terms of the Wightman function of the black hole. We find

$$W_{geon}(\mathbf{x}, \mathbf{x}') = W_{BH}(\mathbf{x}, \mathbf{x}') + W_{BH}(\mathbf{x}, J(\mathbf{x}')). \tag{4.8}$$

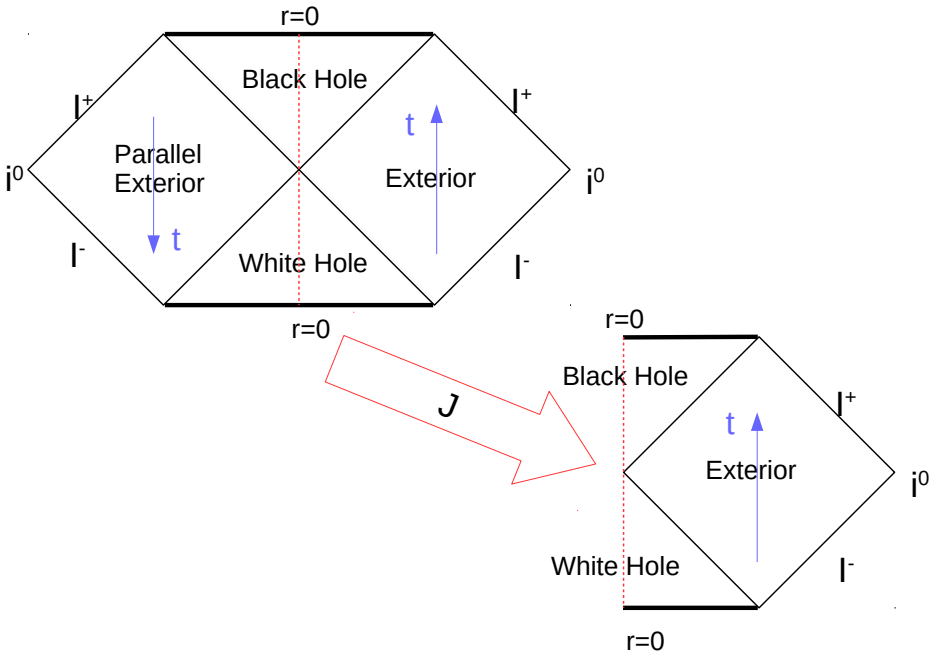

Figure 4.2: The $\mathbb{RP}^3$ geon from the extended Schwarzschild solution.

Therefore, in order to quantify the difference in the quantum state of the field on these two spacetimes, we need to determine the difference in Wightman functions, which is simply $W_J(\mathbf{x}, \mathbf{x}') \equiv W_{BH}(\mathbf{x}, J(\mathbf{x}'))$. However, we are now faced with a unique problem: namely, determining the correlation between points on either side of the black hole. We will deal with this in the next section.

We note here that a second approach to constructing the Hartle-Hawking state of a geon exists. In principle, we could instead start with mode functions that respect the topological identification, then analytically continue them across the horizon, much as is done in Schwarzschild. Indeed, this approach is suggested in [17]. However, for the purposes of distinguishing the geon from the normal black hole, the method of images will prove beneficial. Indeed, since the transition probability of a detector is linear with respect to the Wightman, the difference in transition probabilities between the two spacetimes is *literally* determined by the difference in Wightman functions.

4.2 The mode solutions of the black hole

Let us begin by describing the mode solutions of the Schwarzschild black hole. We will need these to calculate the Wightman function of the black hole, and therefore of the geon. We use a refinement of the methods found in [10, 24, 9]. Let us begin with a familiar ansatz:

$$F^{\text{up,in}}_{\omega lm}(t, r, \theta, \phi) = \frac{1}{\sqrt{4\pi\omega}} e^{-i\omega t} R^{\text{up,in}}_{\omega l}(r) Y_{lm}(\theta, \phi). \tag{4.9}$$

These modes represent the positive frequency solutions, with respect to t, the Schwarzschild coordinate time. That is, they describe particles as observed by a stationary observer. We also include a label, either 'up', or 'in', to represent our choice of particle basis: one set of particles traveling 'up' towards infinity, and another falling 'in' towards the horizon. More precisely, we choose to define the notion of 'particle' relative to two sets of observers in this spacetime: the 'up' particles are defined as purely outgoing particles at infinity, while the 'in' particles are purely ingoing near the event horizon. (While 'down' and 'out' modes can also be defined in the respective asymptotic regions, we will not deal with them.)

Next, let $\tilde{R}_{\omega l} = r R_{\omega l}$, similar to what we did in the shell case. The differential equation then becomes

$$\left(\frac{d^2}{dr^{*2}} + \omega^2 - \left(1 - \frac{2M}{r}\right) \left(\frac{l(l+1)}{r^2} + \frac{2M}{r^3} \right) \right) \tilde{R}_{\omega l} = 0. \tag{4.10}$$

Then, the asymptotic conditions on the 'up' and 'in' modes are:

$$\tilde{R}^{in}_{\omega l} = \begin{cases} B^{in}_{\omega l} e^{-i\omega r^*}, & r \to 2M \\ e^{-\mathrm{i}\omega r^*} + A^{in}_{\omega l} e^{+\mathrm{i}\omega r^*}, & r \to \infty \end{cases} \tag{4.11}$$

$$\tilde{R}^{up}_{\omega l} = \begin{cases} e^{+\mathrm{i}\omega r^*} + A^{up}_{\omega l} e^{-\mathrm{i}\omega r^*}, & r \to 2M \\ B^{up}_{\omega l} e^{+i\omega r^*}, & r \to \infty \end{cases} \tag{4.12}$$

It is then a matter of integrating the modes from their asymptotic solutions to an intermediate region, and matching the two parts together.

While we could, in principle, use the asymptotic values of the modes directly, better approximate solutions exist, using the Jaffé and asymptotic Coulomb solutions found in [16]. Setting $2M = 1$ as he does, we find:

$$\tilde{R}^{in}_{\omega l} \propto e^{-i\omega r}(r-1)^{-\mathrm{i}\omega} \sum_{n=0}^{\infty} a_n \left(\frac{r-1}{r}\right)^n \tag{4.13}$$

$$\tilde{R}^{up}_{\omega l} \propto \sqrt{\frac{r}{r-1}}(r-1)^{+\mathrm{i}\omega} H^+_{\nu_a}(-\omega, \omega r) e^{-\mathrm{i}\theta_{\omega l}} \tag{4.14}$$

where $H^+_{\nu_a}(\eta, \omega r)$ is the Coulomb wavefunction of possibly complex order $\nu_a = (-1 + \sqrt{(2l+1)^2 - 12\omega^2})/2$, $\theta_{\omega l} = \omega \log(2\omega) - \pi\nu_a/2 - \mathrm{ph}\Gamma(\nu_a + 1 - \mathrm{i}\omega)$ is a phase shift (which Leaver omits) to match $e^{+\mathrm{i}\omega r^*}$, and the coefficients a_n are generated by a recurrence relation,

$$\begin{aligned} a_{-1} =& 0, \\ a_0 =& 1, \\ 0 =& (1+n)(1+n-2i\omega)a_{n+1} \\ &+ (-1 - l(l+1) - 2n(1+n))a_n + n^2 a_{n-1}. \end{aligned} \tag{4.15}$$

4.3 Through the black hole

In order to determine the value of W_J, we will next briefly review [38, 13] how the Hartle-Hawking state is derived, noting differences where they occur. As we will see, the resulting function is quite time dependent, and has a few other exceptional properties. Still, the result can be expressed with respect to the mode solutions of the black hole, and calculating W_J is in principle no harder than calculating W_{BH}.

Previously, we described the Boulware modes, positive frequency solutions to the Klein-Gordon equation with respect to coordinate time t. In principle, one could use these modes to construct a vacuum state on the exterior. However, this Boulware vacuum is ill-behaved: specifically, it has infinite energy density on the horizon. However, this is not the only possible choice of time, nor the only possible choice of vacuum. The Hartle-Hawking vacuum is a vacuum, relative to the Kruskal time T. It is smooth on the horizon (and everywhere else), but does contain (Boulware) particles. Still, it is possible to define modes with respect to which the Hartle-Hawking state is a vacuum, by picking mode functions with positive frequency with respect to the Kruskal time.

First, we note that in the extended Kruskal space, the parallel exterior can be given the same coordinates as the usual exterior, and the same metric. Therefore, the Boulware modes also solve the Klein-Gordon equation on the parallel exterior. Let us then define $F^+_{\omega lm}$ as the usual mode solution on the normal exterior, and $F^-_{\omega lm}$ its 'partner' on the parallel exterior. However, with respect to the global, Kruskal time T, the time coordinate t on the parallel exterior is reversed. Thus, $F^+_{\omega lm}$ is associated with a positive frequency particle, and therefore an annihilation operator $\hat{a}^+$; $F^-_{\omega lm}$ is associated with a negative frequency and therefore a creation operator $\hat{a}^{-\dagger}$. The field operator with respect to these extended Boulware modes is therefore

$$\Phi(x) = \sum_{lm} \int_0^\infty d\omega (a^+_{\omega lm} F^+_{\omega lm} + a^-_{\omega lm} F^{-*}_{\omega lm} + h.c.) \tag{4.16}$$

Of course, in normal circumstances the F^- terms vanish, since those functions are zero in the normal exterior. If we were using the Boulware vacuum, this expression could easily be used to calculate the Wightman function.

As noted previously, we can build modes that annihilate the Hartle-Hawking vacuum, using the Boulware modes. Using the conventions of [13],

$$H^+_{\omega lm} = \frac{1}{\sqrt{2\sinh(4\pi M\omega)}} \left(e^{2\pi M\omega} F^+_{\omega lm} + e^{-2\pi M\omega} F^-_{\omega lm}\right) \tag{4.17}$$

$$H^-_{\omega lm} = \frac{1}{\sqrt{2\sinh(4\pi M\omega)}} \left(e^{2\pi M\omega} F^-_{\omega lm} + e^{-2\pi M\omega} F^+_{\omega lm}\right), \tag{4.18}$$

and the positive frequency solutions ("particles") are H^+, H^{-*}. For large ω, the H^+ solutions are mostly in the normal exterior, while the H^{-*} solutions are mostly in the parallel exterior. Much as before, we associate annihilation operators b^+, b^- with H^+, H^{-*} respectively, and creation operators $b^{+\dagger}, b^{-\dagger}$ with H^{+*}, H^-. Using these modes, the field operator

is now

$$\hat{\Phi} = \sum_{lm} \int_0^\infty d\omega (b^+_{\omega lm} H^+_{\omega lm} + b^-_{\omega lm} H^{-*}_{\omega lm} + h.c.) \tag{4.19}$$

This time, both sets of modes are nonzero in the usual exterior. However, since the Hartle-Hawking vacuum $|0\rangle_{HH}$ is annihilated by $b^\pm$, we can express the Schwarzschild Wightman function as

$$\begin{aligned} W_{BH}(\mathbf{x}, \mathbf{x}') =& {}_{HH}\left\langle 0|\hat{\Phi}(\mathbf{x})\hat{\Phi}(\mathbf{x}')|0\right\rangle_{HH} \\ =& \sum_{lm} \int_0^\infty d\omega \, (H^+_{\omega lm}(x) H^{+*}_{\omega lm}(x') + H^{-*}_{\omega lm}(x) H^-_{\omega lm}(x')). \end{aligned} \tag{4.20}$$

Finally, we re-express this Wightman function with respect to the original Boulware modes, using (4.18). Suppose first that both $\mathbf{x}, \mathbf{x}'$ are in the normal exterior. For brevity, let $\theta = \theta' = \phi = \phi' = 0$. Then, we get the usual result:

$$\begin{aligned} W_{BH}(\mathbf{x}, \mathbf{x}') =& \sum_{lm} \int_0^\infty \frac{d\omega}{2\sinh(4\pi M\omega)} \left(e^{4\pi M\omega} F^+_{\omega lm}(\mathbf{x}) F^{+*}_{\omega lm}(\mathbf{x}') + e^{-4\pi M\omega} F^{+*}_{\omega lm}(\mathbf{x}) F^+_{\omega lm}(\mathbf{x}')\right) \\ =& \sum_{lm} \int_0^\infty \frac{d\omega}{8\pi\omega\sinh(4\pi M\omega)} \Big(e^{4\pi M\omega} e^{-\mathrm{i}\omega(t-t')} R_{\omega l}(r) R^*_{\omega l}(r') Y_{lm}(\theta,\phi) Y^*_{lm}(\theta',\phi') \\ & + e^{-4\pi M\omega} e^{+\mathrm{i}\omega(t-t')} R^*_{\omega l}(r) R_{\omega l}(r') Y^*_{lm}(\theta,\phi) Y_{lm}(\theta',\phi') \Big) \\ =& \sum_{lm} \int_0^\infty \frac{(2l+1)\delta_{m,0} d\omega}{32\pi^2\omega\sinh(4\pi M\omega)} \Big(e^{4\pi M\omega} e^{-\mathrm{i}\omega(t-t')} R_{\omega l}(r) R^*_{\omega l}(r') \\ & + e^{-4\pi M\omega} e^{+\mathrm{i}\omega(t-t')} R^*_{\omega l}(r) R_{\omega l}(r') \Big) \end{aligned} \tag{4.21}$$

Note that we include $\delta_{m,0}$ to indicate that only the $m = 0$ modes need to be evaluated.

On the other hand, once we apply J to $\mathbf{x}'$, we find:

$$\begin{aligned}
W_{BH}(\mathbf{x},J(\mathbf{x}')) &= \sum_{lm}\int_0^\infty \frac{d\omega}{2\sinh(4\pi M\omega)}\left(F^+_{\omega lm}(\mathbf{x})F^-_{\omega lm}(J(\mathbf{x}')) + F^{+*}_{\omega lm}(\mathbf{x})F^{-*}_{\omega lm}(J(\mathbf{x}'))\right)\\
&= \sum_{lm}\int_0^\infty \frac{d\omega}{8\pi\omega\sinh(4\pi M\omega)}\Big(e^{-\mathrm{i}\omega(t+t')}R_{\omega l}(r)R^*_{\omega l}(r')Y_{lm}(\theta,\phi)Y_{lm}(\pi-\theta',\phi'+\pi)\\
&\qquad + e^{+\mathrm{i}\omega(t+t')}R^*_{\omega l}(r)R_{\omega l}(r')Y^*_{lm}(\theta,\phi)Y^*_{lm}(\pi-\theta',\phi'+\pi)\Big)\\
&= \sum_{lm}\int_0^\infty \frac{(-1)^l(2l+1)\delta_{m,0}d\omega}{32\pi^2\omega\sinh(4\pi M\omega)}\left(e^{-\mathrm{i}\omega(t+t')}R_{\omega l}(r)R^*_{\omega l}(r') + e^{+\mathrm{i}\omega(t+t')}R^*_{\omega l}(r)R_{\omega l}(r')\right)
\end{aligned} \tag{4.22}$$

This new Wightman function has a few unusual properties. Most immediately apparent is the fact that the usual $e^{4\pi M\omega}$ term is completely absent. That is, for large ω, both terms are equally suppressed. Also evident is a violation of time translation symmetry, since the Wightman depends explicitly on $t+t'$, rather than $t-t'$. These two facts suggest that the strongest contributions are due to small ω. Also, the antipodal part of the map results in the $(-1)^l$ factor, which will also serve to suppress higher energy values.

For further simplicity, let us assume our detector remains static. Then, since $J(\mathbf{x})$ has the same r as $\mathbf{x}$, $r = r' = J(r')$. Therefore:

$$W_{BH}(\mathbf{x},\mathbf{x}') = \sum_{l=0}^\infty\int_0^\infty \frac{(2l+1)d\omega}{16\pi^2\omega\sinh(4\pi M\omega)}\cosh(4\pi M\omega - \mathrm{i}\omega(t-t'))|R_{\omega l}(r)|^2, \tag{4.23}$$

$$W_{BH}(\mathbf{x},J(\mathbf{x}')) = \sum_{l=0}^\infty\int_0^\infty \frac{(-1)^l(2l+1)d\omega}{16\pi^2\omega\sinh(4\pi M\omega)}\cos(\omega(t+t'))|R_{\omega l}(r)|^2. \tag{4.24}$$

At this point, it should be fairly clear that the geon contribution, W_J, is maximized when $t+t'=0$. In some sense this is not too surprising, since $t=0$ is the time when the two exterior regions are 'closest' on the Kruskal diagram. Still, the introduction of time dependence adds another parameter to explore.

For completeness, we also include the Unruh vacua. In this case, since the black hole does not receive radiation, there is no correlation in the 'in' modes between the two exterior

regions; the geon contribution is only in the 'up' modes.

$$W_{BH,U} = \sum_l \int_0^\infty \frac{(2l+1)d\omega}{16\pi^2\omega} \left(\frac{\cosh(4\pi M\omega - \mathrm{i}\omega(t-t'))}{\sinh(4\pi M\omega)} |R^{\mathrm{up}}_{\omega l}(r)|^2 \right.$$
$$\left. + e^{-\mathrm{i}\omega(t-t')} |R^{\mathrm{in}}_{\omega l}(r)|^2 \right) \tag{4.25}$$

$$W_{J,U} = \sum_l \int_0^\infty \frac{(-1)^l(2l+1)d\omega}{16\pi^2\omega} \frac{\cos(\omega(t+t'))}{\sinh(4\pi M\omega)} |R^{\mathrm{up}}_{\omega l}(r)|^2. \tag{4.26}$$

4.4 Switching the detector

Since the Hartle-Hawking vacuum of the $\mathbb{RP}^3$ geon is now time-dependent, it is of paramount importance how we switch the detector on and off. In the spirit of the previous section, we will seek to derive an expression for the transition function in terms of the Fourier transform of the switching function,

$$\hat{\chi}(\tilde{\omega}) = \frac{1}{\sqrt{2\pi}} \int_{-\infty}^{\infty} e^{\mathrm{i}\tilde{\omega}\tau} \chi(\tau). \tag{4.27}$$

While the presence of multiple bases and 'negative frequency' parts complicates matters, we may once again interpret the integrals with $e^{\mathrm{i}(\tilde{\omega}+\Omega)t}$ factors and similar as Fourier transforms, and find

$$F_{BH}(\Omega) = \sum_{l=0}^{\infty} \int_0^\infty \frac{(2l+1)d\tilde{\omega}}{16\pi\omega\sinh(2\pi\omega)} \left(|R^{\mathrm{in}}_{\omega l}|^2 + |R^{\mathrm{up}}_{\omega l}|^2 \right)$$
$$\times \left(e^{-2\pi\omega} |\hat{\chi}(\tilde{\omega}-\Omega)|^2 + e^{+2\pi\omega} |\hat{\chi}(\tilde{\omega}+\Omega)|^2 \right), \tag{4.28}$$

$$F_J(\Omega) = \sum_{l=0}^{\infty} \int_0^\infty \frac{(-1)^l(2l+1)d\tilde{\omega}}{16\pi\omega\sinh(2\pi\omega)} \left(|R^{\mathrm{in}}_{\omega l}|^2 + |R^{\mathrm{up}}_{\omega l}|^2 \right) 2\Re \left(\hat{\chi}(\tilde{\omega}-\Omega)\hat{\chi}(\tilde{\omega}+\Omega) \right), \tag{4.29}$$

Notably, while the geon contribution is time-dependent, its dependence is fairly simple to express. Let $\xi(\tau) = \chi(\tau - \tau_0)$. Then, since $\hat{\xi} = e^{-\mathrm{i}\tilde{\omega}\tau_0}\hat{\chi}(\tilde{\omega})$, the translated geonic transition function becomes

$$F_{J,\tau_0}(\Omega) = \sum_{l=0}^{\infty} \int_0^\infty \frac{(-1)^l(2l+1)d\tilde{\omega}}{16\pi\omega\sinh(2\pi\omega)} \left(|R^{\mathrm{in}}_{\omega l}|^2 + |R^{\mathrm{up}}_{\omega l}|^2 \right) 2\Re \left(e^{-2\mathrm{i}\tilde{\omega}\tau_0} \hat{\chi}(\tilde{\omega}-\Omega)\hat{\chi}(\tilde{\omega}+\Omega) \right) \tag{4.30}$$

demonstrating a 'dephasing' effect.

It is now a simple matter to substitute in a Gaussian switching function. Let $\chi(\tau) = e^{-\tau^2/2\sigma^2}$, where σ is the proper switching time. The Fourier transform is then $\hat{\chi}(\tilde{\omega}) = \sigma e^{-\sigma^2\tilde{\omega}^2/2}$, and so:

$$\begin{aligned}
F_{BH}(\Omega) =& \sum_{l=0}^{\infty} \int_0^{\infty} \frac{(2l+1)d\tilde{\omega}}{16\pi\omega\sinh(2\pi\omega)} \left(|R^{\text{in}}_{\omega l}|^2 + |R^{\text{up}}_{\omega l}|^2\right) \\
& \times \sigma \left(e^{-2\pi\omega - \sigma^2(\tilde{\omega}-\Omega)^2} + e^{+2\pi\omega - \sigma^2(\tilde{\omega}+\Omega)^2}\right) \\
=& \sum_{l=0}^{\infty} \int_0^{\infty} \frac{(2l+1)d\tilde{\omega}}{8\pi\omega\sinh(2\pi\omega)} \left(|R^{\text{in}}_{\omega l}|^2 + |R^{\text{up}}_{\omega l}|^2\right) \\
& \times \sigma e^{-\sigma^2(\tilde{\omega}^2+\Omega^2)} \cosh(2\pi\omega - 2\sigma^2\tilde{\omega}\Omega) \qquad (4.31) \\
F_J(\Omega) =& 2\sum_{l=0}^{\infty} \int_0^{\infty} \frac{(-1)^l(2l+1)d\tilde{\omega}}{16\pi\omega\sinh(2\pi\omega)} \left(|R^{\text{in}}_{\omega l}|^2 + |R^{\text{up}}_{\omega l}|^2\right) \sigma e^{-\frac{\sigma^2}{2}\left((\tilde{\omega}-\Omega)^2+(\tilde{\omega}+\Omega)^2\right)} \\
=& \sum_{l=0}^{\infty} \int_0^{\infty} \frac{(-1)^l(2l+1)d\tilde{\omega}}{8\pi\omega\sinh(2\pi\omega)} \left(|R^{\text{in}}_{\omega l}|^2 + |R^{\text{up}}_{\omega l}|^2\right) \sigma e^{-\sigma^2(\tilde{\omega}^2+\Omega^2)} \\
=& e^{-\sigma^2\Omega^2} F_J(0) \qquad (4.32) \\
F_{J,\tau_0}(\Omega) =& \sum_{l=0}^{\infty} \int_0^{\infty} \frac{(-1)^l(2l+1)d\tilde{\omega}}{16\pi\omega\sinh(2\pi\omega)} \left(|R^{\text{in}}_{\omega l}|^2 + |R^{\text{up}}_{\omega l}|^2\right) \\
& \times 2\sigma e^{-\sigma^2(\tilde{\omega}^2+\Omega^2)} \cos(2\tilde{\omega}\tau_0)\,. \qquad (4.33)
\end{aligned}$$

Strangely, it appears that the geonic response depends on the gap in a very simple way, at least if the switching is centred about $t = 0$. It is also fairly easy to see that for sufficiently large σ, the small ω modes dominate, as the $\cosh(2\pi\omega)$ factor from F_{BH} is absent in F_J. In that limit, we find that $F_J(0)/F_BH(0) \approx 1$. In other words, in the slow switching limit, the geonic part of the response is equal to the black hole part in magnitude, a 100% effect! This clearly shows that the geon and the black hole can, in principle, be distinguished.

Again, for completeness, we include the Unruh vacuum responses. For $F_{J,U}$, one simply

drops the 'in' modes, while for $F_{BH,U}$,

$$F_{BH,U} = \sum_{l=0}^{\infty} \int_0^{\infty} \frac{(2l+1)d\tilde{\omega}}{8\pi\omega} \sigma \left(e^{-\sigma^2(\tilde{\omega}-\Omega)^2} |R^{\text{in}}_{\omega l}|^2 + e^{-\sigma(\tilde{\omega}^2+\Omega^2)} \frac{\cosh(2\pi\omega - 2\sigma\tilde{\omega}\Omega)}{\sinh(2\pi\omega)} |R^{\text{up}}_{\omega l}|^2 \right) . \tag{4.34}$$

We do not expect a 100% effect in this case; the precise magnitude of the effect remains to be seen.

4.5 Transition rate

In order to compare our work with a previous paper [35] on a (2+1)-dimensional geon, we also calculate *instantaneous* transition rates. More precisely, instead of switching the detector on and off smoothly, we switch on the detector asymptotically far into the past, switch off the detector *suddenly*, and calculate the derivative of the transition function with respect to switchoff time. As one might expect, the transition probability of a suddenly switched detector is divergent; however, the divergence is independent of the state of the field [18]. In particular, it is possible to compare different trajectories, simply by subtracting their Wightman functions, much as we have done here; and as the vacuum of an ordinary black hole is time independent, the detector's absolute transition probability in that case can be found fairly easily, as a point of comparison. Of course, such a divergent switching cannot be experimentally implemented. Nonetheless, it is still possible to consider this as the field-dependent part of the transition rate in the appropriate limit.

We use the sudden switching function $\chi_{\tau_0}(\tau) = \Theta(\tau_0 - \tau)$, switching the detector on in the asymptotic past and off at τ_0. Its Fourier transform is then

$$\hat{\chi}_{\tau_0}(\tilde{\omega}) = \sqrt{\frac{\pi}{2}}\delta(\tilde{\omega}) - \frac{ie^{i\tau_0\tilde{\omega}}}{\sqrt{2\pi}\tilde{\omega}}$$

and so, the geonic time dependence becomes

$$\tilde{\chi}_{\tau_0}(\tilde{\omega}-\Omega)\tilde{\chi}_{\tau_0}(\tilde{\omega}+\Omega) = -\frac{e^{2i\tau_0\tilde{\omega}}}{2\pi(\tilde{\omega}^2-\Omega^2)} - \frac{ie^{i\tau_0(\tilde{\omega}-\Omega)}}{2(\tilde{\omega}-\Omega)}\delta(\tilde{\omega}+\Omega) - \frac{ie^{i\tau_0(\tilde{\omega}+\Omega)}}{2(\tilde{\omega}+\Omega)}\delta(\tilde{\omega}-\Omega)$$

for $\Omega \neq 0$. Since $\tilde{\omega} > 0$, and we only need the real part, we can simplify this to

$$\partial_{\tau_0} 2\Re\left(\tilde{\chi}_{\tau_0}(\tilde{\omega}-\Omega)\tilde{\chi}_{\tau_0}(\tilde{\omega}+\Omega)\right) = \cos(2\tau_0\Omega)\delta(\tilde{\omega}-|\Omega|) + \frac{2\tilde{\omega}\sin(2\tau_0\tilde{\omega})}{\pi(\tilde{\omega}^2-\Omega^2)}. \tag{4.35}$$

We then take the time derivative to find the transition rate. Note that this last term is a Cauchy principle value. As well, this expression does approach a well-defined value as $\Omega \to 0$.

As for the normal black hole, we need $|\tilde{\chi}(\tilde{\omega} - \Omega)|^2$

$$|\tilde{\chi}_{\tau_0}(\tilde{\omega} - \Omega)|^2 = \frac{\pi}{2}\delta(\tilde{\omega} - \Omega)^2 - \frac{ie^{i\tau_0(\tilde{\omega}-\Omega)}}{2(\tilde{\omega} - \Omega)}\delta(\tilde{\omega} - \Omega) + \frac{ie^{-i\tau_0(\tilde{\omega}-\Omega)}}{2(\tilde{\omega} - \Omega)}\delta(\tilde{\omega} - \Omega) + \frac{1}{2\pi\tilde{\omega}} \tag{4.36}$$

Taking the time derivative, we find

$$\partial_{\tau_0}|\tilde{\chi}_{\tau_0}(\tilde{\omega} - \Omega)|^2 = e^{i\tau_0(\tilde{\omega}-\Omega)}\delta(\tilde{\omega} - \Omega) = \delta(\tilde{\omega} - \Omega), \tag{4.37}$$

and similarly $\partial_{\tau_0}|\tilde{\chi}_{\tau_0}(\tilde{\omega} + \Omega)|^2 = \delta(\tilde{\omega} + \Omega)$. Therefore,

$$\partial_{\tau_0}\left(e^{-2\pi\omega}|\tilde{\chi}_{\tau_0}(\tilde{\omega} - \Omega)|^2 + e^{+2\pi\omega}|\tilde{\chi}_{\tau_0}(\tilde{\omega} + \Omega)|\right) = e^{-\Omega/2T_{loc}}\delta(\tilde{\omega} - |\Omega|) \tag{4.38}$$

where $T_{loc} = T_H/\sqrt{f(r)} = 1/(4\pi\sqrt{1 - 1/r})$.

Finally, using these expressions for the time-derivative of the Fourier-transformed switching functions, we get

$$\begin{aligned}
\dot{F}_{BH}(\Omega) &= \sum_{l=0}^{\infty} \frac{(2l+1)e^{-2\pi\tilde{\Omega}}}{16\pi\tilde{\Omega}\sinh(2\pi\tilde{\Omega})}(|R^{in}_{\tilde{\Omega}l}|^2 + |R^{up}_{\tilde{\Omega}l}|^2) \\
\dot{F}_{J}(\Omega) &= \sum_{l=0}^{\infty} \frac{(-1)^l(2l+1)\cos(2\tau_0\Omega)}{16\pi\tilde{\Omega}\sinh(2\pi\tilde{\Omega})}(|R^{in}_{\tilde{\Omega}l}|^2 + |R^{up}_{\tilde{\Omega}l}|^2) \\
&\quad + \sum_{l=0}^{\infty}\int_0^{\infty} \frac{(-1)^l(2l+1)d\tilde{\omega}}{16\pi\omega\sinh(2\pi\omega)}\left(|R^{\text{in}}_{\omega l}|^2 + |R^{\text{up}}_{\omega l}|^2\right)\frac{2\tilde{\omega}\sin(2\tau_0\tilde{\omega})}{\pi(\tilde{\omega}^2 - \Omega^2)}
\end{aligned} \tag{4.39}$$

where $\tilde{\Omega} = \Omega\sqrt{f(r)}$ is the detector gap with respect to t, rather than τ.

4.6 Results

There is a large potential parameter space to explore. As we have shown, the transition rate depends on the detector gap, the switching time, the time translation, the choice of the vacuum, and the position of the detector. We will explore how each of these affect the transition probability for the Gaussian switching, as well as the transition rate for sudden switching.

Since we have demonstrated that the low energy modes contribute the most to the geon contribution, and that the geon contribution is strongest at $t = 0$, we will set $\Omega = 0$, $r = 3r_S$, $\sigma = 100r_S/c$, $\tau_0 = 0$, unless otherwise specified. While such a long switching time is not numerically 'natural', it is not unreasonable; for a small black hole of 10 solar masses, it would be on the order of 10 milliseconds.

We first vary the gap of the detector. As noted earlier, under this manipulation the geon contribution varies as a Gaussian. Since the black hole contribution behaves thermally, for the Hartle-Hawking vacuum we get the transition functions shown in Fig. 4.3. As predicted, for small gap, the geonic contribution and the black hole contribution are equal. However, for larger gap, the geon contribution is quickly suppressed. Notably, the Unruh vacuum results are qualitatively similar.

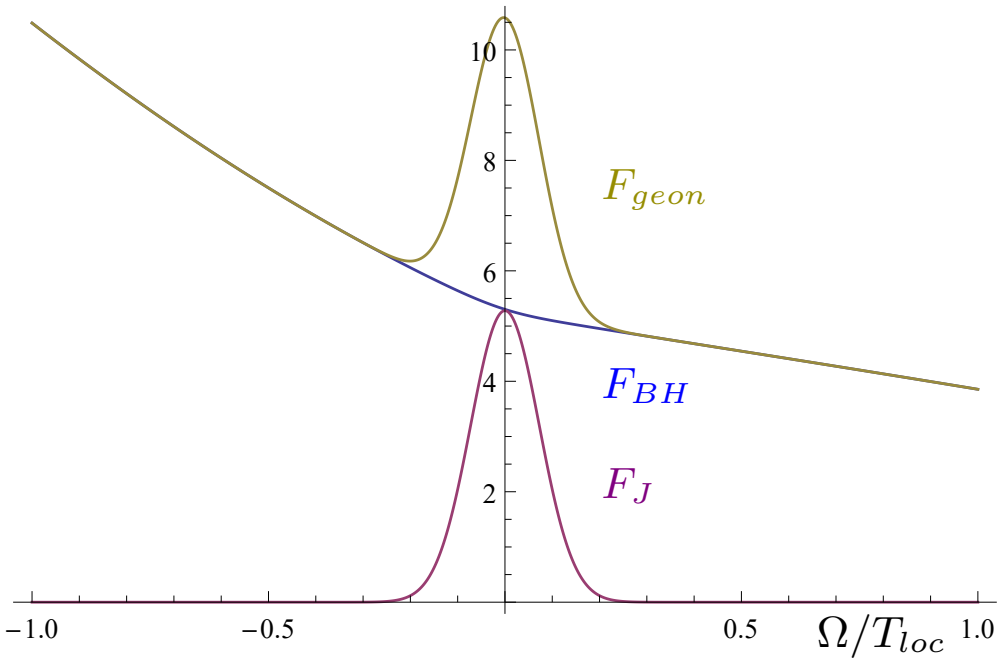

Figure 4.3: Response functions for black hole (blue), geon part (red), and geon total (green) versus Ω. $F_{geon} = F_{BH} + F_J$.

Next, we consider the effect of distance from the black hole. We plot the Hartle-Hawking response function in Fig. 4.4a, and the Unruh response in Fig. 4.4b Since the Unruh vacuum does not include infalling radiation, while the Hartle-Hawking vacuum does,

there is a much more noticeable difference in transition functions here. Namely, the Hartle-Hawking black hole response appears to level off as distance increases, even as the geon part decays.

As we noted earlier, the low energy modes contribute most to F_J. As can be seen in (4.28), (4.29), if the Fourier transform of the switching function is too broad, the higher energy modes will be weighted more strongly, suppressing the signal. In other words, if we switch too quickly, the geon part of the response will become much smaller than the black hole part. We demonstrate this dependence on σ by plotting the relative signal, F_J/F_{BH}, in Fig. 4.5. While the signal is fairly stable at large σ, as we might expect, it quickly decays if σ is too small.

Next, we consider the effects of time-translating the Gaussian switching function, as plotted in Fig. 4.6. As expected, the geon signal decays as τ_0 increases. This presents an interesting problem: were we to discover a geon 'in the wild', there would be no way to detect the topological identification, unless we were present during the critical moment $t = 0$. Otherwise, the 'dephasing' effect we noted earlier destroys the geon contribution.

As for the transition rate, we first tested our formalism by plotting ordinary black hole transition rates with varying Ω in Fig. 4.7. The three curves, representing the Hartle-Hawking, Unruh, and Boulware vacua, accurately replicate those found in [9]

Finally, we tested the dependence of the $\mathbb{RP}^3$ geon transition rate on the gap, for $\Omega/T_{\text{loc}} = -2, 0.01, 2$, and on the local time τ. The results, plotted in Fig. 4.8a, bear striking resemblance to the (2+1)-dimensional BTZ geon results from [35], seen in Fig. 4.8b. For $\tau < 0$, the geon transition rate is dominated by the black hole contribution; however, as the critical moment passes, the geonic contribution switches on, as can be seen by increasing time variance. However, the use of the switching function $\Theta(\tau_0 - \tau)$ suggests a switch-on in the distant past; experimentally, it may be better to consider a finite-time switching, even if the interpretation of the results is more complicated.

Our results demonstrate that the geon vacuum is time-dependent, and that it can be distinguished from the black hole vacuum, at least if the vacuum in question is not Boulware. We have also demonstrated how the geon contribution is largest at $t = 0$, with small gap, long switching, and near to the black hole, confirming the results found in [35] apply to (3+1)-dimensional geons. It seems that the Hawking radiation of a black hole does carry some information—namely, regarding the topology of its interior—and that this information can be retrieved by a single, pointlike observer on its exterior. Thus, the Unruh-DeWitt detector can, in a certain sense, see into the black hole, both in (2+1) and (3+1) dimensions.

(a) Hartle-Hawking vacuum

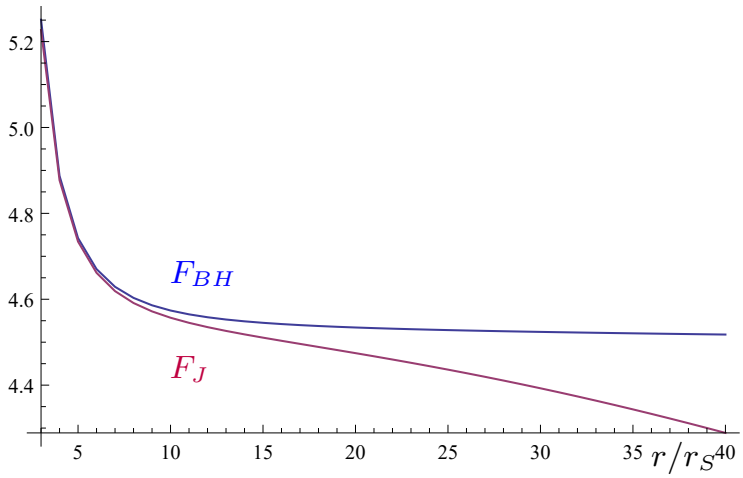

(b) Unruh vacuum

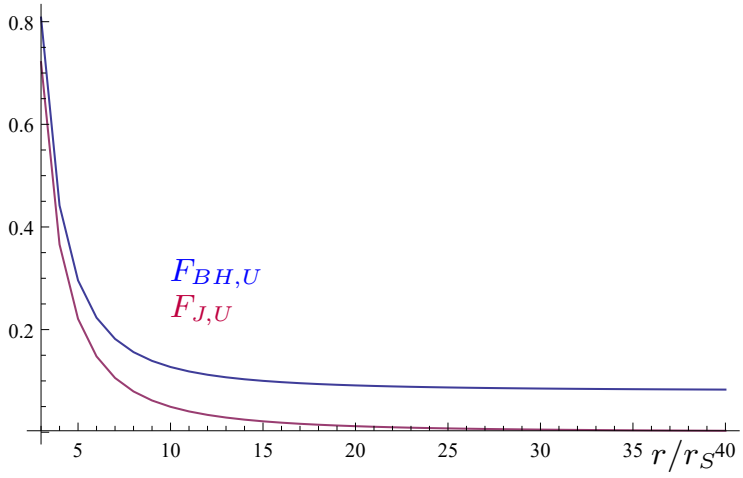

Figure 4.4: Response functions for varying detector radius, Hartle-Hawking and Unruh vacua.

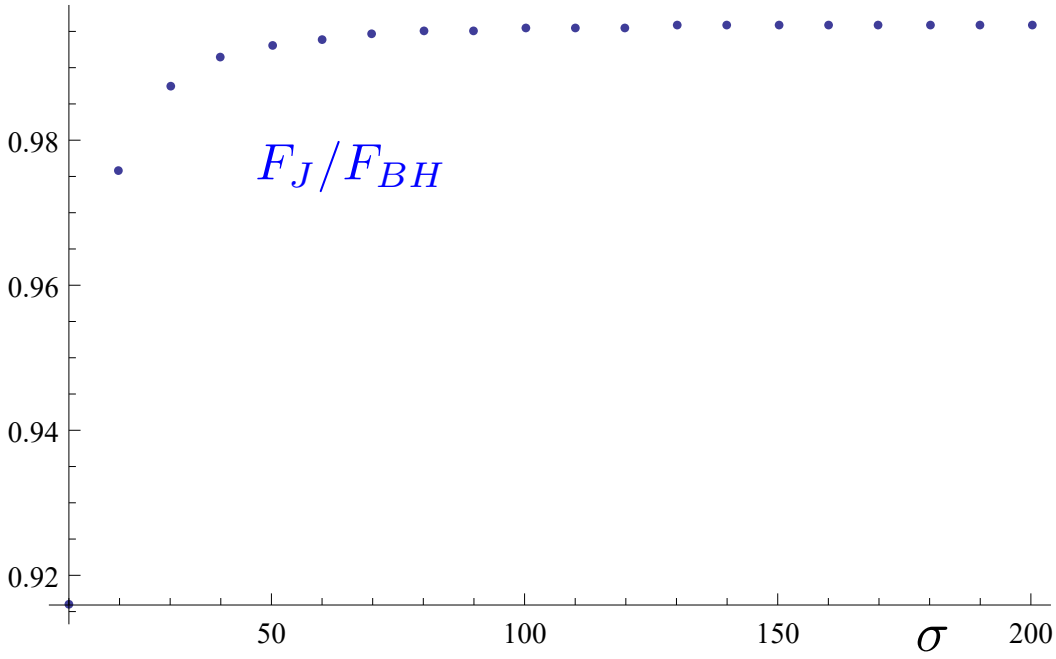

Figure 4.5: Geon relative signal for varying switching width σ.

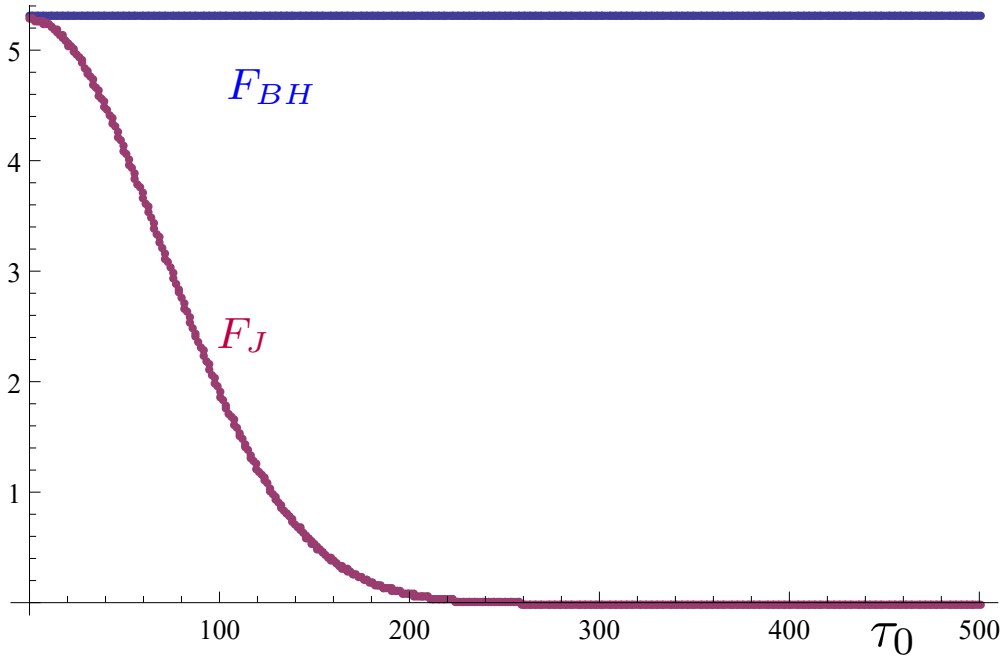

Figure 4.6: Response functions for black hole (blue) and geon part (red) versus time translation.

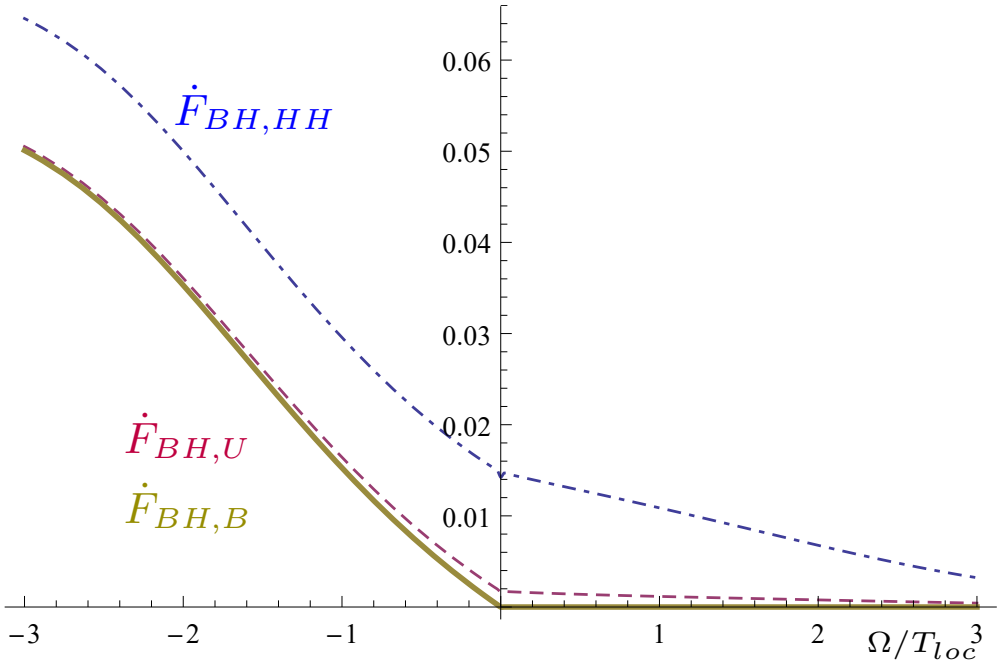

Figure 4.7: Transition rates for black hole versus gap, for the Hartle-Hawking (dot-dashed), Unruh (dashed), and Boulware (solid) vacuum states.

(a) (3+1)-dimensional $\mathbb{RP}^3$ geon

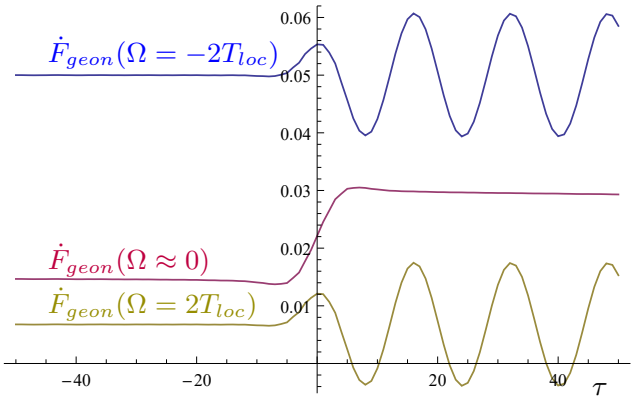

(b) (2+1)-dimensional BTZ geon

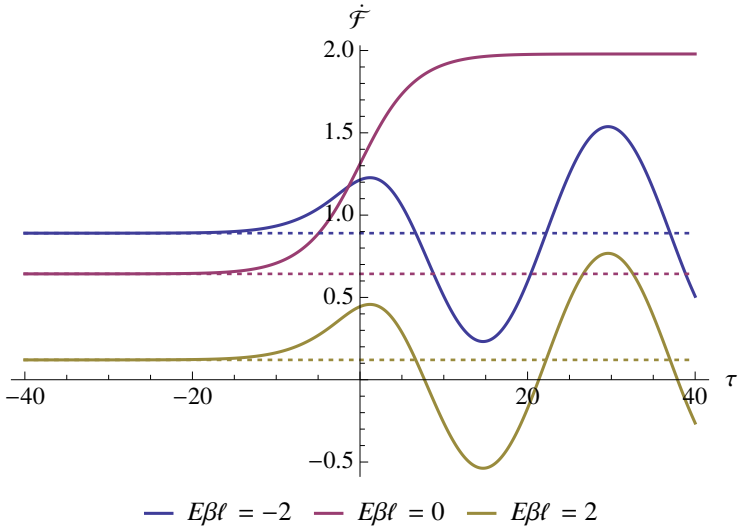

Figure 4.8: Transition rate for Ω/T_{loc} = -2 (top), 0 (middle), 2 (bottom), for $\mathbb{RP}^3$ and BTZ geons.

Chapter 5

Harvesting entanglement: a new approach

Having explored the potential of a single Unruh-DeWitt detector, we now move on to the observations of two. More specifically, we have previously considered how the excitations of a single detector coupled to a vacuum state can be used to distinguish different spacetimes. Now, suppose we were to couple a pair of detectors to the vacuum instead. As was shown by [39] (and revisited later by [33]), these detectors can become entangled, even if they are spacelike separated. This process is known as 'entanglement harvesting'. It has been shown that the quantity of entanglement harvested is also sensitive to the motion of the detector [34], and the structure of spacetime [36, 22]. Thus, calculating the entanglement harvested by two detectors in various spacetimes can tell us more about how much particle detectors can detect about spacetime.

However, calculating the entanglement harvested by two detectors is more difficult than calculating the transition probability of one detector. We will begin this chapter by summarizing the formalism used to calculate the entanglement harvested. As we will see, the form of the entangling terms in the density matrix pose challenges, frustrating many of the simplifications possible in the single detector case. However, this does not mean no simplification is possible. We will demonstrate that the entangling term may be expressed as a sum of two parts, both of which may be more easily calculated in any spacetime. In fact, if the two detectors are spacelike separated for the duration of their interaction with the field, we show that the entangling term simplifies drastically, aiding calculations in the situation which draws the most theoretical interest.

While this chapter is based on [28], here we will use the more general formalism found

in [27]. This is in anticipation of application of this chapter's results in curved spacetimes.

5.1 The perturbative density matrix

As before, let us define the interaction Hamiltonian of our system. Summing over both detectors, we have

$$\begin{aligned}\hat{H}_I(t) = &\sum_{I=A,B} \lambda_I \chi_I(\tau_I(t)) \hat{\mu}_I(t) \\ &\times F_I(\tau_I, \xi_I) \hat{\Phi}(t, x),\end{aligned} \tag{5.1}$$

where the monopole operator of detector I is

$$\hat{\mu}_I(t) = e^{\mathrm{i}\Omega_I \tau_I(t)} \hat{\sigma}_I^+ + e^{-\mathrm{i}\Omega_I \tau_I(t)} \hat{\sigma}_I^- \tag{5.2}$$

and where $F_I(\tau_I, \xi_I)$ is the smearing function of detector I, describing its spatial extent.

In this chapter, we will use the pointlike smearing function

$$F_I(\tau_I, \xi_I) = \delta(\xi_I) = \delta(\mathbf{x_I})/\sqrt{-h_I(t, \mathbf{x}_I)}$$

where $h_I(t, \mathbf{x})$ is the determinant of the spatial three-metric *of the detector's proper frame*. For stationary spacetime trajectories, $\frac{\mathrm{d}\tau}{\mathrm{d}t} = \sqrt{g(t, \mathbf{x})/h(t, \mathbf{x})}$, where $g(t, \mathbf{x})$ is the determinant of the ambient metric of our spacetime. However, this is not the only possibility: we could, for instance, use a Gaussian smearing function. However, interpretation of detector smearing becomes troublesome in curved spacetimes; the pointlike smearing is simplest. Spatially extended detectors can also cause problems with causality: see e.g. [20] for more information.

As before, we initialize both detectors in a reference state $|0\rangle$. The initial joint density matrix of the detectors and field is then $\hat{\rho}(t_0) = |0_A 0_B\rangle|\Psi\rangle\langle\Psi|\langle 0_A 0_B|$. Our task is to now calculate the reduced state of the detectors as a function of t: that is, the time-evolved state after tracing out the field. If we had direct access to the unitary evolution operator $\hat{U}(t, t_0)$, we could simply calculate

$$\hat{\rho}_{\mathrm{AB}}(t) = \mathrm{Tr}_\phi[\hat{U}(t, t_0)\hat{\rho}(t_0)\hat{U}^\dagger(t, t_0)] \tag{5.3}$$

directly.

In practice, we do not have access to the unitary evolution operator. Instead, we can use the Dyson expansion to approximate it via the interaction Hamiltonian. With respect to the coupling constant λ, this expansion is:

$$\hat{U}(t,t_0) = \sum_{n=0}^{\infty} \hat{U}_n(t,t_0), \tag{5.4}$$

$$\hat{U}_n(t,t_0) = \frac{(-i)^n}{n!} \int_{t_0}^{t} \mathrm{d}t_1 \int_{t_0}^{t} \mathrm{d}t_2 \cdots \int_{t_0}^{t} \mathrm{d}t_n \mathcal{T}\left(\hat{H}_I(t_1)\hat{H}_I(t_2)\cdots\hat{H}_I(t_n)\right). \tag{5.5}$$

Note that in the interaction picture, $\hat{U}_0 = \mathrm{Id}$, the identity operator. In order to express the final density matrix of the detectors we then sum up:

$$\hat{\rho}_{\mathrm{AB}}(t) = \mathrm{Tr}_{\phi}\left[\sum_{n,m=0}^{n+m\leq N} \hat{U}_n(t,t_0)\hat{\rho}(t_0)\hat{U}_m^{\dagger}(t,t_0)\right] + \cdots \tag{5.6}$$

where N is the highest order of perturbation. Note that since the order of λ in each term is given by $n+m$, we need to consider both terms like $\hat{U}_2\hat{\rho}$ and $\hat{U}_1\hat{\rho}\hat{U}_1^{\dagger}$, in order to capture all possible terms. If we include all such terms, then the unit trace of the density matrix is maintained to all orders, even though we have truncated the sum at finite order.

Now, for any quantum state where the one-point function, $\langle\Phi(\mathbf{x})\rangle$, vanishes everywhere, it is easy to show that the density matrix is unchanged to first order. Such states include vacuum field states, Fock states, and free thermal states more generally. In those cases, the leading order contribution to the density matrix is at second order.

Let us define the following basis for the density matrix:

$$\begin{array}{ll} |0_{\mathrm{A}}0_{\mathrm{B}}\rangle = (1,0,0,0)^{\dagger} & |\Omega_{\mathrm{A}}0_{\mathrm{B}}\rangle = (0,1,0,0)^{\dagger} \\ |0_{\mathrm{A}}\Omega_{\mathrm{B}}\rangle = (0,0,1,0)^{\dagger} & |\Omega_{\mathrm{A}}\Omega_{\mathrm{B}}\rangle = (0,0,0,1)^{\dagger}. \end{array} \tag{5.7}$$

Then, we find [31]

$$\hat{\rho}_{\mathrm{AB}} = \begin{bmatrix} 1-\mathcal{L}_{\mathrm{AA}}-\mathcal{L}_{\mathrm{BB}} & 0 & 0 & \mathcal{M}^* \\ 0 & \mathcal{L}_{\mathrm{AA}} & \mathcal{L}_{\mathrm{AB}} & 0 \\ 0 & \mathcal{L}_{\mathrm{BA}} & \mathcal{L}_{\mathrm{BB}} & 0 \\ \mathcal{M} & 0 & 0 & 0 \end{bmatrix} + O(\lambda_I^4), \tag{5.8}$$

where

$$\mathcal{M} = -\lambda_{\mathrm{A}}\lambda_{\mathrm{B}} \int_{-\infty}^{\infty} \mathrm{d}t \int_{-\infty}^{t} \mathrm{d}t' \int \mathrm{d}^n\mathbf{x} \int \mathrm{d}^n\mathbf{x}' \sqrt{g(t,\mathbf{x})g(t',\mathbf{x}')}\mathcal{M}(t,\mathbf{x},t',\mathbf{x}')W(t,\mathbf{x},t',\mathbf{x}') \tag{5.9}$$

$$\mathcal{L}_{IJ} = \lambda_I\lambda_J \int_{-\infty}^{\infty} \mathrm{d}t \int_{-\infty}^{\infty} \mathrm{d}t' \int \mathrm{d}^n\mathbf{x} \int \mathrm{d}^n\mathbf{x}' \sqrt{g(t,\mathbf{x})g(t',\mathbf{x}')}\mathcal{L}_I(t,\mathbf{x})\mathcal{L}_J^*(t',\mathbf{x}')W(t,\mathbf{x},t',\mathbf{x}') \tag{5.10}$$

and

$$\mathcal{L}_I(t,\mathbf{x}) = \chi_I(\tau_I(t,\mathbf{x}))F_I(\tau_I,\xi_I)e^{\mathrm{i}\Omega_I\tau_I(t,\mathbf{x})} \tag{5.11}$$

$$\mathcal{M}(t,\mathbf{x},t',\mathbf{x}') = \mathcal{L}_{\mathrm{A}}(t,\mathbf{x})\mathcal{L}_{\mathrm{B}}(t',\mathbf{x}') + \mathcal{L}_{\mathrm{A}}(t',\mathbf{x}')\mathcal{L}_{\mathrm{B}}(t,\mathbf{x}) \tag{5.12}$$

where $I = \mathrm{A}, \mathrm{B}$. Notably, $\mathcal{L}_{\mathrm{AA}}$ is the transition rate of detector A, the quantity calculated in previous chapters. $\mathcal{L}_{\mathrm{BA}}$ is associated with mutual information, while $\mathcal{M}$ is associated with entanglement. It is thus $\mathcal{M}$ we are most interested in calculating.

5.2 The problem with the entangling term

In order to measure entanglement, we will use the logarithmic negativity, an entanglement monotone. More precisely, we will use an estimator for the logarithmic negativity, $\mathcal{N}^{(2)}$:

$$\mathcal{N}^{(2)} = -\frac{1}{2}\left(\mathcal{L}_{\mathrm{AA}} + \mathcal{L}_{\mathrm{BB}} - \sqrt{(\mathcal{L}_{\mathrm{AA}} - \mathcal{L}_{\mathrm{BB}})^2 + 4|\mathcal{M}|^2}\right). \tag{5.13}$$

The logarithmic negativity is then

$$\mathcal{N} = \max[0, \mathcal{N}^{(2)}]. \tag{5.14}$$

When the logarithmic negativity $\mathcal{N} > 0$, the detectors are entangled. In fact, in the case of a two-qubit system like ours, the logarithmic negativity is a faithful measure of entanglement.

In the special case where the detectors have equal transition probability,$\mathcal{L}_{\mathrm{AA}} = \mathcal{L}_{\mathrm{BB}}$, this simplifies to

$$\mathcal{N}^{(2)} = |\mathcal{M}| - \mathcal{L}_{II}. \tag{5.15}$$

Thus, $\mathcal{M}$ is referred to as the 'entangling term', and the transition rate of the detector acts as a local noise term, suppressing entanglement.

In previous chapters, we showed that the transition functions $\mathcal{L}_{\text{AA}}$ of detectors could be expressed in terms of the Fourier transforms of the switching functions. Indeed, it is not hard to see that this is also possible for (5.10), given a Wightman function of simple time dependence. However, for (5.9), the inner integration limit, expressing the time ordering in the Dyson expansion, frustrates this interpretation. We are therefore left with the daunting task of integrating over the worldlines of both detectors, and summing over all modes inside the double integral. This is computationally very costly. Fortunately, we can show that the problem can be simplified dramatically.

5.3 Symmetry

In order to begin our simplification, we note that in (5.12), $\mathcal{M}(t, \mathbf{x}, t', \mathbf{x}')$ is completely symmetric: exchanging the primed and unprimed points in space has no effect. A similar statement can be made about the volume element $\sqrt{g(t, \mathbf{x})g(t', \mathbf{x}')}$. However, two parts of the integral in (5.9) do not share this symmtery: $t' < t$, and the Wightman function $W(t, \mathbf{x}, t', \mathbf{x}')$.

Now, for the scalar field, the real and imaginary parts of the Wightman function each have a definite symmetry under this exchange: the real part is symmetric, while the imaginary part is antisymmetric.

$$W(t, \mathbf{x}, t', \mathbf{x}') = \Re\left[W(t, \mathbf{x}, t', \mathbf{x}')\right] + \mathrm{i}\Im\left[W(t, \mathbf{x}, t', \mathbf{x}')\right]. \tag{5.16}$$

Let us define a sign function $\varepsilon(\tau) = 2\Theta(\tau) - 1$, where $\Theta(\tau)$ is the Heaviside switching function. Then, splitting the Wightman function into parts of definite symmetry allow us to remove the time ordering of the integral. Thus, we find:

$$\begin{aligned}\mathcal{M} = -\lambda_A\lambda_B\frac{1}{2}\int_{-\infty}^{\infty}\mathrm{d}t\int_{-\infty}^{\infty}\mathrm{d}t'\int\mathrm{d}^n\mathbf{x}\int\mathrm{d}^n\mathbf{x}'\sqrt{g(t, \mathbf{x})g(t', \mathbf{x}')}\mathcal{M}(t, \mathbf{x}, t', \mathbf{x}') \\ \times\left(\Re\left[W(t, \mathbf{x}, t', \mathbf{x}')\right] + \mathrm{i}\varepsilon(t - t')\Im\left[W(t, \mathbf{x}, t', \mathbf{x}')\right]\right)\end{aligned} \tag{5.17}$$

Now, this combination of the real and imaginary parts of the Wightman function corresponds to the Feynman Green's function:

$$\begin{aligned}\mathrm{i}G_F(t, \mathbf{x}, t', \mathbf{x}') = \Re\left[W(t, \mathbf{x}, t', \mathbf{x}')\right] \\ + \mathrm{i}\varepsilon(t - t')\Im\left[W(t, \mathbf{x}, t', \mathbf{x}')\right]\end{aligned} \tag{5.18}$$

This allows us to derive our first major result of this chapter:

$$\mathcal{M} = -\lambda_A\lambda_B\frac{1}{2}\int_{-\infty}^{\infty}\mathrm{d}t\int_{-\infty}^{\infty}\mathrm{d}t'\int\mathrm{d}^n\mathbf{x}\int\mathrm{d}^n\mathbf{x}' \\ \times\sqrt{g(t,\mathbf{x})g(t',\mathbf{x}')}\mathcal{M}(t,\mathbf{x},t',\mathbf{x}')\mathrm{i}G_F(t,\mathbf{x},t',\mathbf{x}'). \tag{5.19}$$

In cases where an analytic form of the Feynman Green's function is known, this expression may be of great use. In fact, one could also use the Feynman diagram formalism found in [11] to calculate the Feynman Green's function, and use it here. It may even be possible to extend this result to higher spin fields.

However, in some cases, the Feynman Green's function may not be available. To find our next expression, we note that the real and imaginary parts of the scalar Wightman function are associated with the commutator and anti-commutator:

$$\mathcal{C}^+(t,\mathbf{x},t',\mathbf{x}') \equiv \left\langle[\hat{\Phi}(t,\mathbf{x}),\hat{\Phi}(t',\mathbf{x}')]_+\right\rangle_{\hat{\rho}(t_0)}, \tag{5.20}$$

$$\mathrm{i}\mathcal{C}^-(t,\mathbf{x},t',\mathbf{x}') \equiv \left\langle[\hat{\Phi}(t,\mathbf{x}),\hat{\Phi}(t',\mathbf{x}')]_-\right\rangle_{\hat{\rho}(t_0)}, \tag{5.21}$$

$$\mathcal{C}^+(t,\mathbf{x},t',\mathbf{x}') = 2\Re\left[W(t,\mathbf{x},t',\mathbf{x}')\right], \tag{5.22}$$

$$\mathcal{C}^-(t,\mathbf{x},t',\mathbf{x}') = 2\Im\left[W(t,\mathbf{x},t',\mathbf{x}')\right]. \tag{5.23}$$

where $[,]_-$ and $[,]_+$ denote the commutator and anti-commutator respectively. Of course, the commutator is anti-symmetric, and the anti-commutator symmetric.

Using the commutators, we can rewrite (5.17), and find our second result:

$$\mathcal{M} = -\lambda_A\lambda_B\frac{1}{4}\int_{-\infty}^{\infty}\mathrm{d}t\int_{-\infty}^{\infty}\mathrm{d}t'\int\mathrm{d}^n\mathbf{x}\int\mathrm{d}^n\mathbf{x}'\sqrt{g(t,\mathbf{x})g(t',\mathbf{x}')}\mathcal{M}(t,\mathbf{x},t',\mathbf{x}') \\ \times\left(\mathcal{C}^+(t,\mathbf{x},t',\mathbf{x}')+\mathrm{i}\varepsilon(t-t')\mathcal{C}^-(t,\mathbf{x},t',\mathbf{x}')\right). \tag{5.24}$$

This expression allows us to separate the integral into two parts: one depending exclusively on the commutator, and one on the anti-commutator. Since the commutator vanishes outside the light cone, by causality, it follows that only the anti-commutator term participates in spacelike entanglement. In fact, to leading order, the commutator is the only part that participates in signalling [20]; the anti-commutator part is therefore nonsignalling. We can therefore argue that the anti-commutator part of this integral is exclusively due to pre-existing correlations in the quantum state of the field.

There is another way to express (5.17), in terms of the Wightman function. Since $\mathcal{C}^-$ is antisymmetric, its integral over the entire t, t' domain must vanish. Therefore, we may simply add it to the integrand.

$$\begin{aligned}\mathcal{M} = &- \lambda_A \lambda_B \frac{1}{4} \int_{-\infty}^{\infty} \mathrm{d}t \int_{-\infty}^{\infty} \mathrm{d}t' \int \mathrm{d}^n\mathbf{x} \int \mathrm{d}^n\mathbf{x}' \sqrt{g(t,\mathbf{x})g(t',\mathbf{x}')}\mathcal{M}(t,\mathbf{x},t',\mathbf{x}') \\ &\times \left(\mathcal{C}^+(t,\mathbf{x},t',\mathbf{x}') + \mathrm{i}(1+\varepsilon(t-t'))\mathcal{C}^-(t,\mathbf{x},t',\mathbf{x}')\right). \end{aligned} \tag{5.25}$$

However, recall that

$$2W(t,\mathbf{x},t',\mathbf{x}') = \mathcal{C}^+(t,\mathbf{x},t',\mathbf{x}') + \mathrm{i}\mathcal{C}^-(t,\mathbf{x},t',\mathbf{x}'). \tag{5.26}$$

We may then put the Wightman function back into the integral, leaving us with

$$\begin{aligned}\mathcal{M} = &- \lambda_A \lambda_B \frac{1}{2} \int_{-\infty}^{\infty} \mathrm{d}t \int_{-\infty}^{\infty} \mathrm{d}t' \int \mathrm{d}^n\mathbf{x} \int \mathrm{d}^n\mathbf{x}' \sqrt{g(t,\mathbf{x})g(t',\mathbf{x}')}\mathcal{M}(t,\mathbf{x},t',\mathbf{x}') \\ &\times \left(W(t,\mathbf{x},t',\mathbf{x}') + \frac{\mathrm{i}}{2}\varepsilon(t-t')\mathcal{C}^-(t,\mathbf{x},t',\mathbf{x}')\right) \end{aligned} \tag{5.27}$$

which is our key result. Suppose the commutator vanishes; that is, the detectors do not communicate directly. This is always the case if the detectors are spacelike separated. This can also occur in spacetimes that respect the strong Huygens principle (i.e. if the commutator is supported on the lightcone), if the detectors are *timelike* separated. In those cases, the only remaining term is an integral of the Wightman function over all t, t', much like $\mathcal{L}_{\mathrm{IJ}}$ in (5.10). This extension of the domain of integration when the commutator vanishes in the support of the switching and smearing function of the detector is at the core of the simplification obtained here.

In fact, the similarity with $\mathcal{L}_{\mathrm{IJ}}$ is even closer than it first appears. Let us first define

$$\mathcal{M}^+ = - \lambda_A \lambda_B \frac{1}{2} \int_{-\infty}^{\infty} \mathrm{d}t \int_{-\infty}^{\infty} \mathrm{d}t' \int \mathrm{d}^n\mathbf{x} \int \mathrm{d}^n\mathbf{x}' \sqrt{g(t,\mathbf{x})g(t',\mathbf{x}')}\mathcal{M}(t,\mathbf{x},t',\mathbf{x}')W(t,\mathbf{x},t',\mathbf{x}'), \tag{5.28}$$

$$\begin{aligned}\mathcal{M}^- = &- \lambda_A \lambda_B \frac{1}{4} \int_{-\infty}^{\infty} \mathrm{d}t \int_{-\infty}^{\infty} \mathrm{d}t' \varepsilon(t-t') \int \mathrm{d}^n\mathbf{x} \int \mathrm{d}^n\mathbf{x}' \\ &\times \sqrt{g(t,\mathbf{x})g(t',\mathbf{x}')}\mathcal{M}(t,\mathbf{x},t',\mathbf{x}')\mathrm{i}\mathcal{C}^-(t,\mathbf{x},t',\mathbf{x}') \end{aligned} \tag{5.29}$$

so that $\mathcal{M} = \mathcal{M}^+ + \mathcal{M}^-$. Therefore, if the commutator vanishes while the detectors are switched on, $\mathcal{M}^-$ vanishes, and thus $\mathcal{M} = \mathcal{M}^+$. Note that (5.28) is unchanged if we replace W by $\mathcal{C}^+/2$, justifying the name.

Now, consider the $\mathcal{L}_I(t,\mathbf{x})$ terms in (5.11). It is easy to see that most of the components are real, leaving us with

$$\mathcal{L}_I^*(\Omega;t,\mathbf{x}) = \mathcal{L}_I(-\Omega;t,\mathbf{x}). \tag{5.30}$$

We can then rewrite (5.12) as follows:

$$\mathcal{M}(t,\mathbf{x},t',\mathbf{x}') = \mathcal{L}_A(\Omega_A;t,\mathbf{x})\mathcal{L}_B^*(-\Omega_B;t',\mathbf{x}') + \mathcal{L}_B(\Omega_B;t,\mathbf{x})\mathcal{L}_A^*(-\Omega_A;t',\mathbf{x}'). \tag{5.31}$$

This demonstrates a deep relation between (5.28) and the definition of $\mathcal{L}_{IJ}$ found in (5.10). If we consider the dependence of $\mathcal{L}_{IJ}[\Omega_I,\Omega_J]$, on the detector gaps, we can finally write:

$$\mathcal{M}^+ = -\frac{1}{2}\left(\mathcal{L}_{AB}[\Omega_A,-\Omega_B] + \mathcal{L}_{BA}[\Omega_B,-\Omega_A]\right), \tag{5.32}$$

which represents our final key result of this chapter.

Since $\mathcal{M} = \mathcal{M}^+ + \mathcal{M}^-$, we can express the full entangling term with respect to $\mathcal{L}_{IJ}$ and the commutator:

$$\begin{aligned}\mathcal{M} = &-\frac{1}{2}\left(\mathcal{L}_{AB}[\Omega_A,-\Omega_B] + \mathcal{L}_{BA}[\Omega_B,-\Omega_A]\right)\\ &- \lambda_A\lambda_B\frac{1}{4}\int_{-\infty}^{\infty}\mathrm{d}t\int_{-\infty}^{\infty}\mathrm{d}t'\varepsilon(t-t')\int\mathrm{d}^n\mathbf{x}\int\mathrm{d}^n\mathbf{x}'\\ &\times\sqrt{g(t,\mathbf{x})g(t',\mathbf{x}')}\mathcal{M}(t,\mathbf{x},t',\mathbf{x}')\mathrm{i}\mathcal{C}^-(t,\mathbf{x},t',\mathbf{x}')\ .\end{aligned} \tag{5.33}$$

When the commutator vanishes, $\mathcal{M}^-$ vanishes; thus, if the detectors cannot communicate, the entangling term may be written in terms of the mutual information terms with modified gaps.

As a demonstration of the power of these results, suppose additionally that

$$W(t,\mathbf{x},t',\mathbf{x}') = \sum_{nlm}\frac{1}{2\omega_{nlm}}e^{-\mathrm{i}\omega_{nlm}(t-t')}\varphi_{nlm}(x)\overline{\varphi}_{nlm}(x'), \tag{5.34}$$

for some time-independent mode functions $\varphi_{nlm}(x)$. Now, the imaginary part of this Wightman function is proportional to the commutator; however, since the commutator is divergent on the light cone, the Wightman function is also UV-divergent there. Using this mode sum expression, we may now express (5.28) as another Fourier transform of switching functions:

$$\begin{aligned}\mathcal{M}^+ = -\frac{1}{2}\lambda_B\lambda_A\sum_{nlm}\frac{\pi}{\omega}\Bigg(&\hat{\chi}_B\left(\Omega_B - \frac{dt}{\mathrm{d}\tau_B}\omega\right)\hat{\chi}_A\left(\Omega_A + \frac{dt}{\mathrm{d}\tau_A}\omega\right)\varphi_{nlm}(x_B)\varphi^*_{\omega lm}(x_A)\\ &+ \hat{\chi}_A\left(\Omega_A - \frac{dt}{\mathrm{d}\tau_A}\omega\right)\hat{\chi}_B\left(\Omega_B + \frac{dt}{\mathrm{d}\tau_B}\omega\right)\varphi_{nlm}(x_A)\varphi^*_{\omega lm}(x_B)\Bigg).\end{aligned} \tag{5.35}$$

Compare this to (5.10):

$$\begin{aligned}\mathcal{L}_{IJ} =&\lambda_J\lambda_I \sum_{\omega lm} \frac{\pi}{\omega}\varphi_{nlm}(x_J)\varphi^*_{\omega lm}(x_I) \\ &\times \hat{\chi}_I\left(\omega\frac{dt}{\mathrm{d}\tau_I}+\Omega_I\right)\hat{\chi}^*_J\left(\omega\frac{dt}{\mathrm{d}\tau_J}+\Omega_J\right).\end{aligned} \tag{5.36}$$

In the particular case where the commutator vanishes while the detectors are switched on, this means the entangling term can simply be expressed in terms of the modes and the Fourier transform of the switching functions. The unwieldy double-integral-and-sum is no longer necessary: our calculation is now reduced to a single mode sum, and we can Fourier transform the switching functions separately. This represents a massive computational savings.

It is important to emphasize the great generality of our results. No matter whether the detector gaps are equal or not, no matter whether their trajectories are similar or different, no matter whether the detector *times* are equal or not, the symmetry in (5.12) and in the Wightman function allow us to derive Equation (5.27), our key result. Additionally, in the spacelike case, the case which is of most interest theoretically, we have shown that the entangling term can be expressed entirely in terms of mutual information terms, which are typically much simpler to calculate. It is our hope that this result may be used to aid calculations in much more complicated configurations and spacetimes.

5.4 A demonstration in flat space

Let us compare our results with those found in flat space, in [31]. Consider two identical detectors, switched according to

$$\chi_I(t) = e^{-(t-t_I)^2/T^2}, \tag{5.37}$$

where T is the switching time.

Now, the expression found in [31] for $\mathcal{L}_{AB}$ assumes the detectors have equal gap. This is not the case in our expression (5.33) for $\mathcal{M}$; therefore, our expression will also depend on $t_B + t_A$, at least in intermediate stages. While this is typical for detectors with unequal gaps, it means we will have to interpret our results very carefully.

Using their notation, let us take $t_A = -t_B = -t_0/2$; that is, detector A switches first, and we divide the delays equally in coordinate time. We then find:

$$\mathcal{M}^+ = -\frac{1}{2}\left(\mathcal{L}_{AB}[\alpha,-\alpha] + \mathcal{L}_{BA}[\alpha,-\alpha]\right) \tag{5.38}$$

$$= -\frac{\lambda^2}{8\pi^2 T^2 \beta}\int_0^\infty d|\kappa|\sin(\kappa\beta)e^{-\frac{1}{2}\kappa^2\delta^2}\left(G_1(\kappa,-\gamma/2,\alpha)G_1(\kappa,\gamma/2,-\alpha)^* + G_1(\kappa,\gamma/2,\alpha)G_1(\kappa,-\gamma/2,-\alpha)^*\right). \tag{5.39}$$

Next, we find G_1, in terms of t_0 and other parameters.

$$G_1(\kappa,-\gamma/2,\alpha)G_1(\kappa,\gamma/2,-\alpha)^* = \pi T^2 e^{\frac{1}{2}(|\kappa|^2+\alpha^2)}e^{-\mathrm{i}|\kappa|\gamma} \tag{5.40}$$

$$G_1(\kappa,\gamma/2,\alpha)G_1(\kappa,-\gamma/2,-\alpha)^* = \pi T^2 e^{\frac{1}{2}(|\kappa|^2+\alpha^2)}e^{+\mathrm{i}|\kappa|\gamma} \tag{5.41}$$

Thus, our integral becomes

$$\mathcal{M}^+ = -\frac{\lambda^2 e^{-\frac{1}{2}\alpha^2}}{4\pi\beta}\int_0^\infty d|\kappa|\sin(\kappa\beta)\cos(\kappa\gamma)e^{-\frac{1}{2}\kappa^2(\delta^2+1)} \tag{5.42}$$

$$= -\frac{\lambda^2 e^{\frac{1}{2}\alpha^2}}{8\sqrt{2\pi}\beta\sqrt{1+\delta^2}}\left(e^{-\frac{(\beta-\gamma)^2}{2(1+\delta^2)}}\mathrm{erfi}\left(\frac{\beta-\gamma}{\sqrt{2}\sqrt{1+\delta^2}}\right) + e^{-\frac{(\beta+\gamma)^2}{2(1+\delta^2)}}\mathrm{erfi}\left(\frac{\beta+\gamma}{\sqrt{2}\sqrt{1+\delta^2}}\right)\right) \tag{5.43}$$

The commutator part $\mathcal{M}^-$ requires a little more work. In Minkowski (3+1)-space,

$$\mathrm{i}\mathcal{C}^- = \frac{\mathrm{i}}{4\pi|\mathbf{x}-\mathbf{x}'|}(\delta(t-t'+|\mathbf{x}-\mathbf{x}'|) - \delta(t-t'-|\mathbf{x}-\mathbf{x}'|)). \tag{5.44}$$

Since the commutator has support on the lightcone, it is inherently a UV feature. Therefore, any attempt to approximate the Wightman function at finite energy will smear the commutator, and cause causality issues [20]: for instance, a signalling contribution would appear outside the light cone, in violation of causality. However, our closed expression will allow us to avoid that. After translating the integrand in t for greater symmetry, we find:

$$\mathcal{M}^- = \frac{\mathrm{i}\lambda^2}{8\pi}\int_{-\infty}^\infty \mathrm{d}\tau \int \mathrm{d}^3\beta \int \mathrm{d}^3\beta' \frac{e^{-2\tau^2+2\mathrm{i}\alpha\tau}}{|\beta-\beta'|} \times \left(e^{-\frac{1}{2}(|\beta-\beta'|+\gamma)^2}F_A(\mathbf{x})F_B(\mathbf{x}') + e^{-\frac{1}{2}(|\beta-\beta'|-\gamma)^2}F_B(\mathbf{x})F_A(\mathbf{x}')\right) \tag{5.45}$$

For pointlike detectors, under the notation of [31], $\delta = 0$, allowing us to do this integral analytically:

$$\mathcal{M}^- = \frac{\mathrm{i}\lambda^2 e^{-\frac{1}{2}\alpha^2}}{8\sqrt{2\pi}\beta}\left(e^{-\frac{(\beta+\gamma)^2}{2}} + e^{-\frac{(\beta-\gamma)^2}{2}}\right). \tag{5.46}$$

Therefore, for pointlike detectors, we find:

$$\mathcal{M} = -\frac{\lambda^2 e^{-\frac{1}{2}\alpha^2}}{8\sqrt{2\pi}\beta}\left(e^{-\frac{(\beta-\gamma)^2}{2}}\left[\mathrm{erfi}\left(\frac{\beta-\gamma}{\sqrt{2}}\right) - \mathrm{i}\right] + e^{-\frac{(\beta+\gamma)^2}{2}}\left[\mathrm{erfi}\left(\frac{\beta+\gamma}{\sqrt{2}}\right) - \mathrm{i}\right]\right) \tag{5.47}$$

This new expression is extremely close to $\mathcal{M}_{non}$, the analytical result found by [31] when the detector switching functions do not overlap. The main difference is simply the sign of the imaginary summands. Therefore, $\mathcal{M} \approx \mathcal{M}_{non}$ unless both β and γ are small; that is, unless the detector switching functions overlap, as we would expect.

In order to continue our comparison, we took the numerical expression for $\mathcal{M}$ from [31], and compared it with our analytic expression. Notably, after dividing out a common factor $\frac{\lambda^2 e^{-\alpha^2/2}}{8\sqrt{2\pi}\beta}$, no dependence on α remains: we are left with

$$\begin{aligned}\sqrt{\frac{2}{\pi}}\int_0^\infty d|\kappa|\ \sin(\beta|\kappa|)e^{-\kappa^2/2}(E(\kappa,\gamma) + E(\kappa,-\gamma)) \\ \approx e^{-\frac{(\beta-\gamma)^2}{2}}\left[\mathrm{erfi}\left(\frac{\beta-\gamma}{\sqrt{2}}\right) - \mathrm{i}\right] + e^{-\frac{(\beta+\gamma)^2}{2}}\left[\mathrm{erfi}\left(\frac{\beta+\gamma}{\sqrt{2}}\right) - \mathrm{i}\right]\end{aligned} \tag{5.48}$$

where

$$E(\kappa,\gamma) = e^{\mathrm{i}\gamma|\kappa|}\mathrm{erfc}\left(\frac{\gamma + \mathrm{i}|\kappa|}{\sqrt{2}}\right). \tag{5.49}$$

We therefore chose $\delta = 0$ and $\beta = 1, 5, 10$ in Fig. 5.1, 5.2, 5.3 respectively, and plotted with respect to γ. We believe the numerical agreement to be quite satisfactory, with residuals of less than 1 part in 10^6.

Finally, in Fig. 5.4 we plot $\mathcal{M}^\pm$ for $\beta = 5$. Note that the sign difference in the imaginary part we noted for $\mathcal{M}_{\text{non}}$ means that that estimate is inaccurate here, as we would expect. Notably, it appears that $\mathcal{M}^+$ vanishes near the light cone, where $\mathcal{M}^-$ is largest. While this is not why we called $\mathcal{M}^+$ the 'non-communicating' part of $\mathcal{M}$, this is still a matter of some interest. This graph also demonstrates how, in the spacelike region $|\gamma| \gg 1$, $\mathcal{M}^+$ is dominant. We note that by contrast, $\mathcal{M}^-$ is positive for all values of τ.

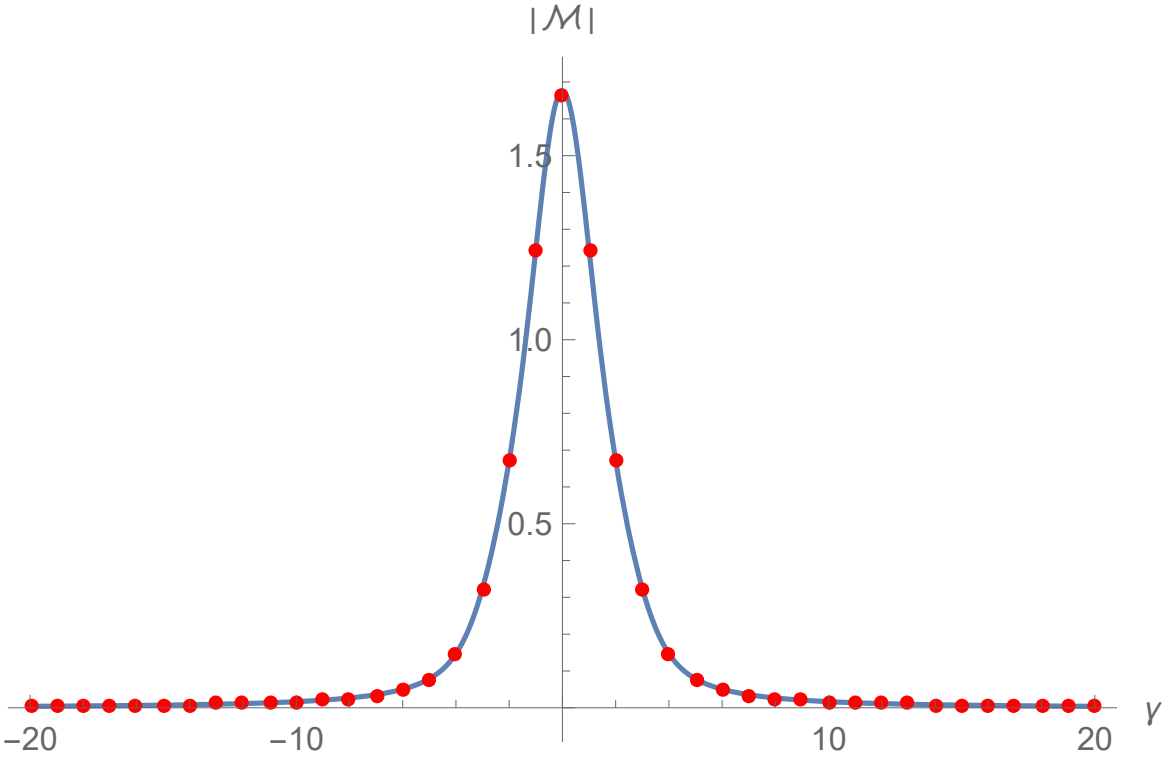

Figure 5.1: A plot of our expression for $\mathcal{M}$ (blue line) against the results in [32] (red points) for $\beta = 1$.

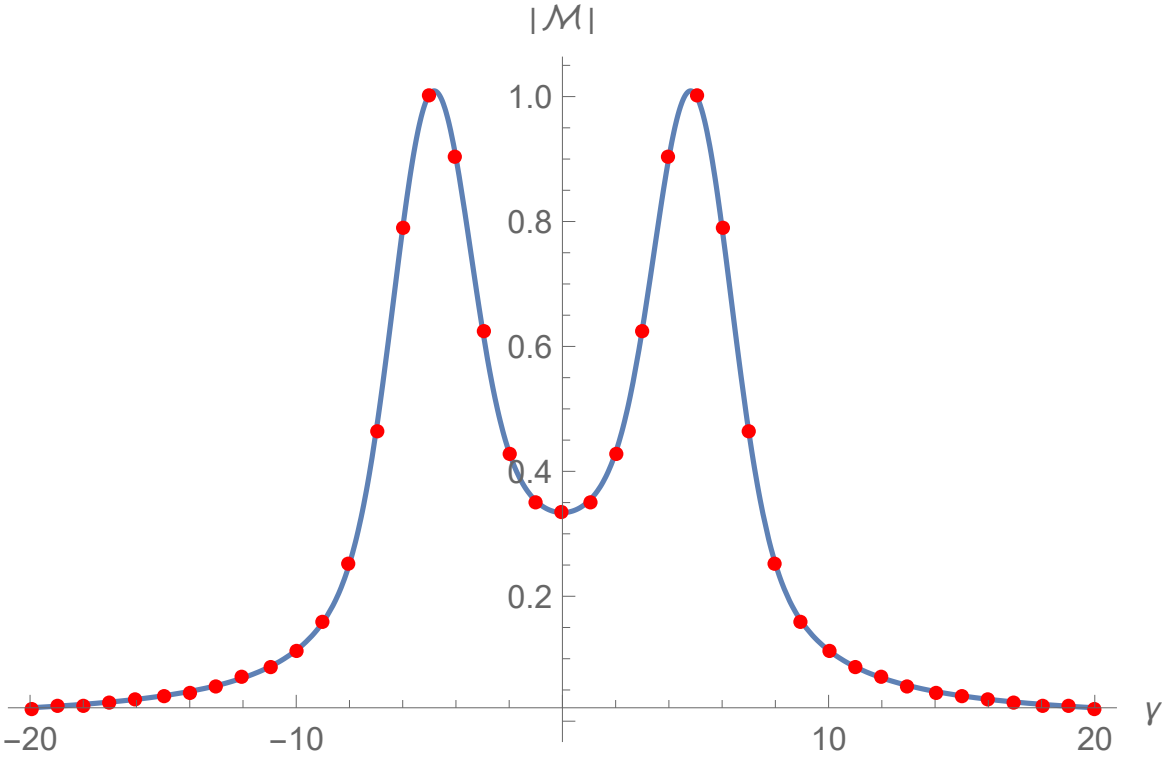

Figure 5.2: A plot of our expression for $\mathcal{M}$ (blue line) against the results in [32] (red points) for $\beta = 5$.

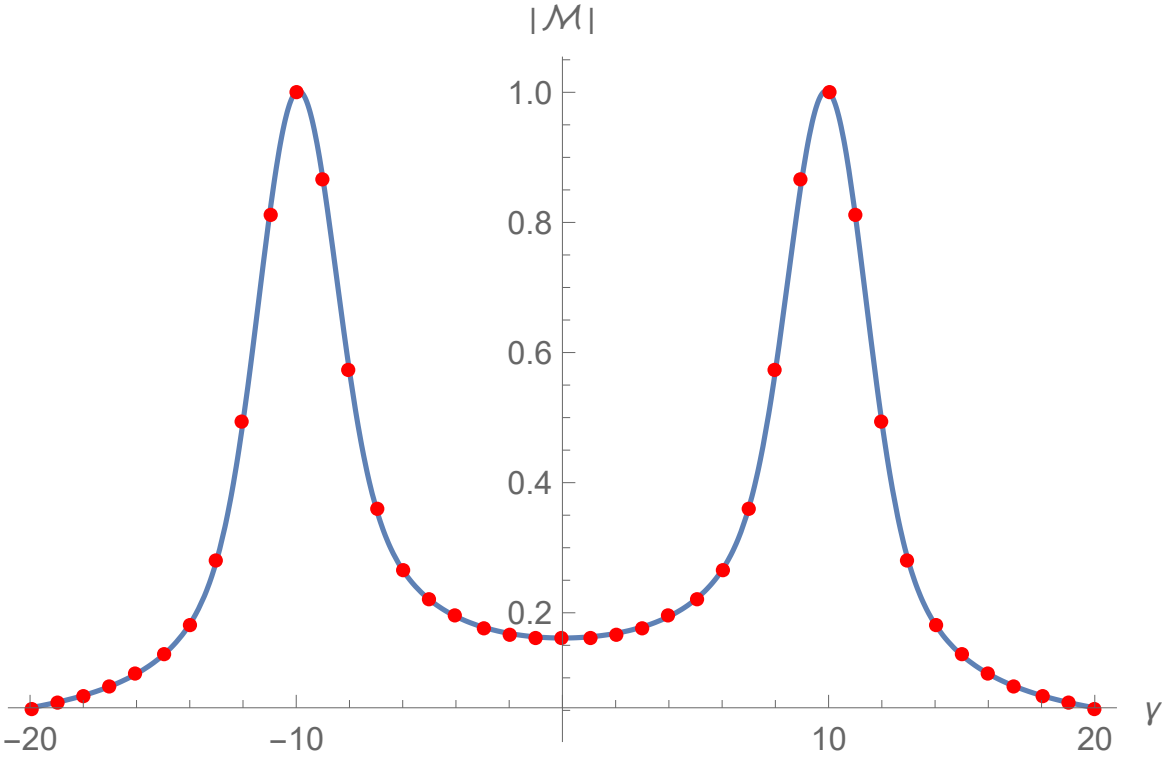

Figure 5.3: A plot of our expression for $\mathcal{M}$ (blue line) against the results in [32] (red points) for $\beta = 10$.

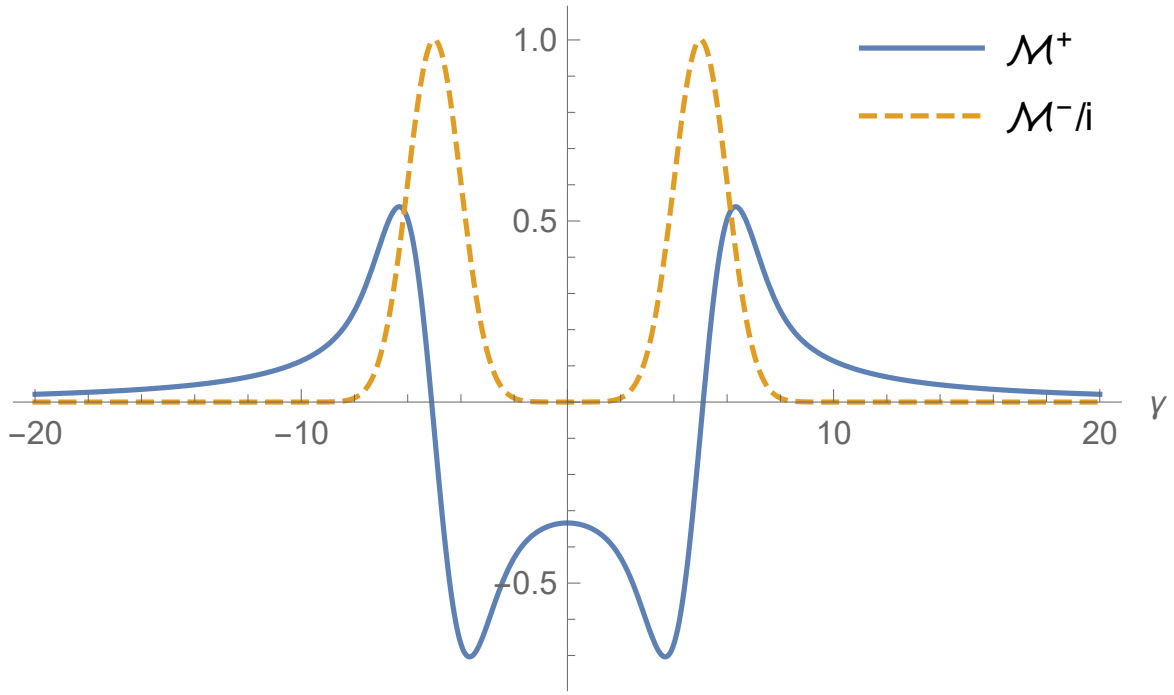

Figure 5.4: Comparing $\mathcal{M}^{\pm}$ for $\beta = 5$: $\mathcal{M}^+$ solid blue, $\mathcal{M}^-/\mathrm{i}$ dashed orange. Note that $\mathcal{M}^+$ appears to be smallest in magnitude on the light cone, where $\mathcal{M}^-$ is largest.

5.5 Conclusions on the new method

In many spacetimes, the Wightman function is only known with respect to a mode expansion. Those wishing to calculate the entangling term $\mathcal{M}$ are then left with the daunting task of calculating a triple integral: twice over time, and once over mode energy. Additionally, since the causal structure of the field is extremely sensitive to the UV limit, the usual practice of truncating at finite energy will cause violations of causality.

In this section, we have found a number of extremely general expressions for $\mathcal{M}$, including equations (5.27) and (5.33), which allow us to split the entangling terms into two parts: one dependent on the commutator, and one dependent only on the anti-commuting part. By doing this, we allow ourselves to isolate the UV divergence to the commutator part $\mathcal{M}^-$. The anti-commuting part $\mathcal{M}^+$ can often also be turned into a Fourier transform, with considerable computational savings, as we have demonstrated in the Minkowski case; in fact, if the detectors are spacelike separated, as one often posits, then this term is equal to $\mathcal{M}$ in its entirety.

The generality of this result suggests its application in almost any spacetime. It remains to be seen, however, how much this generalizes to higher spin fields, interacting fields, or even higher order couplings. It also raises the question of whether placing a UV cutoff can cause causality violations not just in $\mathcal{M}^-$, but also in $\mathcal{M}^+$. Still, we expect this result to be quite productive for those researching entanglement harvesting. In the next chapter, we will use it ourselves to explore the properties of Anti-de Sitter space.

Chapter 6

Entanglement harvesting in Anti-de Sitter space

In previous chapters, we have calculated how a single detector responds to the structure of various spacetimes. However, two detectors are capable of much more than one: using the entanglement harvested by two detectors, we can probe even more structural features of spacetime [36, 22]. However, as we saw in the previous chapter, calculating the entanglement harvesting by two detectors is, in general, a computational challenge. In the absence of an analytic expression for the Wightman function, we must sum over the modes for each point in a double integral. Thus, calculations in all but the simplest spacetimes are quite difficult.

In the previous chapter, we found an expression that allows for the calculation of entanglement harvesting with greater ease than before. We will now apply this to Anti-de Sitter space in (3+1) dimensions, a highly symmetric space of constant curvature. While the metric of this spacetime is fairly simple, calculating its characteristics is still of great scientific interest: understanding AdS is crucial to understanding the AdS/CFT duality. In particular, the entanglement structure of AdS may serve as another means to match theories on the boundary with theories in the bulk. We will also compare our results with those found concurrently in AdS in (2+1) dimensions with more traditional methods [7], and see how the difference in dimensions leads to different phenomena.

6.1 Life in Anti-de Sitter space

Anti-de Sitter space is a highly symmetric spacetime of negative curvature. While there are several possible choices for a metric, we will choose the following, from [2]:

$$\mathrm{d}s^2 = L^2 \sec^2 \varrho \left(\mathrm{d}t^2 - d\varrho^2 - \sin^2 \varrho(\mathrm{d}\theta^2 + \sin^2\theta \, \mathrm{d}\phi^2)\right) \tag{6.1}$$

where L is the AdS curvature length, and $\varrho \in [0, \pi/2]$ is the coordinate radius. Notably, ϱ has the same units as the angular coordinates θ, ϕ: none at all. Unlike the well-known Poincaré metric, this global metric is not manifestly conformally flat. However, it does have the advantage of covering the whole space, rather than only half.

AdS possesses an unusual property, which we need to address before we continue. It is fairly simple to show that lightlike geodesics reach $\varrho = \pi/2$ in finite coordinate time; that is, light emitted from the centre of AdS can reach the boundary in finite time, interact with it, then return, within time $\Delta t = \pi$. We will therefore need to assign a boundary condition to the conformal boundary. We will consider three possible choices, indicated by ε:

$$\varepsilon = \begin{cases} -1, & \text{Dirichlet} \\ 1, & \text{Neumann} \\ 0, & \text{transparent} \end{cases} \tag{6.2}$$

However, in some sense, AdS is still a spacetime of infinite extent. One can also calculate the *proper* length Δx between the centre and a point at equal time and radius ϱ :

$$\Delta x = L \log(\tan \varrho + \sec \varrho) \tag{6.3}$$

$$\varrho = \arctan \sinh(\Delta x / L). \tag{6.4}$$

We therefore have the strange situation where light 'crosses' infinite proper distance in finite 'time'.

The 'transparent' condition also causes some special considerations. Briefly, in order to quantize AdS, it is necessary to ensure it is Cauchy-complete; that is, the state of the field at all times is determined by its state on some initial surface. Even if the boundary of AdS allows particles to escape, it is possible to restore Cauchy-completeness by embedding it into one half of an Einstein static universe [2]. Since the Einstein static universe is closed, these waves *return* some time later through the AdS boundary. Thus, in a certain sense, unitarity is preserved in this boundary condition; one can even pick a Cauchy surface entirely inside AdS, although a rather strange one, spanning two values of t rather than one.

This metric conceals an unusual symmetry possessed by AdS. Much like Minkowski space, AdS has the property that all geodesics are related by a coordinate isometry. For the purposes of understanding the geodesic structure, AdS may be thought of as a 'bowl', where a particle can take a circular orbit around the coordinate centre; this symmetry allows us to pick another coordinate system, where this particle remains stationary at the centre. The AdS vacuum shares this symmetry: the analytic form of the Wightman function is [4]

$$8\pi^2 L^2 W(x,x') = X[1+\varepsilon(1+2X)^{-1}], \tag{6.5}$$

where X is a simple function of the geodesic distance between the two points. Thus, for the purposes of calculating detector statistics, we will usually map one detector to the centre, for simplicity. In particular, unlike in the Schwarzschild solution, a detector in circular motion does *not* become excited [15].

For the purposes of probing the entanglement structure of AdS, we will consider two families of trajectories. First, we consider detectors that are geodesic at constant radius: these include circular geodesics, and detectors at the centre. While it is less obvious, AdS does possess another symmetry: all circular geodesics experience the same proper time, and the same angular velocity. This first family of trajectories thus is simpler to handle conceptually:

$$t = \tau_I/L, \tag{6.6}$$
$$\phi = \tau_I/L. \tag{6.7}$$

Therefore, our 'geodesic' detector configuration is as follows: detector A will be static at the centre, while detector B will be at a fixed distance, in geodesic circular motion.

The other family of trajectories we will consider are the static trajectories, those of constant spatial coordinate in time. Obviously, these trajectories have a proper time dependent on their distance from the centre; if we place one detector at the centre, and one further out, they will not share a proper time. Thus, we will have to carefully manage the proper gap and time of the two detectors. However, this situation is perhaps more generic: in most spacetimes, even if two detectors are geodesic, their proper times will not agree. For a detector at coordinate radius ϱ_I, its proper time is

$$\tau_I = Lt\sec\varrho_I. \tag{6.8}$$

Our 'static' detector configuration is as follows: detector A is static at the centre, while detector B is static a fixed distance away.

In order to handle detectors at different redshifts, we need to be clear about our conventions. We let Ω_I be the proper gap of the detector, τ_I be the proper time of the detector, and $\tilde{\Omega}_I$ be the 'coordinate frequency' of the detector, i.e. the frequency such that $\tilde{\Omega}_I \mathrm{d}t = \Omega_I \mathrm{d}\tau_I$, where I =A,B. We will also define $\tilde{\chi}_I(t) = \chi_I(\tau_I(t))\mathrm{d}\tau_I/\mathrm{d}t$ as the 'coordinate switching function' of detector I, so that its integral over time remains constant. This will greatly simplify future expressions.

6.2 The AdS vacuum

Let us first begin by writing the mode solutions of AdS. Recall that the curved-space Klein-Gordon equation is

$$(\Box - \zeta R)\Phi = 0, \tag{6.9}$$

where ζ is the coupling of the scalar field to the Ricci curvature R. (In 3+1 dimensions, $\zeta = 1/6$ defines the conformal coupling.) Since our coordinate system is static, we can then define a basis of positive frequency modes via

$$\Phi_{nlm}(t,x) = \frac{1}{\sqrt{2\omega_{nlm}}} e^{-\mathrm{i}\omega_{nlm}t}\varphi_{nlm}(x). \tag{6.10}$$

where n, l, m are non-negative integers, with $l \geq m$.

Under these conventions, the modes are given by [2]:

$$\varphi_{nlm}(x) = \sqrt{2}^{\varepsilon^2} N_{\omega l} \cos\varrho (\sin\varrho)^l C^{(l+1)}_{\omega-l-1}(\cos\varrho) Y^m_l(\theta,\phi), \tag{6.11}$$

$$N_{\omega l} = \frac{2^l l!}{L}\sqrt{\frac{2\omega(\omega-l-1)!}{\pi(\omega+l)!}}, \tag{6.12}$$

where C^b_a are the Gegenbauer polynomials, and the mode energy is given by

$$\omega = \begin{cases} l+n+1 & \text{if } \varepsilon = 0 \\ l+2n+1 & \text{if } \varepsilon = 1 \\ l+2n+2 & \text{if } \varepsilon = -1 \end{cases}. \tag{6.13}$$

Notably, AdS has a discrete spectrum; the modes are indexed by integers, rather than real values. This is due to the presence of the conformal boundary, a peculiarity of AdS. As well, it seems that the Neumann modes take even energy values, starting at $\omega = 2$, while

the Dirichlet modes take odd energy values, starting at $\omega = 3$; the transparent modes take both energy values, as one might have expected. At this point, we also note that since the Cauchy surface of the transparent boundary condition $\varepsilon = 0$ is twice as large, the normalization is different by a factor of $\sqrt{2}$. This is the source of the factor $\sqrt{2}^{\varepsilon^2}$ in (6.12).

Now, since we are primarily interested in detectors in static and circular geodesic trajectories, we can specialize to the equatorial plane. In this case, the modes take on the value

$$\begin{aligned}\varphi_{nlm}(x(t)) =& \sqrt{2}^{\varepsilon^2} N_{\omega l} \cos\varrho (\sin\varrho)^l C^{(l+1)}_{\omega-l-1}(\cos\varrho) \\ &\times \sqrt{\frac{2l+1}{4\pi}\frac{(l-m)!}{(l+m)!}} P_l(\cos\theta) e^{\mathrm{i}m\phi}.\end{aligned} \tag{6.14}$$

where $\phi = t$ in the circular geodesic case, and $\phi = 0$ in the static case. Notably, in the circular geodesic case, the existence of a factor $e^{\mathrm{i}mt}$ in the modes affects the 'effective frequency' of the mode, as seen by the detector. However, it is simple to show that this effective frequency cannot become negative, and so detectors in circular geodesic orbit cannot become excited [15].

Now, we can describe the Wightman function of the vacuum in terms of these modes. As noted previously, we can express the field operator and the vacuum Wightman function with respect to the annihilator a_{nlm} of a particle of indices n, l, m. Summing over all mode indices yields the following:

$$\hat{\Phi}(t,x) = \sum_{nlm}\left[\hat{a}_{nlm}(t,x)\Phi_{nlm}(t,x) + \hat{a}^\dagger_{nlm}(t,x)\bar{\Phi}_{nlm}(t,x)\right] \tag{6.15}$$

$$W(t,x,t',x') = \sum_{nlm}\frac{1}{2\omega_{nlm}} e^{-\mathrm{i}\omega_{nlm}(t-t')}\varphi_{nlm}(x)\overline{\varphi}_{nlm}(x'). \tag{6.16}$$

Thus, in principle, we have completely described the vacuum, at least for our purposes.

AdS in (3+1) dimensions also has an analytic expression for the commutator. In particular, AdS_4 obeys the strong Huygens principle: the commutator has support strictly on the light cone. When one detector is located at the centre, the commutator is given by [2]

$$\mathrm{i}\mathcal{C}^-(x,0) = -\frac{\mathrm{i}}{4\pi L^2}\varsigma^0(t)[\delta(\sigma^0(x)) + \varepsilon\delta(\sigma^0(x)-2)] \tag{6.17}$$

where $\sigma^0 = 1 - \cos t \sec\varrho$ is half of the geodesic distance in the embedding space, and $\varsigma^0(t) = \mathrm{sgn}(\sin(t))$ [1]. Notably, this implies that the commutator is 2π periodic. In our

[1] Note that our sign convention differs from that of [2].

case, since our detectors will always be at constant ϱ, we can then write:

$$\begin{aligned}
\mathrm{i}\mathcal{C}^-(x,t,0,t') = \sum_{N=-\infty}^{\infty} & -\frac{\mathrm{i}}{4\pi L^2}(\tan\varrho)^{-1} \\
& [\delta(\Delta t - \varrho - 2N\pi) \\
& + \varepsilon\delta(\Delta t + \varrho - (2N+1)\pi) \\
& - \varepsilon\delta(\Delta t - \varrho - (2N+1)\pi) \\
& - \delta(\Delta t + \varrho - (2N+2)\pi)] \qquad (6.18) \\
\mathrm{i}\mathcal{C}^-(0,t,x',t') = \sum_{N=-\infty}^{\infty} & -\frac{\mathrm{i}}{4\pi L^2}(\tan\varrho')^{-1} \\
& [\delta(\Delta t - \varrho' - 2N\pi) \\
& + \varepsilon\delta(\Delta t + \varrho' - (2N+1)\pi) \\
& - \varepsilon\delta(\Delta t - \varrho' - (2N+1)\pi) \\
& - \delta(\Delta t + \varrho' - (2N+2)\pi)] \qquad (6.19)
\end{aligned}$$

where $\Delta t = t - t'$. Note that, as written, $t > t'$ corresponds to $N \geq 0$.

6.3 The geodesic detector

Now that we have described the Wightman function and the commutator, we can calculate the behaviour of detectors in geodesic motion. To keep things simple, we place detector A at the centre, and B at proper separation Δx, which may be converted to a coordinate separation via (6.4). As noted earlier, since all geodesics are equivalent, we need only consider the transition probability of a detector at the centre: the answer greatly resembles that found in previous chapters. Using the mode definitions (6.12) to express the Wightman and substituting into (5.10) yields

$$\mathcal{L}_{II} = \lambda_I^2 \sum_n \frac{\pi}{\omega_n}\varphi_n^2(x_{\mathrm{A}})|\hat{\chi}_I(\omega_n/L + \Omega_I)|^2 \qquad (6.20)$$

where for brevity, we write φ_n and ω_n instead of φ_{n00} and ω_{n00}, and use the fact that φ_n is real to omit the absolute value function.

Next, since detector A is located at the centre, we need only consider the $l = 0$ modes. These modes are spherically symmetric, and so the value of the spatial modes at B is time

independent. Thus, we can also write

$$\mathcal{L}_{\mathrm{AB}} = \lambda_{\mathrm{B}}\lambda_{\mathrm{A}} \sum_n \frac{\pi}{\omega_n} \varphi_n(x_{\mathrm{B}})\varphi_n(x_{\mathrm{A}})\hat{\chi}_{\mathrm{A}}(\omega_n/L + \Omega_{\mathrm{A}})\hat{\chi}^*_{\mathrm{B}}(\omega_n/L + \Omega_{\mathrm{B}}). \tag{6.21}$$

$\mathcal{M}^+$ can now be expressed using the simplified expression found in (5.35):

$$\begin{aligned}\mathcal{M}^+ = -\lambda_{\mathrm{B}}\lambda_{\mathrm{A}} \sum_{n=0}^{\infty} \frac{\pi}{2\omega_n} \varphi_n(x_{\mathrm{B}})\varphi_n(x_{\mathrm{A}})(\hat{\chi}_{\mathrm{B}}(\Omega_{\mathrm{B}} - \omega_n/L)\hat{\chi}_{\mathrm{A}}(\Omega_{\mathrm{A}} + \omega_n/L) \\ + \hat{\chi}_{\mathrm{A}}(\Omega_{\mathrm{A}} - \omega_n/L)\hat{\chi}_{\mathrm{B}}(\Omega_{\mathrm{B}} + \omega_n/L))\end{aligned} \tag{6.22}$$

As noted previously, this may be expressed with respect to $\mathcal{L}_{BA}$:

$$\mathcal{M}^+(\Omega_{\mathrm{A}}, \Omega_{\mathrm{B}}) = -\frac{1}{2}\mathcal{L}_{\mathrm{AB}}(\Omega_{\mathrm{A}}, -\Omega_{\mathrm{B}}) - \frac{1}{2}\mathcal{L}_{\mathrm{BA}}(\Omega_{\mathrm{B}}, -\Omega_{\mathrm{A}}). \tag{6.23}$$

We may also use the commutator expression in (6.18), (6.19) to find $\mathcal{M}^-$, although this expression is more complicated. Assuming for simplicity that the detector gaps are equal, we find:

$$\begin{aligned}\mathcal{M}^- =& -\frac{1}{2}\lambda_{\mathrm{B}}\lambda_{\mathrm{A}} \int_{-\infty}^{\infty} \mathrm{d}t \int_{-\infty}^{t} \mathrm{d}t' e^{\mathrm{i}\tilde{\Omega}(t+t')} \\ & \times (\tilde{\chi}_{\mathrm{B}}(t)\tilde{\chi}_{\mathrm{A}}(t')\mathrm{i}\mathcal{C}^-(t, x_{\mathrm{B}}; t', x_{\mathrm{A}}) + \tilde{\chi}_{\mathrm{A}}(t)\tilde{\chi}_{\mathrm{B}}(t')\mathrm{i}\mathcal{C}^-(t, x_{\mathrm{A}}; t', x_{\mathrm{B}})) \\ =& \frac{\mathrm{i}\lambda_{\mathrm{A}}\lambda_{\mathrm{B}}}{8\pi \tan\varrho} \int_{-\infty}^{\infty} \mathrm{d}t\, e^{2\mathrm{i}\tilde{\Omega}t} \sum_{N=0}^{\infty} \\ & (e^{-\mathrm{i}\tilde{\Omega}(\varrho+2N\pi)}\tilde{\chi}_{\mathrm{B}}(t)\tilde{\chi}_{\mathrm{A}}(t - \varrho - 2N\pi) \\ & + e^{-\mathrm{i}\tilde{\Omega}(\varrho+2N\pi)}\tilde{\chi}_{\mathrm{A}}(t)\tilde{\chi}_{\mathrm{B}}(t - \varrho - 2N\pi) \\ & + \varepsilon e^{-\mathrm{i}\tilde{\Omega}(-\varrho+(2N+1)\pi)}\tilde{\chi}_{\mathrm{B}}(t)\tilde{\chi}_{\mathrm{A}}(t + \varrho - (2N+1)\pi) \\ & + \varepsilon e^{-\mathrm{i}\tilde{\Omega}(-\varrho+(2N+1)\pi)}\tilde{\chi}_{\mathrm{A}}(t)\tilde{\chi}_{\mathrm{B}}(t + \varrho - (2N+1)\pi) \\ & - \varepsilon e^{-\mathrm{i}\tilde{\Omega}(\varrho+(2N+1)\pi)}\tilde{\chi}_{\mathrm{B}}(t)\tilde{\chi}_{\mathrm{A}}(t - \varrho - (2N+1)\pi) \\ & - \varepsilon e^{-\mathrm{i}\tilde{\Omega}(\varrho+(2N+1)\pi)}\tilde{\chi}_{\mathrm{A}}(t)\tilde{\chi}_{\mathrm{B}}(t - \varrho - (2N+1)\pi) \\ & - e^{-\mathrm{i}\tilde{\Omega}(-\varrho+(2N+2)\pi)}\tilde{\chi}_{\mathrm{B}}(t)\tilde{\chi}_{\mathrm{A}}(t + \varrho - (2N+2)\pi) \\ & - e^{-\mathrm{i}\tilde{\Omega}(-\varrho+(2N+2)\pi)}\tilde{\chi}_{\mathrm{A}}(t)\tilde{\chi}_{\mathrm{B}}(t + \varrho - (2N+2)\pi))\end{aligned}$$

$$
\begin{aligned}
=&\frac{\mathrm{i}\lambda_{\mathrm{A}}\lambda_{\mathrm{B}}}{8\pi L^2\tan\varrho}\int_{-\infty}^{\infty}\mathrm{d}t\, e^{2\mathrm{i}\tilde{\Omega}t}\sum_{N=-\infty}^{\infty}\varsigma(N+1/2)\\
&\left(\tilde{\chi}_{\mathrm{B}}\left(t+\frac{\varrho+2N\pi}{2}\right)\tilde{\chi}_{\mathrm{A}}\left(t-\frac{\varrho+2N\pi}{2}\right)\right.\\
&+\tilde{\chi}_{\mathrm{A}}\left(t+\frac{\varrho+2N\pi}{2}\right)\tilde{\chi}_{\mathrm{B}}\left(t-\frac{\varrho+2N\pi}{2}\right)\\
&-\varepsilon\tilde{\chi}_{\mathrm{B}}\left(t+\frac{\varrho+(2N+1)\pi}{2}\right)\tilde{\chi}_{\mathrm{A}}\left(t-\frac{\varrho+(2N+1)}{2}\right)\\
&\left.-\varepsilon\tilde{\chi}_{\mathrm{A}}\left(t+\frac{\varrho+(2N+1)}{2}\right)\tilde{\chi}_{\mathrm{B}}\left(t-\frac{\varrho+(2N+1)}{2}\right)\right)\\
=&\frac{\mathrm{i}\lambda_{\mathrm{A}}\lambda_{\mathrm{B}}}{8\pi L^2\tan\varrho}\int_{-\infty}^{\infty}\mathrm{d}t\, e^{2\mathrm{i}\tilde{\Omega}t}\sum_{N=-\infty}^{\infty}\varsigma(N+1/2)(-\varepsilon)^{p(N)}\\
&\left(\tilde{\chi}_{\mathrm{B}}\left(t+\frac{\varrho+N\pi}{2}\right)\tilde{\chi}_{\mathrm{A}}\left(t-\frac{\varrho+N\pi}{2}\right)\right.\\
&\left.+\tilde{\chi}_{\mathrm{A}}\left(t+\frac{\varrho+N\pi}{2}\right)\tilde{\chi}_{\mathrm{B}}\left(t-\frac{\varrho+N\pi}{2}\right)\right),
\end{aligned}
\tag{6.24}
$$

where $\varsigma(n)=\mathrm{sgn}(n)$ is the sign function, $\tilde{\Omega}\,\mathrm{d}t=\Omega\,\mathrm{d}\tau$, $p(n)=0$ if n is even and 1 otherwise, and we use the convention that $0^0=1$.

Now, one of the features highlighted by this expression is the necessity, in principle, of summing over all N, which in this case is related to the number of reflections of the light cone off the boundary. In practice, if the detector is switched over a finite length of time, we need only consider a finite maximum N. However, it implies that $\mathcal{M}^-$ extends infinitely in time: no matter how far we displace the switching functions in time, we will always get some contribution from the commutator. This, of course, is quite peculiar to AdS, as a closed spacetime with reflecting boundaries: in most other spacetimes, waves either escape to infinity, or are absorbed by some other feature, such as a black hole.

We also note that the relative simplicity of this result is due to the nature of AdS_4 as strong Huygens; that is, that the commutator is supported on the light cone. This is not the case in AdS3, for instance: there, the commutator is nonzero inside the light cone as well. In that case, we would have to integrate over the interior of the light cone, instead of simply taking the value of the switching functions on the light cone. However, the technique of separating $\mathcal{M}^-$ still allows us to isolate the singularity on the light cone from the rest of the expression; in particular, if the two detectors are spacelike separated, the singularity disappears.

6.4 Static detectors

We next tackle the more generic case, where the detectors are static, and have different redshifts. As before, we locate B at a proper distance Δx from A, then use (6.4) to convert to a coordinate radius ϱ. For convenience, we place B on the z-axis, so we only need consider modes with axial angular momentum $m = 0$. This time, the proper time of B is given by

$$\tau_B = Lt \sec \varrho, \tag{6.25}$$

so the coordinate switching functions are scaled respectively. We also have to remember to apply the Fourier transforms in proper time: that is, we apply the Fourier transform as follows:

$$\hat{\chi}_{\mathrm{B}}(\tau) = \mathcal{F}_{\tau_{\mathrm{B}}}[\chi_{\mathrm{B}}(\tau_{\mathrm{B}}(t))]. \tag{6.26}$$

First, since the detector at B is not geodesic, the transition rate of B is now different from A:

$$\begin{aligned}\mathcal{L}_{\mathrm{BB}} =& \lambda_{\mathrm{B}}^2 \sum_{n,l} \frac{\pi}{\omega_{nl}} \varphi_{n,l,0}^2(x_{\mathrm{B}}) \\ &\times |\hat{\chi}_{\mathrm{B}}(\omega_{nl}/(L \sec \varrho_{\mathrm{B}}) + \Omega_{\mathrm{B}})|^2.\end{aligned} \tag{6.27}$$

Surprisingly, the expression found in (6.21) for $\mathcal{L}_{JI}$ and in (6.22) for $\mathcal{M}^+$ remains completely valid: this is because, much as before, since detector A is at the centre, only $l = 0$ modes matter, and thus the value of the spatial mode at B is time-independent.

Unfortunately, $\mathcal{M}^-$ is now significantly more difficult to calculate. Beginning as before,

we find

$$\begin{aligned}
\mathcal{M}^- =& -\frac{1}{2}\lambda_{\mathrm{B}}\lambda_{\mathrm{A}}\int_{-\infty}^{\infty}\mathrm{d}t\int_{-\infty}^{t}\mathrm{d}t' \\
&\times (e^{i\tilde{\Omega}_{\mathrm{B}}t}\tilde{\chi}_{\mathrm{B}}(t)e^{\mathrm{i}\tilde{\Omega}_{\mathrm{A}}t'}\tilde{\chi}_{\mathrm{A}}(t')\mathrm{i}\mathcal{C}^-(t,x_{\mathrm{B}};t',x_{\mathrm{A}}) \\
&+ (e^{\mathrm{i}\tilde{\Omega}_{\mathrm{A}}t}\tilde{\chi}_{\mathrm{A}}(t)e^{\mathrm{i}\tilde{\Omega}_{\mathrm{B}}t'}\tilde{\chi}_{\mathrm{B}}(t')\mathrm{i}\mathcal{C}^-(t,x_{\mathrm{A}};t',x_{\mathrm{B}})) \\
=&\frac{\mathrm{i}\lambda_{\mathrm{B}}\lambda_{\mathrm{A}}}{8\pi L^2\tan\varrho_{\mathrm{B}}}\int_{-\infty}^{\infty}\mathrm{d}t\, e^{\mathrm{i}(\tilde{\Omega}_{\mathrm{A}}+\tilde{\Omega}_{\mathrm{B}})t}\sum_{N=0}^{\infty} \\
&(e^{-\mathrm{i}\tilde{\Omega}_{\mathrm{A}}(\varrho_{\mathrm{B}}+2N\pi)}\tilde{\chi}_{\mathrm{B}}(t)\tilde{\chi}_{\mathrm{A}}(t-\varrho_{\mathrm{B}}-2N\pi) \\
&+ e^{-\mathrm{i}\tilde{\Omega}_{\mathrm{B}}(\varrho_{\mathrm{B}}+2N\pi)}\tilde{\chi}_{\mathrm{A}}(t)\tilde{\chi}_{\mathrm{B}}(t-\varrho_{\mathrm{B}}-2N\pi) \\
&+ \varepsilon e^{-\mathrm{i}\tilde{\Omega}_{\mathrm{A}}(-\varrho_{\mathrm{B}}+(2N+1)\pi)}\tilde{\chi}_{\mathrm{B}}(t)\tilde{\chi}_{\mathrm{A}}(t+\varrho_{\mathrm{B}}-(2N+1)\pi) \\
&+ \varepsilon e^{-\mathrm{i}\tilde{\Omega}_{\mathrm{B}}(-\varrho_{\mathrm{B}}+(2N+1)\pi)}\tilde{\chi}_{\mathrm{A}}(t)\tilde{\chi}_{\mathrm{B}}(t+\varrho_{\mathrm{B}}-(2N+1)\pi) \\
&- \varepsilon e^{-\mathrm{i}\tilde{\Omega}_{\mathrm{A}}(\varrho_{\mathrm{B}}+(2N+1)\pi)}\tilde{\chi}_{\mathrm{B}}(t)\tilde{\chi}_{\mathrm{A}}(t-\varrho_{\mathrm{B}}-(2N+1)\pi) \\
&- \varepsilon e^{-\mathrm{i}\tilde{\Omega}_{\mathrm{B}}(\varrho_{\mathrm{B}}+(2N+1)\pi)}\tilde{\chi}_{\mathrm{A}}(t)\tilde{\chi}_{\mathrm{B}}(t-\varrho_{\mathrm{B}}-(2N+1)\pi) \\
&- e^{-\mathrm{i}\tilde{\Omega}_{\mathrm{A}}(-\varrho_{\mathrm{B}}+(2N+2)\pi)}\tilde{\chi}_{\mathrm{B}}(t)\tilde{\chi}_{\mathrm{A}}(t+\varrho_{\mathrm{B}}-(2N+2)\pi) \\
&- e^{-\mathrm{i}\tilde{\Omega}_{\mathrm{B}}(-\varrho_{\mathrm{B}}+(2N+2)\pi)}\tilde{\chi}_{\mathrm{A}}(t)\tilde{\chi}_{\mathrm{B}}(t+\varrho_{\mathrm{B}}-(2N+2)\pi)), \qquad (6.28)
\end{aligned}$$

and now, the usual t-translation trick no longer neutralizes the phase factors. We can still try to use the same t-translation, but the answer is no longer purely imaginary. However, the summands can be compressed as before, leading to:

$$\begin{aligned}
\mathcal{M}^- =& \frac{\mathrm{i}\lambda_{\mathrm{B}}\lambda_{\mathrm{A}}}{8\pi L^2\tan\varrho_{\mathrm{B}}}\int_{-\infty}^{\infty}\mathrm{d}t\, e^{i(\tilde{\Omega}_{\mathrm{A}}+\tilde{\Omega}_{\mathrm{B}})t}\sum_{N=-\infty}^{\infty}(-\varepsilon)^{p(N)}\varsigma(N+1/2) \\
&\left(e^{i(\tilde{\Omega}_{\mathrm{B}}-\tilde{\Omega}_{\mathrm{A}})(\varrho_{\mathrm{B}}+N\pi)/2}\tilde{\chi}_{\mathrm{B}}\left(t+\frac{\varrho_{\mathrm{B}}+N\pi}{2}\right)\tilde{\chi}_{\mathrm{A}}\left(t-\frac{\varrho_{\mathrm{B}}+N\pi}{2}\right)\right. \\
&\left.+\, e^{-\mathrm{i}(\tilde{\Omega}_{\mathrm{B}}-\tilde{\Omega}_{\mathrm{A}})(\varrho_{\mathrm{B}}+N\pi)/2}\tilde{\chi}_{\mathrm{A}}\left(t+\frac{\varrho_{\mathrm{B}}+N\pi}{2}\right)\tilde{\chi}_{\mathrm{B}}\left(t-\frac{\varrho_{\mathrm{B}}+N\pi}{2}\right)\right). \qquad (6.29)
\end{aligned}$$

We are thus left with an answer only slightly more complicated than (6.24).

6.5 Gaussian switching functions

At this point, let us consider a more concrete switching function:

$$\chi_I(\tau) = e^{-(\tau-\tau_{0I})^2/2\sigma^2}. \tag{6.30}$$

Note that τ_{0I}, σ are expressed in proper time, rather than in coordinate time. Thus, the detectors are switched identically in their proper frames, but not necessarily in the coordinate frame. The Fourier transform of the switching function in proper time is now

$$\hat{\chi}_I(k) = \sigma e^{-k^2\sigma^2/2+\mathrm{i}k\tau_{0I}}. \tag{6.31}$$

We may now proceed to substitute this into our previous results.

In the geodesic case, let us assume that $\lambda_{\mathrm{A}} = \lambda_{\mathrm{B}} = \lambda$, $\tilde{\Omega}_{\mathrm{A}} = \tilde{\Omega}_{\mathrm{B}} = \Omega L, t_{0A} = -t_{0B} = -t_0/2 = -\tau_0/2L$, $\tilde{\sigma}_{\mathrm{A}} = \tilde{\sigma}_{\mathrm{B}} = \sigma/L$. For $t_0 > 0$, this implies A switches first. We will also use the proper separation Δx as a physical parameter, rather than the coordinate ϱ; we then find ϱ_{B} using (6.4). Since all circular geodesics in AdS share a common proper time, these detectors are identical. Given these parameters, we find that

$$\mathcal{L}_{II} = \lambda^2 \sum_n \frac{\pi}{\omega_n} \varphi_n^2(x_{\mathrm{A}}) \sigma^2 e^{-(\omega_n/L+\Omega)^2\sigma^2} \tag{6.32}$$

$$\begin{aligned}\mathcal{L}_{\mathrm{AB}} =& \lambda^2 \sum_n \frac{\pi}{\omega_n} \varphi_n(x_{\mathrm{B}}) \varphi_n(x_{\mathrm{A}}) \\ &\times \sigma^2 e^{-(\omega_n/L+\Omega)^2\sigma^2 - \mathrm{i}(\omega_n/L+\Omega)\tau_0}.\end{aligned} \tag{6.33}$$

As usual, the commutators in $\mathcal{M}^-$ are more complicated.

$$\begin{aligned}&\tilde{\chi}_{\mathrm{B}}(t + (\varrho_{\mathrm{B}} + N\pi)/2)\tilde{\chi}_{\mathrm{A}}(t - (\varrho_{\mathrm{B}} + N\pi)/2) \\ &= L^2 e^{-((\varrho_{\mathrm{B}}+N\pi-t_0)/2)^2/\tilde{\sigma}^2} e^{-t^2/\tilde{\sigma}^2},\end{aligned} \tag{6.34}$$

$$\begin{aligned}&\chi_{\mathrm{A}}(t + (\varrho_{\mathrm{B}} + N\pi)/2)\chi_{\mathrm{B}}(t - (\varrho_{\mathrm{B}} + N\pi)/2) \\ &= L^2 e^{-((\varrho_{\mathrm{B}}+N\pi+t_0)/2)^2/\tilde{\sigma}^2} e^{-t^2/\tilde{\sigma}^2}.\end{aligned} \tag{6.35}$$

Finally, we find the entangling term, $\mathcal{M} = \mathcal{M}^+ + \mathcal{M}^-$:

$$\begin{aligned}\mathcal{M}^+ =& -\lambda^2 \sum_{n=0}^{\infty} (-\varepsilon)^{p(N)} \frac{\pi}{\omega_n} \varphi_n(x_{\text{B}}) \varphi_n(x_{\text{A}}) \\ & \times \sigma^2 \cos[\omega_n \tau_0 / L] e^{-(\Omega^2 + \omega_n^2/L^2)\sigma^2} \end{aligned} \tag{6.36}$$

$$\begin{aligned}\mathcal{M}^- =& \lambda^2 \frac{\mathrm{i}}{8\pi \tan \varrho_{\text{B}}} \tilde{\sigma} \sqrt{\pi} e^{-\tilde{\sigma}^2 \tilde{\Omega}^2} \sum_{N=-\infty}^{\infty} (-\varepsilon)^{p(N)} \varsigma(N + 1/2) \\ & \times (e^{-((\varrho_{\text{B}} + N\pi - t_0)/2)^2/\tilde{\sigma}^2} + e^{-((\varrho_{\text{B}} + N\pi + t_0)/2)^2/\tilde{\sigma}^2}) \\ =& \lambda^2 \frac{\mathrm{i}}{4\sqrt{\pi} L \tan \varrho_{\text{B}}} \sigma e^{-\sigma^2 \Omega^2} \sum_{N=-\infty}^{\infty} (-\varepsilon)^{p(N)} \varsigma(N + 1/2) \\ & \times e^{-((\varrho_{\text{B}} + N\pi)^2 L^2 + \tau_0^2)/4\sigma^2} \cosh(2(\varrho_{\text{B}} + N\pi)\tau_0 L / 4\sigma^2) \end{aligned} \tag{6.37}$$

Notably, $\mathcal{M}^+$ is real, while $\mathcal{M}^-$ is pure imaginary. This has interesting consequences, as we will later see.

In the static case, we once again set the proper gaps and switching functions of the two detectors equal. Thus, $\tilde{\Omega}_{\text{A}} = \Omega L$, $\tilde{\Omega}_{\text{B}} = \Omega(L \sec \varrho_{\text{B}})$, $\tilde{\sigma}_{\text{A}} = \sigma / L$, $\tilde{\sigma}_{\text{B}} = \sigma / (L \sec \varrho_{\text{B}})$. As for the time-displacement, we choose it to be equal and opposite in *coordinate* time: $t_{0A} = -t_{0B} = -t_0/2$. The total time displacement is still t_0, but there may now be effects on the total phases. Since t_0 is not a proper time, we instead derive it according to $t_0 = \tau_0 / L = -2\tau_{0A}/L$, holding the proper time τ_0 constant; that is, we scale the coordinate-time displacement as though it were measured at the center.

Under this choice of parameters, we find:

$$\mathcal{L}_{II} = \lambda^2 \sigma^2 \sum_{nl} \frac{\pi}{\omega_{nl}} \varphi_{nl}^2(x_I) e^{-\sigma^2(\Omega + \omega_{nl}/(L \sec \varrho_{\text{B}} I))^2}, \tag{6.38}$$

$$\begin{aligned}\mathcal{L}_{IJ} =& \lambda^2 \sigma^2 \sum_{n} \frac{\pi}{\omega_n} \varphi_n(x_J) \varphi_n(x_I) e^{-\sigma^2(\Omega + \omega_n/(L \sec \varrho_{\text{B}} I))^2/2} \\ & \times e^{-\sigma^2(\Omega + \omega_n/(L \sec \varrho_{\text{B}} J))^2/2} \, e^{-i(\omega_n + \bar{\Omega})\tau_0/L}, \end{aligned} \tag{6.39}$$

where $\bar{\Omega} = (\tilde{\Omega}_{\text{A}} + \tilde{\Omega}_{\text{B}})/2 = \Omega L(1 + \sec \varrho_{\text{B}})/2$.

Next, we calculate $\mathcal{M}^+$:

$$\begin{aligned}\mathcal{M}^+ = &-\frac{\lambda^2}{2}\sum_n \frac{\pi}{\omega_n}\varphi_n(x_{\rm B})\varphi_n(x_{\rm A})\sigma^2 \\ &\Big(e^{-(\sigma^2(\frac{\omega_n}{L\sec\varrho_{\rm B}}-\Omega)^2+\sigma^2(\frac{\omega_n}{L}+\Omega)^2)/2-{\rm i}(2n+2+(\tilde\Omega_{\rm A}-\tilde\Omega_{\rm B}))t_0} \\ &+ e^{-(\sigma^2(\frac{\omega_n}{L}-\Omega)^2+\sigma^2(\frac{\omega_n}{L\sec\varrho_{\rm B}}+\Omega)^2)/2+{\rm i}(\omega_n-(\tilde\Omega_{\rm A}-\tilde\Omega_{\rm B}))t_0}\Big) \\ &= -\lambda^2\sigma^2 e^{-\sigma^2\Omega^2+i\Omega\tau_0(\sec\varrho_{\rm B}-1)}\sum_n\frac{\pi}{\omega_n}\varphi_n(x_{\rm B})\varphi_n(x_{\rm A}) \\ &\times e^{-\sigma^2(\omega_n)^2(1+\cos^2\varrho_{\rm B})/2L^2} \\ &\times\cosh(\sigma^2\Omega(\omega_n)(1-\cos\varrho_{\rm B})/L-{\rm i}(\omega_n)\tau_0/L) \end{aligned} \tag{6.40}$$

employing the identity (5.32), where we use the fact $\tilde\sigma_I\tilde\Omega_I=\sigma\Omega$ to simplify the final result. Clearly, $\mathcal{M}^+$ is no longer real.

The switching functions appearing in $\mathcal{M}^-$ become

$$\begin{aligned}&\tilde\chi_{\rm B}\left(t+\frac{\varrho_{\rm B}+N\pi}{2}\right)\tilde\chi_{\rm A}\left(t-\frac{\varrho_{\rm B}+N\pi}{2}\right) \\ &=L^2(\sec\varrho_{\rm B})e^{-(t+\frac{\varrho_{\rm B}+N\pi-t_0}{2})^2/2\tilde\sigma_{\rm B}^2}e^{-(t-\frac{\varrho_{\rm B}+N\pi-t_0}{2})^2/2\tilde\sigma_{\rm A}^2} \\ &=L^2(\sec\varrho_{\rm B})e^{-\frac{(\varrho_{\rm B}+N\pi-t_0)^2}{2(\tilde\sigma_{\rm A}^2+\tilde\sigma_{\rm B}^2)}}e^{-\left(t+(\varrho_{\rm B}+N\pi-t_0)\frac{\tilde\sigma_{\rm A}^2-\tilde\sigma_{\rm B}^2}{\tilde\sigma_{\rm A}^2+\tilde\sigma_{\rm B}^2}\right)^2/2\tilde\sigma_{\rm AB}^2}, \end{aligned} \tag{6.41}$$

$$\begin{aligned}&\tilde\chi_{\rm A}\left(t+\frac{\varrho_{\rm B}+N\pi}{2}\right)\tilde\chi_{\rm B}\left(t-\frac{\varrho_{\rm B}+N\pi}{2}\right) \\ &=L^2(\sec\varrho_{\rm B})e^{-(t+\frac{\varrho_{\rm B}+N\pi+t_0}{2})^2/2\tilde\sigma_{\rm A}^2}e^{-(t-\frac{\varrho_{\rm B}+N\pi+t_0}{2})^2/2\tilde\sigma_{\rm B}^2} \\ &=L^2(\sec\varrho_{\rm B})e^{-\frac{(\varrho_{\rm B}+N\pi+t_0)^2}{2(\tilde\sigma_{\rm A}^2+\tilde\sigma_{\rm B}^2)}}e^{-\left(t-(\varrho_{\rm B}+N\pi+t_0)\frac{\tilde\sigma_{\rm A}^2-\tilde\sigma_{\rm B}^2}{\tilde\sigma_{\rm A}^2+\tilde\sigma_{\rm B}^2}\right)^2/2\tilde\sigma_{\rm AB}^2}, \end{aligned} \tag{6.42}$$

where $\tilde\sigma_{\rm AB}^2=\tilde\sigma_{\rm A}^2\tilde\sigma_{\rm B}^2/(\tilde\sigma_{\rm A}^2+\tilde\sigma_{\rm B}^2)$. Applying the final integral term-by-term, we find:

$$\begin{aligned}\mathcal{M}^- =&\frac{{\rm i}\lambda^2}{8\pi\sin\varrho_{\rm B}}\sum_{N=-\infty}^{\infty}(-\varepsilon)^{p(N)}\varsigma(N+1/2) \\ &\times\tilde\sigma_{\rm AB}\sqrt{2\pi}e^{-2\sigma_{\rm AB}^2\bar\Omega^2+2{\rm i}t_0\bar\Omega\frac{\tilde\sigma_{\rm A}^2-\tilde\sigma_{\rm B}^2}{\tilde\sigma_{\rm A}^2+\tilde\sigma_{\rm B}^2}} \\ &\times\Big(e^{-\frac{(\varrho_{\rm B}+N\pi-t_0)^2}{2(\tilde\sigma_{\rm A}^2+\tilde\sigma_{\rm B}^2)}-{\rm i}(\varrho_{\rm B}+N\pi)\frac{\tilde\sigma_{\rm A}^2\tilde\Omega_{\rm A}-\tilde\sigma_{\rm B}^2\tilde\Omega_{\rm B}}{\tilde\sigma_{\rm A}^2+\tilde\sigma_{\rm B}^2}} \\ &+e^{-\frac{(\varrho_{\rm B}+N\pi+t_0)^2}{2(\tilde\sigma_{\rm A}^2+\tilde\sigma_{\rm B}^2)}+{\rm i}(\varrho_{\rm B}+N\pi)\frac{\tilde\sigma_{\rm A}^2\tilde\Omega_{\rm A}-\tilde\sigma_{\rm B}^2\tilde\Omega_{\rm B}}{\tilde\sigma_{\rm A}^2+\tilde\sigma_{\rm B}^2}}\Big)\end{aligned}$$

$$
\begin{aligned}
=&\frac{i\lambda^2}{8\pi\sin\varrho_{\rm B}}\tilde{\sigma}_{\rm AB}\sqrt{2\pi}e^{-2\sigma_{\rm AB}^2\bar{\Omega}^2+2{\rm i}t_0\bar{\Omega}\frac{\tilde{\sigma}_{\rm A}^2-\tilde{\sigma}_{\rm B}^2}{\tilde{\sigma}_{\rm A}^2+\tilde{\sigma}_{\rm B}^2}}\\
&\times\sum_{N=-\infty}^{\infty}(-\varepsilon)^{p(N)}\varsigma(N+1/2)e^{-\frac{(\varrho_{\rm B}+N\pi)^2+t_0^2}{2(\tilde{\sigma}_{\rm A}^2+\tilde{\sigma}_{\rm B}^2)}}\\
&\times 2\cosh\left[\frac{\varrho_{\rm B}+N\pi}{\tilde{\sigma}_{\rm A}^2+\tilde{\sigma}_{\rm B}^2}\left(t_0-{\rm i}(\tilde{\sigma}_{\rm A}^2\tilde{\Omega}_{\rm A}-\tilde{\sigma}_{\rm B}^2\tilde{\Omega}_{\rm B})\right)\right]\\
=&\frac{i\lambda^2}{8\pi L\sin\varrho_{\rm B}}\sigma\sqrt{\frac{2\pi}{1+\sec^2\varrho_{\rm B}}}\\
&\times e^{-\frac{(1+\sec\varrho_{\rm B})^2}{1+\sec^2\varrho_{\rm B}}\sigma^2\Omega^2/2+{\rm i}\tau_0\Omega\frac{(1-\cos^2\varrho_{\rm B})(1+\sec\varrho_{\rm B})}{1+\cos^2\varrho_{\rm B}}}\\
&\times\sum_{N=-\infty}^{\infty}(-\varepsilon)^{p(N)}\varsigma(N+1/2)e^{-\frac{(\varrho_{\rm B}+N\pi)^2L^2+\tau_0^2}{2\sigma^2(1+\cos^2\varrho_{\rm B})}}\\
&\times 2\cosh\left[\frac{(\varrho_{\rm B}+N\pi)L}{1+\cos^2\varrho_{\rm B}}\left(\tau_0/\sigma^2-{\rm i}\Omega(1-\cos\varrho_{\rm B})\right)\right]
\end{aligned}
\tag{6.43}
$$

Evidently $\mathcal{M}^-$ is no longer pure imaginary either. These phase shifts are a symptom of the unequal $\tilde{\Omega}_I$; were the coordinate gaps equal, this would not happen. However, it is not clear whether the relative phase between $\mathcal{M}^\pm$ can be predicted merely from the coordinate gaps.

As before, the two physical quantities we would like to calculate are (the estimator $\mathcal{N}^{(2)}$ of) the logarithmic negativity, an entanglement monotone; and the mutual information. Recall (5.13): in the geodesic case, because $\mathcal{L}_{\rm AA}=\mathcal{L}_{\rm BB}$, this is simply

$$
\mathcal{N}^{(2)}=|\mathcal{M}|-\mathcal{L}_{II}. \tag{6.44}
$$

As for the mutual information,

$$
I(\rho_{\rm AB})=S(\rho_{\rm A})+S(\rho_{\rm B})-S(\rho_{\rm AB}) \tag{6.45}
$$

where $S=-Tr(\rho\log\rho)$ is the von Neumann entropy and $\rho_I=Tr_J(\rho_{IJ})$ is the partial trace of the total state of two detectors. In terms of our density matrix terms, we find [31]:

$$
\begin{aligned}
I(\rho_{\rm AB})=&\mathcal{L}_+\log\mathcal{L}_+ + \mathcal{L}_-\log\mathcal{L}_-\\
&-\mathcal{L}_{\rm AA}\log\mathcal{L}_{\rm AA}-\mathcal{L}_{\rm BB}\log\mathcal{L}_{\rm BB}
\end{aligned}
\tag{6.46}
$$

where

$$
\mathcal{L}_\pm=\frac{1}{2}\left(\mathcal{L}_{\rm AA}+\mathcal{L}_{\rm BB}\pm\sqrt{(\mathcal{L}_{\rm AA}-\mathcal{L}_{\rm BB})^2+4|\mathcal{L}_{\rm AB}|^2}\right). \tag{6.47}
$$

In the geodesic case, this can be simplified to

$$\mathcal{L}_{\pm} = \mathcal{L}_{\text{AA}} \pm |\mathcal{L}_{\text{AB}}|. \tag{6.48}$$

6.6 Results

Let us begin by characterizing the transition probability of a single detector. While the transition probability of a uniformly accelerating single detector in AdS_4 was previously calculated in [14], that was in the context of asymptotically slow switching; our finite time switching may therefore lead to qualitatively different results. We also consider negative gaps, i.e. where the detector is initially excited. For brevity, we will mostly plot the Dirichlet case, $\varepsilon = 1$; we will describe any differences between boundary conditions in text.

6.6.1 Transition rates

We compute L_{II} for a static detector as a function of gap and position, where we use $\sigma = 1$ as our reference length scale, and plot it in Fig. 6.1. Notably, there is essentially no dependence on the position of the detector, at least at this scale. Since we are switching for finite time, even a detector with positive gap can become excited. On the other hand, a detector of negative gap spontaneously de-excites; the larger the gap, the faster this occurs. Fig. 6.1a also exhibits some resonances for $L = \sigma$, where the detector couples to different AdS modes. Different boundaries have different modes, and thus different boundary conditions: as we previously noted, the Neumann modes are offset from the Dirichlet modes, while the transparent modes contain both the Neumann and Dirichlet modes. Notably, the first mode has a lower energy in the Neumann case: as shown in Fig. 6.1a, this also causes the transition rate to decay faster for positive Ω. Since the transition rate acts as a noise term in our entanglement, however, we will typically seek to minimize it. We thus will mostly focus our attention on positive gaps. (Of course, as discussed earlier, the geodesic detector has the same behaviour regardless of its position.) We also note that the analytic Wightman function yields identical results.

6.6.2 Geodesic entanglement harvesting

We now analyze the entanglement harvested by two geodesic detectors, via the logarithmic negativity estimator $\mathcal{N}^{(2)}$. This quantity has a certain advantage over the negativity proper:

(a) $\delta x = 0$

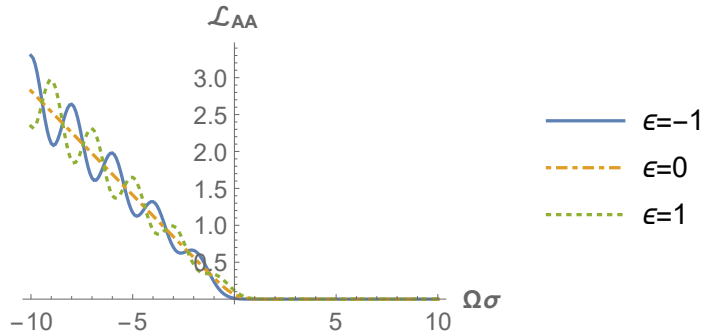

(b) $\Omega = 2/\sigma$

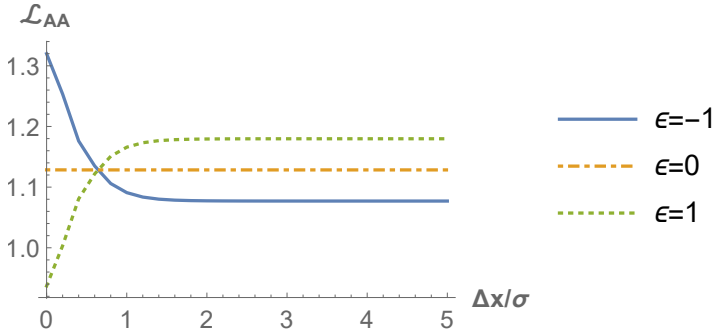

Figure 6.1: The one-detector transition rate for the static detector, $L = \sigma$, varying Ω and δx separately. Note the resonances visible in Fig. 6.1a.

namely, it provides an intuitive way to think of 'almost' entangled systems. A similar scenario was previously calculated by [31] in flat space, and will serve as a comparison. However, AdS is not flat, so some special considerations come into play. First, the curvature scale L acts as an additional parameter: $L \to \infty$ is the flat space limit, while $L \to 0$ is the limit of infinite curvature. In particular, one would imagine that for $L < \sigma$, qualitative differences from flat space should be apparent: at that point, the detector can probe the discrete spectrum of AdS. However, it seems that the existence of entanglement does not change: for any separation, there exists some threshold gap, above which entanglement exists. We show a gap/separation plot for $L = 5\sigma$ in Figure 6.2, where we have plotted $\mathcal{N}^{(2)}$ from (5.15). Notably, much as in flat space, the curve where $\mathcal{N}^{(2)} = 0$ is almost linear, independent of the value of ε. In fact, even for $L = \sigma$, the entire gap/separation plot is almost identical, with the threshold in the same place.

The fact that the zero contour is a line is more interesting than it appears. In [31], it was demonstrated that the boundary is a straight line for both (3+1)-D and (1+1)-D Minkowski space, when the detector is switched via Gaussian, suggesting the dimension is not a factor here; [8] found similar results in AdS_3. However, both papers show this linear relation breaks down at small gap and separation. In this regime, we have instead found that AdS_4 still appears linear; in particular, it appears that even degenerate detectors can harvest entanglement, while this is not possible in Minkowski space. Since the finite switching implies the detectors are in causal contact, the theorem of [30] does not apply; however, this is still one factor that separates AdS_4 from both AdS3 and Minkowski space and may merit further investigation.

Another feature of AdS becomes relevant once L becomes comparable to σ. As noted previously, it takes a coordinate time of π for a signal to go from the origin to the boundary and back again; thus, the time it takes for a signal to travel from one detector to the other is bounded by $\pi/2$. Therefore, no matter how large the proper separation of two detectors, they will become causally connected for small L. (In fact, this is also true for nonconformal fields: two detectors will be causally connected for sufficiently small L.) This makes maintaining spacelike separation problematic. Nevertheless, despite the lack of spacelike separation, we may still study the quantity of entanglement harvested. In this regime, the boundary condition will become more important.

With these caveats in mind, we plot the dependence of $\mathcal{N}^{(2)}$on curvature length and proper separation, keeping the gap constant at $\Omega = 3\sigma$, shown in Fig. 6.3a. Selected slices of this graph are shown in Figs. 6.3b and 6.3c for greater detail. As we would expect, at large L we approach the results found in flat space. On the other hand, entanglement decreases to zero for small L. However, it seems that even as $L \to 0$, the maximum distance at which entanglement exists *increases*. This is perhaps due to the previously mentioned

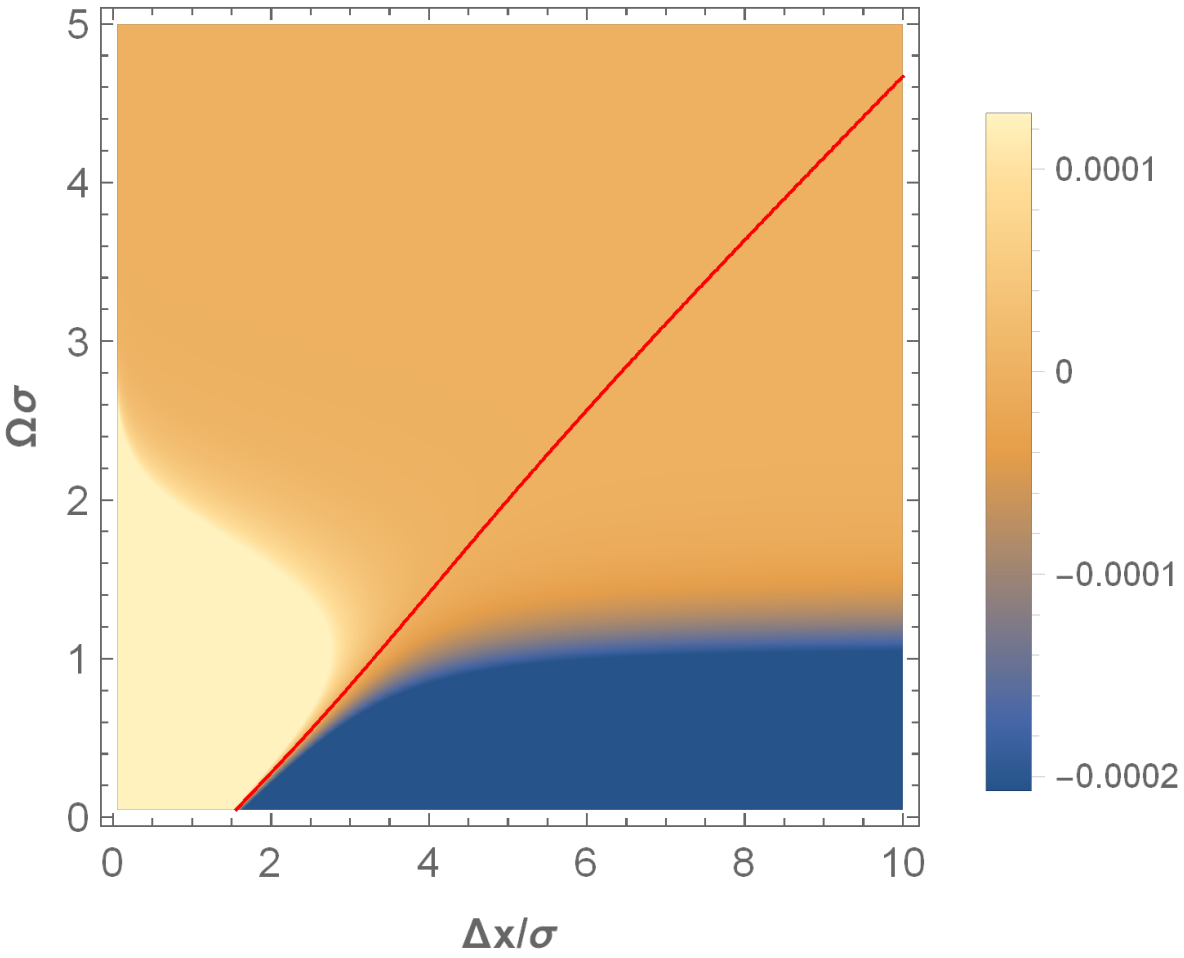

Figure 6.2: $\mathcal{N}^{(2)}$ values for varying separation and gap. $\varepsilon = -1$. Zero contour marked in red. Region where $\mathcal{N}^{(2)} > 0$ appears to be limited in size, even as $L \to \infty$.

caveat: at sufficiently high curvature, all detectors are causally connected.

At this point, we refer to Figs. 6.3b and 6.3c for the effect of different boundary conditions. While little difference is visible at large L, the small L limit shows drastic effects. This is due to the different lowest energy modes of AdS: while the first Dirichlet mode decays with distance, the first Neumann mode (and thus the first transparent mode) is evenly spread out over all of space; thus, the Dirichlet entanglement decays much faster with distance. (Notably, the lowest energy Neumann mode would, under different conventions, be a zero mode. However, the coupling to the Ricci scalar prevents this mode from having zero energy.)

Next, we plot in Fig. 6.4 the negativity and mutual information, changing the separation of detectors in time and space. The support of the commutator, the light cones, can be seen reflecting off the boundary in Fig. 6.4a. There are also subtler signatures of the boundary conditions: notably, it is only in the von Neumann condition $\varepsilon = 1$ in Fig. 6.4e that entanglement can vanish for zero separation. Of course, since the boundaries are reflective, the negativity and mutual information are nearly periodic. (In the transparent case in Fig. 6.4c, while the light cone does not reflect off the boundary, it does return at a later time, after passing through the embedding ESU space.) However, it is less obvious why $\mathcal{M}^+$ is also affected by the boundary conditions: in Figs. 6.4b-6.4f; the mutual information still is affected by the boundary conditions, despite not involving the commutator. This may merit further investigation.

The periodicity of $\mathcal{N}^{(2)}$ is not perfect, however: careful study shows the maximum at $\Delta t = 0$ is different from the others. For smaller L, e.g. $L = sigma$, while the other peaks blur together, the central peak grows dramatically, as shown in Figure 6.5. However, even as time displacement is increased to infinity, the negativity does not decay, but instead takes on a periodic pattern. By contrast, in a normal cavity, the negativity will decay to zero as time displacement is increased. This oddity is due to the fact that all field operators of AdS are periodic. (This is true even in the minimally coupled case.) In this limit, although the graphs look fairly similar, different boundary conditions lead to wildly different values of entanglement extracted. While we also calculated $I(\rho_{\text{AB}})$ for $L = \sigma, \Omega = 2/\sigma$, there was no variation with respect to Δt; therefore, we have omitted these graphs.

6.6.3 Static Entanglement Harvesting

We now consider the static detector case. First, we plot another gap/separation graph, for curvature scales $L = 5\sigma$ in Fig. 6.6, with qualitatively similar results (not illustrated)

(a) $\Omega = 3/\sigma, \varepsilon = -1$

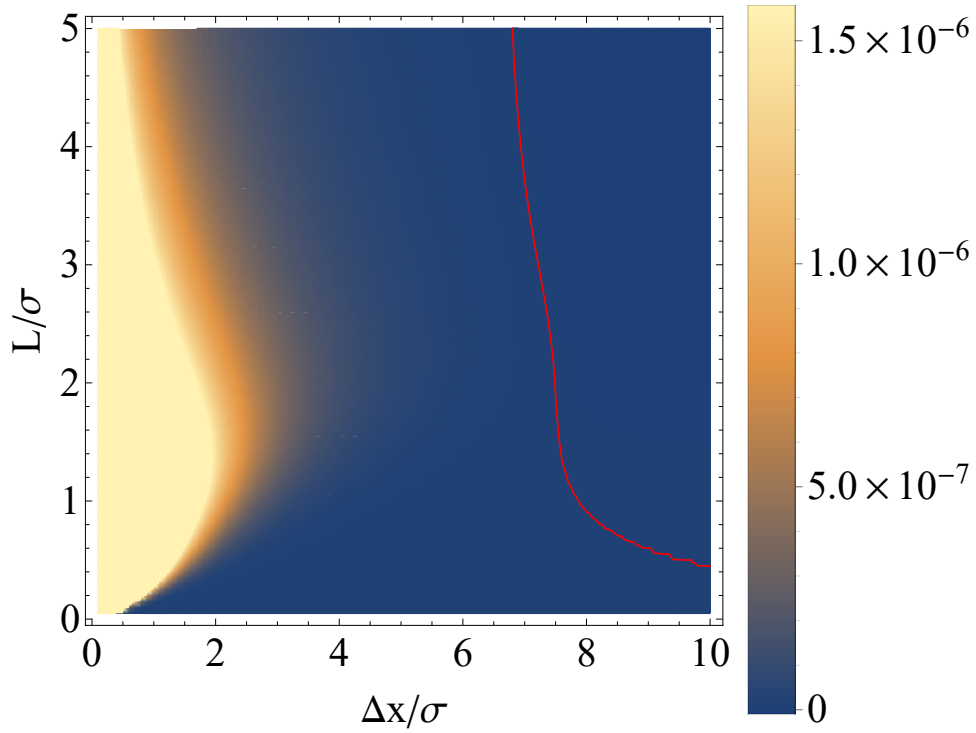

(b) $\Omega = 3/\sigma, \Delta x = 6\sigma$

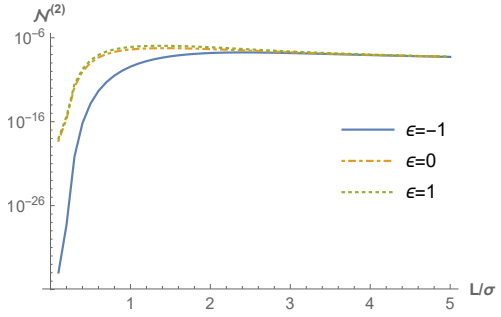

(c) $\Omega = 3/\sigma, L = \sigma$

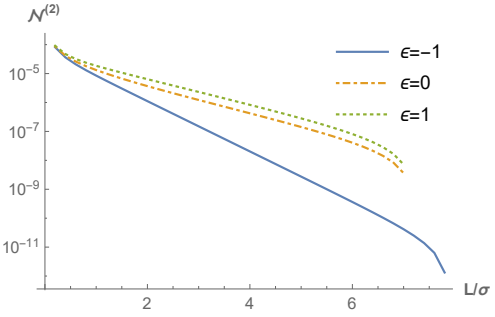

Figure 6.3: $\mathcal{N}^{(2)}$ two geodesic detectors for varying boundary conditions, one at the origin, one at proper separation Δx.

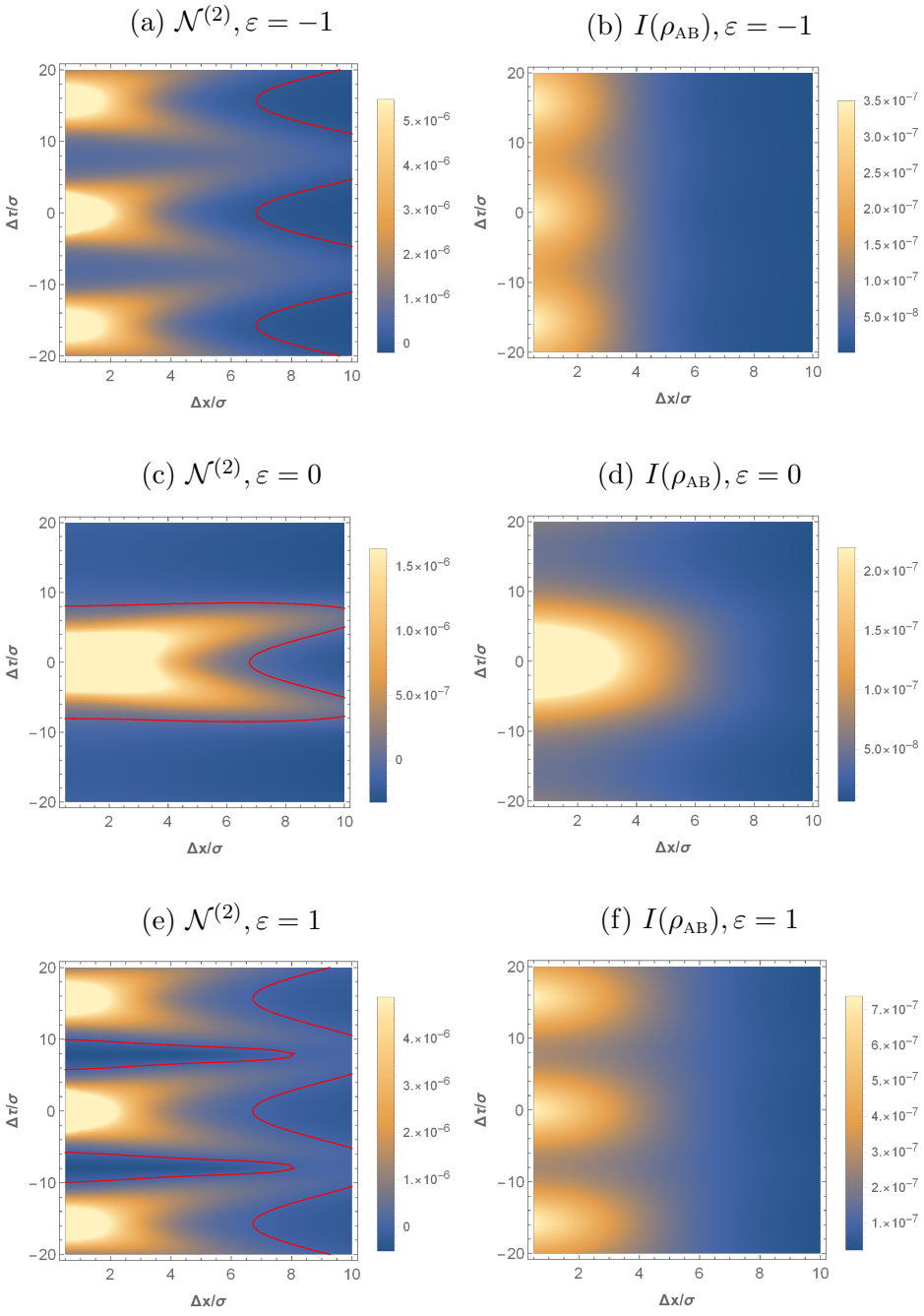

Figure 6.4: $\mathcal{N}^{(2)}$ and $I(\rho_{AB})$ for geodesic detectors configuration vs. separation in space and time. $L = 5\sigma, \Omega = 3/\sigma$. Zero contour in red.

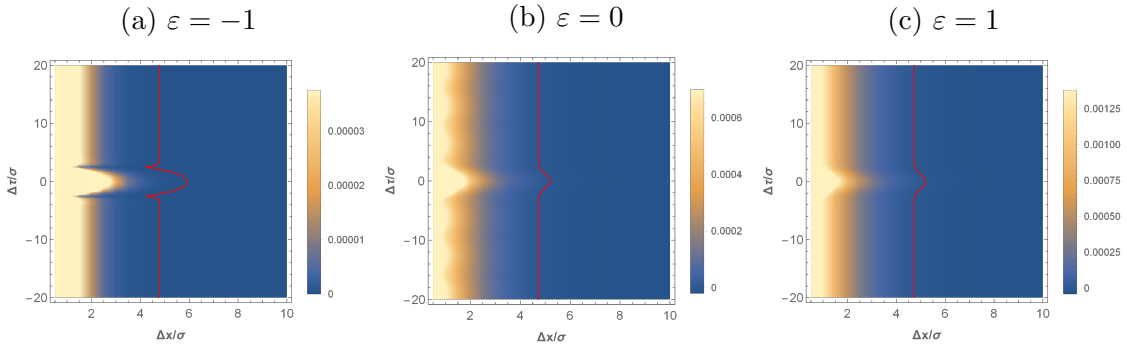

Figure 6.5: $\mathcal{N}^{(2)}$ for geodesic detectors, one at the origin, as a function of separation in space and time. $L = \sigma, \Omega = 2/\sigma$. Zero contour in red.

for $L = \sigma$. Much as in the geodesic case, there is a straight line separating the region of entanglement from the region of separability.

We next plot the dependence of negativity on the separation and curvature scale in Fig. 6.7. However, in order to calculate $\mathcal{L}_{\text{BB}}$, larger separations require exponentially more resources in the static case. Here we see our first major difference from the geodesic case: an island of separability, bounded by the red line in the figure. While unusual, this feature does not appear to be an artifact, persisting even when the precision of the calculation is increased. This feature is also visible in all boundary conditions. (Notably, the Dirichlet condition has the smallest island.) This phenomenon is not particular to AdS_4; a similar island has been shown to appear in AdS_3 with similar parameters, using different methods [8]. There are no obvious resonances at this choice of parameters; the meaning of this island is a matter for further study. The behaviour as L becomes small is also different from the geodesic case: for sufficiently small L, there is a local maximum in negativity as a function of separation. However, our calculations show that for even smaller L, the negativity does indeed vanish.

Next, the dependence of the negativity and the mutual information on the time/space separation is shown in Fig. 6.8, for parameters $L = 5\sigma, \Omega = 3/\sigma$. The difference from the geodesic case is stark. Compared to the geodesic case, it appears that entanglement is possible at much larger distances. However, a series of 'waves' also appears, negativity fluctuating wildly with time and distance. In fact, within the troughs, there are small regions where negativity vanishes. As these features are not apparent in $\mathcal{M}^+$ and $\mathcal{M}^-$ individually, we conclude that they are due to their relative phase; however, we do not yet have a way to predict that phase.

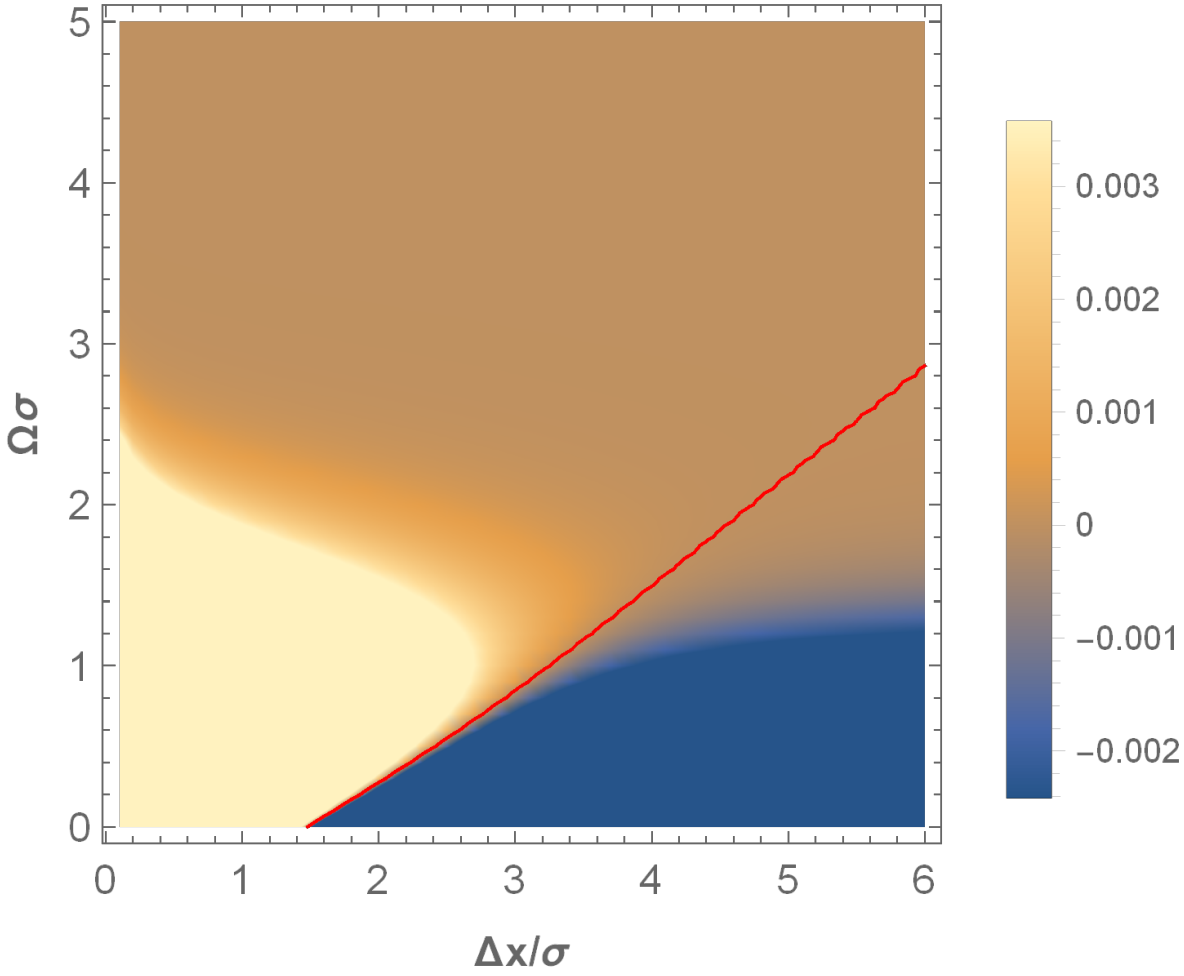

Figure 6.6: $\mathcal{N}^{(2)}$ for a pair of static detectors separated by Δx and having proper gap Ω, with AdS length $L = 5\sigma$. Note that coarseness of $\mathcal{N}^{(2)}$ appears to be an artifact of the plot grid. The zero contour is in red; we see it bounds an island of spacelike entanglement.

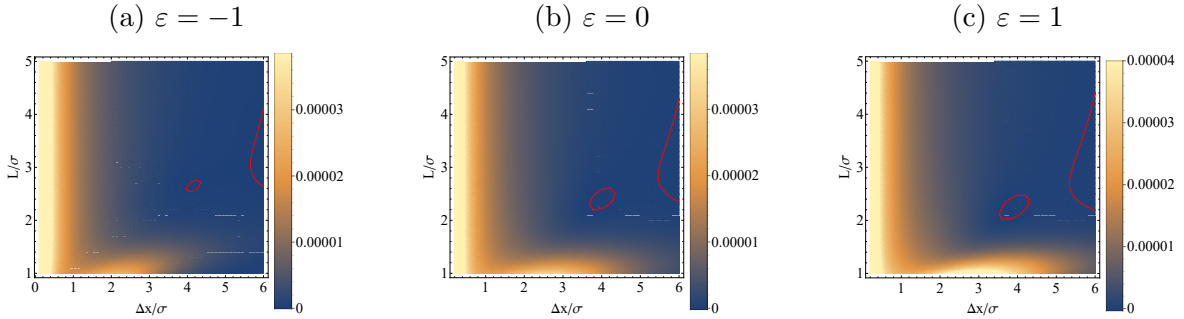

Figure 6.7: $\mathcal{N}^{(2)}$ for the static detector configuration vs. curvature length L and proper separation Δx. Zero contours in red. Note the island of separability, in which there is no entanglement.

Calculating for smaller curvature, $L = \sigma, \Omega = 2/\sigma$ in Figs. 6.9a-6.9e, we get similar results: entanglement reaches further than in the geodesic case, but the waves also appear. Strangely, there appears to be a local maximum in negativity achieved at some finite distance. We believe that both the greater reach of entanglement and this local maximum are due to an enhancement of negativity, from the mismatch in redshifts. However, once again we lack a comprehensive understanding of this effect.

There is also a subtle, but significant time asymmetry: that is, the negativity changes depending on which detector switches first. Something similar happens in AdS_3 [8], albeit with much larger effect: when detector A, at the centre, switches first, $\Delta t > 0$, the quantity of entanglement becomes much larger. In both cases this effect disappears for larger AdS curvatures. We suspect that the effect is much stronger in AdS_3 due to the violation of the strong Huygens principle: in that spacetime, the commutator lingers inside the light cone, allowing for stronger asymmetries in time.

On the other hand, the mutual information, shown in Figs. 6.8b-6.8f and 6.9b-6.9f does not have any notable differences from the geodesic case: in some sense, the mutual information appears to have less information about the spacetime than the entanglement. Notably, there is still a subtle dependence on which detector switches first. This may not be entirely surprising, since the detectors are in different physical situations. However, one feature from the entanglement case remains: there is a finite non-zero distance at which mutual information is also maximized. While we believe this to be a result of the different redshifts, once again more information is required.

In summary, the static detector case shows many interesting phenomena compared to the geodesic detector case. We believe that the "waves" are a consequence of the detector

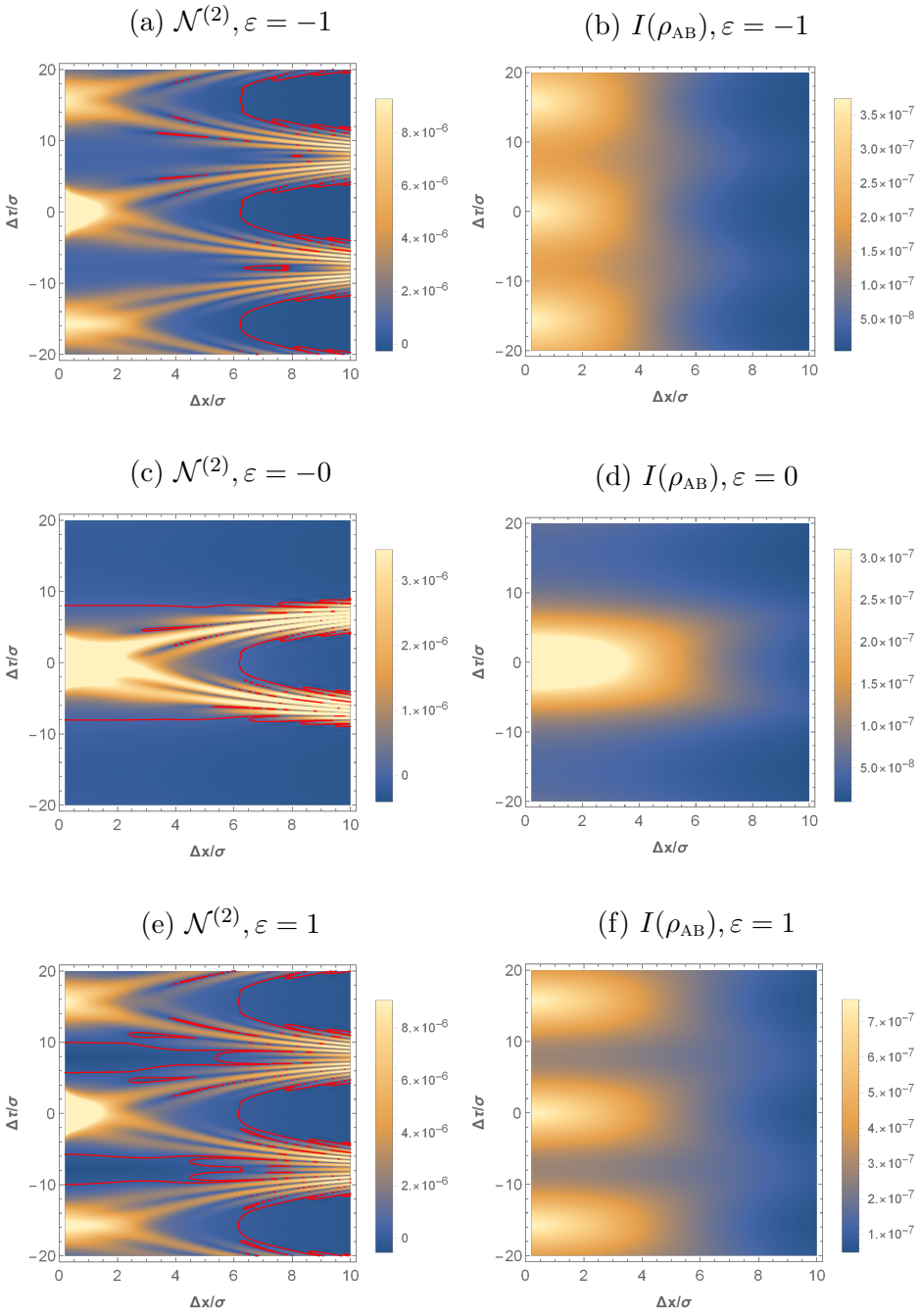

Figure 6.8: $\mathcal{N}^{(2)}$ and $I(\rho_{AB})$ for the static detector configuration vs. separation in space and time. $L = 5\sigma, \Omega = 3/\sigma$. Zero contours in red.

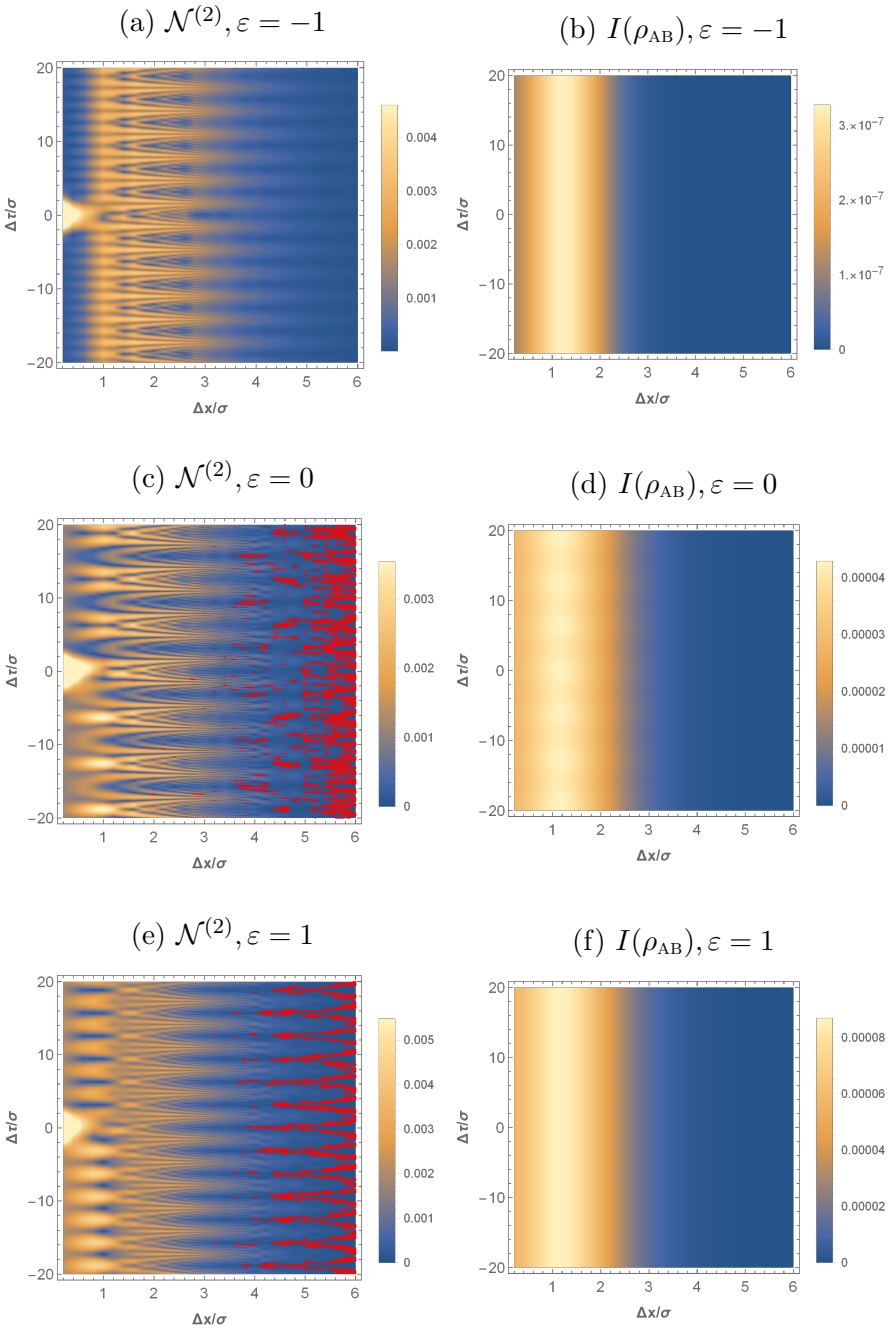

Figure 6.9: $\mathcal{N}^{(2)}$ and $I(\rho_{AB})$ for the static detector configuration vs. separation in space and time. $L = \sigma, \Omega = 2/\sigma$. Zero contours in red.

gaps being unequal in the coordinate frame. However, this theory would require further evidence to be verified. In particular, the unequal gap case has not been studied very much, even in flat space, while the other cases of static detector entanglement in curved space are not immediately comparable (e.g. being in (2+1) dimensions, as in [8, 7]). Many questions yet remain.

6.6.4 Summary of results

As a curved, highly symmetric spacetime, AdS_4 serves as an ideal testbed for the methods we developed in the previous chapter. Using (5.27), and the analytic form of the commutator, we were able to compute the entanglement harvested by a pair of detectors, both in geodesic and static configurations. We then plotted their dependence on various parameters, and compared them to findings both in flat space [31] and in AdS_3 [8].

While we found that the entanglement negativity is sensitive to the curvature of AdS and the boundary condition, many unanswered questions remain. In particular, while the static case is the most generic, many new and unprecedented phenomena were observed, and still defy explanation. If entanglement harvesting is to be used to probe less symmetric spacetimes, these oddities will need to be studied further.

Chapter 7

Closing remarks

The aim of this thesis was to demonstrate the ability of the Unruh-DeWitt detector to probe the structure of the spacetime around it, and to characterize the behaviour of its one- and two-detector statistics. We have seen how the transition rate of a detector responds to an enclosing shell, and to a topological black hole geon. Then, we developed a formalism to calculate detector entanglement more efficiently, and deployed it to find a novel analytic expression in flat space, before applying it to (3+1)-dimensional Anti-de Sitter space.

However, while our research has answered some questions, it raises many more. From the shell case, we noted that it may, in principle, be possible to characterize the mass distribution about the detector using the entire transition function. There are two possibilities: either the transition function contains enough information to reconstruct an entire spherically-symmetric spacetime; or two spherically-symmetric spacetimes share the same spectrum, the same transition function. We believe the former to be more likely, which would imply that the entire radial profile of a spherically-symmetric spacetime is stored in the centre, within the quantum field state.

Next, in the geon case, we showed that a topological feature inside a black hole could be detected outside a black hole. However, while such information is carried away with the Hawking radiation, it is unclear whether the technique generalizes to other infalling information: after all, the geon is an inherently eternal spacetime, while black holes formed by the collapse of matter are not. Of course, the question of what happens to infalling information is the central question of the Information Paradox, so it is not surprising that we have barely scratched the surface.

In these first two cases, we demonstrated how a single detector, interacting locally with a global field state, could retrieve information about the global structure of spacetime. We

have therefore shown that when detectors interact with a quantum field on a spacetime, invoking the Equivalence Principle is not enough; the only way to determine how the detectors behave is to calculate. In the following two cases, we changed tracks: instead of one detector, we investigated how a pair of detectors behaved while interacting with a quantum field on a curved spacetime. The quantity of entanglement harvested is another promising tool to understand the structure of spacetime, which we sought to develop further.

We then demonstrated a powerful new technique for calculating the entanglement harvested by two detectors. We have little doubt that this technique will be quite useful, and find application in many other spacetimes. However, it remains to be seen whether the result generalizes to higher spin fields, interacting fields, or even more exotic objects.

Lastly, we studied (3+1)-dimensional Anti-de Sitter space, and quantified the entanglement harvested by two detectors, using our new method. While we were successful at computing the entanglement in a wide range of parameters, we were unable to explain the broad variety of phenomena that arose in the static case. Where did the waves in the space/time separation graph come from? Why is there a local maximum of entanglement at a finite distance? In most spacetimes, two detectors cannot be deployed at equal redshift, making the static case the norm, not the exception. Therefore, in order to study entanglement harvesting in curved spacetimes, these redshift-related phenomena must be studied and characterized.

It is our hope that our thesis serves a guide to future researchers in the field of entanglement harvesting. We have demonstrated how detectors respond to the structure of spacetime, and shown how this response may be calculated. We have also discovered a wealth of phenomena for the entanglement harvested by two detectors at different redshift. If these phenomena may be understood, and our method used to calculate entanglement harvesting in more spacetimes, it might be possible to fully characterize how UDW detectors interact with spacetime, and use UDW detectors as a tool to understand spacetime in turn. Perhaps one day, this interaction between quantum field theory and general relativity might be fully understood: A small step towards a bright future for physics.

References

[1] Ahmed Almheiri, Donald Marolf, Joseph Polchinski, and James Sully. Black Holes: Complementarity or Firewalls? *JHEP*, 02:062, 2013.

[2] S. J. Avis, C. J. Isham, and D. Storey. Quantum field theory in anti-de sitter space-time. *Phys. Rev. D*, 18:3565–3576, Nov 1978.

[3] N.D. Birrell and P.C.W. Davies. *Quantum Fields in Curved Space*. Cambridge Monographs on Mathematical Physics. Cambridge University Press, 1984.

[4] Stanley Deser and Orit Levin. Accelerated detectors and temperature in (anti)-de Sitter spaces. *Class. Quant. Grav.*, 14:L163–L168, 1997.

[5] Bryce S. DeWitt. QUANTUM GRAVITY: THE NEW SYNTHESIS. In *General Relativity: An Einstein Centenary Survey*, pages 680–745. 1980.

[6] S. W. Hawking. Particle creation by black holes. *Comm. Math. Phys.*, 43:199–220, 1975.

[7] L. J. Henderson, R. A. Hennigar, R. B. Mann, A. R. H. Smith, and J. Zhang. Harvesting Entanglement from the Black Hole Vacuum. 2017.

[8] Laura J. Henderson, Robie A. Hennigar, Robert B. Mann, Alexander R. H. Smith, and Jialin Zhang. Entangling detectors in anti-de Sitter space. 2018.

[9] Lee Hodgkinson. *Particle detectors in curved spacetime quantum field theory*. PhD thesis, 2013.

[10] Lee Hodgkinson, Jorma Louko, and Adrian C. Ottewill. Static detectors and circular-geodesic detectors on the Schwarzschild black hole. *Phys. Rev.*, D89(10):104002, 2014.

[11] Daniel Hümmer, Eduardo Martín-Martínez, and Achim Kempf. Renormalized Unruh-DeWitt Particle Detector Models for Boson and Fermion Fields. *Phys. Rev. D*, 93(2):024019, 2016.

[12] W. Israel. Event Horizons in Static Vacuum Space-Times. *Physical Review*, 164:1776–1779, December 1967.

[13] W. Israel. Thermo field dynamics of black holes. *Phys. Lett.*, A57:107–110, 1976.

[14] David Jennings. On the response of a particle detector in Anti-de Sitter spacetime. *Class. Quant. Grav.*, 27:205005, 2010.

[15] Carl Kent and Elizabeth Winstanley. The global rotating scalar field vacuum on anti-de Sitter space–time. *Phys. Lett. B*, 740:188–191, 2015.

[16] E. W. Leaver. Solutions to a generalized spheroidal wave equation: Teukolsky's equations in general relativity, and the two-center problem in molecular quantum mechanics. *Journal of Mathematical Physics*, 27(5):1238–1265, 1986.

[17] Jorma Louko and Donald Marolf. Inextendible Schwarzschild black hole with a single exterior: How thermal is the Hawking radiation? *Phys. Rev.*, D58:024007, 1998.

[18] Jorma Louko and Alejandro Satz. Transition rate of the Unruh-DeWitt detector in curved spacetime. *Class. Quant. Grav.*, 25:055012, 2008.

[19] Juan Martin Maldacena. The Large N limit of superconformal field theories and supergravity. *Int. J. Theor. Phys.*, 38:1113–1133, 1999. [Adv. Theor. Math. Phys.2,231(1998)].

[20] Eduardo Martín-Martínez. Causality issues of particle detector models in QFT and Quantum Optics. *Phys. Rev. D*, 92(10):104019, 2015.

[21] Eduardo Martín-Martínez and Pablo Rodriguez-Lopez. Relativistic quantum optics: The relativistic invariance of the light-matter interaction models. *Phys. Rev. D*, 97:105026, May 2018.

[22] Eduardo Martín-Martínez, Alexander R. H. Smith, and Daniel R. Terno. Spacetime structure and vacuum entanglement. *Phys. Rev. D*, 93:044001, Feb 2016.

[23] C.W. Misner, K.S. Thorne, J.A. Wheeler, and D.I. Kaiser. *Gravitation*. Princeton University Press, 2017.

[24] Keith K. Ng, Lee Hodgkinson, Jorma Louko, Robert B. Mann, and Eduardo Martín-Martínez. Unruh-DeWitt detector response along static and circular geodesic trajectories for Schwarzschild-AdS black holes. *Phys. Rev. D*, D90(6):064003, 2014.

[25] Keith K. Ng, Robert B. Mann, and Eduardo Martín-Martínez. The equivalence principle and QFT: Can a particle detector tell if we live inside a hollow shell? *Phys. Rev. D*, 94(10):104041, 2016.

[26] Keith K. Ng, Robert B. Mann, and Eduardo Martín-Martínez. Over the horizon: distinguishing the Schwarzschild spacetime and the $\mathbb{RP}^3$ spacetime using an Unruh-DeWitt detector. *Phys. Rev. D*, 96(8):085004, 2017.

[27] Keith K. Ng, Robert B. Mann, and Eduardo Martín-Martínez. Unruh-DeWitt detectors and entanglement: The anti–de Sitter space. *Phys. Rev. D*, 98(12):125005, 2018.

[28] Keith K. Ng, Robert B. Mann, and Eduardo Martíín-Martínez. New techniques for entanglement harvesting in flat and curved spacetimes. *Phys. Rev. D*, 97(12):125011, 2018.

[29] Joseph Polchinski. The Black Hole Information Problem. In *Proceedings, Theoretical Advanced Study Institute in Elementary Particle Physics: New Frontiers in Fields and Strings (TASI 2015): Boulder, CO, USA, June 1-26, 2015*, pages 353–397, 2017.

[30] Alejandro Pozas-Kerstjens, Jorma Louko, and Eduardo Martín-Martínez. Degenerate detectors are unable to harvest spacelike entanglement. *Phys. Rev. D*, 95(10):105009, 2017.

[31] Alejandro Pozas-Kerstjens and Eduardo Martín-Martínez. Harvesting correlations from the quantum vacuum. *Phys. Rev. D*, 92(6):064042, 2015.

[32] Alejandro Pozas-Kerstjens and Eduardo Martín-Martínez. Entanglement harvesting from the electromagnetic vacuum with hydrogenlike atoms. *Phys. Rev. D*, 94:064074, Sep 2016.

[33] Benni Reznik. Entanglement from the vacuum. *Found. Phys.*, 33:167–176, 2003.

[34] Grant Salton, Robert B. Mann, and Nicolas C. Menicucci. Acceleration-assisted entanglement harvesting and rangefinding. *New J. Phys.*, 17(3):035001, 2015.

[35] Alexander R. H. Smith and Robert B. Mann. Looking Inside a Black Hole. *Class. Quant. Grav.*, 31:082001, 2014.

[36] Greg Ver Steeg and Nicolas C. Menicucci. Entangling power of an expanding universe. *Phys. Rev. D*, 79:044027, Feb 2009.

[37] Leonard Susskind, Larus Thorlacius, and John Uglum. The Stretched horizon and black hole complementarity. *Phys. Rev.*, D48:3743–3761, 1993.

[38] W. G. Unruh. Notes on black-hole evaporation. *Phys. Rev. D*, 14:870–892, Aug 1976.

[39] Antony Valentini. Non-local correlations in quantum electrodynamics. *Physics Letters A*, 153(6):321 – 325, 1991.